An Experimental Investigation of Aerodynamic Drag on a Round Parachute Canopy

Project Number: ME-HJ-0502

A Major Qualifying Project Report

Submitted to the Faculty of the

WORCESTER POLYTECHNIC INSTITUTE

in partial fulfillment of the requirements for the

Degree of Bachelor of Science

in Mechanical Engineering

by

Brian P. Day

____

Matthew N. Field

____

Justin P. Gelito

____

April 26, 2006

Approved:

____

keywords
1. Parachute Canopy
2. Rigid Canopy
3. Drag Coefficient

____

Abstract

The objective of this research was to experimentally study the connection between the shape of a parachute canopy during inflation and the aerodynamic forces on the canopy. This was done by comparing the aerodynamics of a series of rigid parachute models, which are similar in shape to the flexible inflating parachute, against unsteady aerodynamics of the flexible parachute during inflation. A series of rigid models were designed, manufactured and tested to see if they could replicate the aerodynamic drag forces on a flexible parachute model inflated under infinite-mass conditions (constant freestream velocity). Experimental results indicate that aerodynamic drag forces on the flexible canopy at specific time instances during the inflation process cannot be replicated using rigid canopy models. These findings suggest that the aerodynamic drag forces on an inflating flexible parachute under infinite-mass conditions are a result of the dynamic motion of the canopy.

Acknowledgements

The authors would like to thank Professor Hamid Johari, Dr. Kenneth Desabrais and Dr. Calvin Lee for their leadership, advice and guidance throughout this project. The authors would also like to thank the US Army Natick Soldier Center for funding this research. Special thanks is reserved for Steve Derosier and Matt Munyon of the WPI Haas Technical Education Center for the countless hours spent discussing machining processes, teaching us how to use CNC software and machines, always finding ways to troubleshoot problems and making us laugh. Additionally, this project would not have been successful without the help of Professor John Sullivan, Mike O'Donnel, Barbara Furhman and Toby Bergstrom. Thank you all.

Table of Contents

List of Figures

List of Tables

1. Introduction

1.1 Background

Round parachute canopies are bluff-body aerodynamic decelerators. Aerodynamic decelerator devices are used to primarily decelerate and/or stabilize an object in freefall, although they are also used in certain ground vehicle applications. Parachutes are used as deceleration devices for airdrop of personnel and equipment and recovery of missiles, rockets and spacecraft. They can also be used to stabilize and retard the delivery of ordinance or to orientate a body in freefall before the primary deceleration system deploys. Today, parachutes have many applications. Parachutes are used to land autonomous exploration rovers on other planets, deliver supplies to natural disaster victims, recover rocket engines from the space shuttle and precisely deliver troops onto the battlefield using steerable ram air canopies. The round parachute canopy has played an important role in US Army operations involving placement of personnel and equipment.

The idea of using a high drag device to slow an object moving through air has been around for centuries. Some of the earliest sketches for this type of device were drawn by Leonardo da Vinci around 1485. In 1783, Sebastien Lenormand gave the name parachute to such drag devices. Jean-Pierre Blanchard demonstrated jumping from a hot air balloon using these parachutes in 1793. In 1797, Andre-Jacques Garnerin jumped using a folded silk parachute. Until the beginning of the twentieth century, parachutes were not all that practical and were mostly used for entertainment purposes similar to earlier eighteenth century hot air balloon jumps (Desabrais, 2002).

However, with the development of flight vehicles in the early 1900s, it became apparent that parachutes could be used for more than just entertainment. As parachute usage increased, a better understanding of the relationship between parachute dynamics and performance characteristics was desired. As a result, in order to refine design and analysis methods, formal studies into the dynamics of parachutes began.

Parachutes can inflate under two types of freestream velocity conditions. These conditions are characterized as either an infinite mass or finite mass condition. It is known that the connection between parachute canopy shape and size as well as the forces on the canopy depend on the freestream flow conditions (Knacke, 1992). Inflation under finite mass conditions means that the velocity of the parachute system decays as it inflates. Eventually after terminal velocity, the velocity of the parachute system becomes relatively constant. The canopy breathing does cause variations in drag forces and subsequently the velocity of the system. This condition is known as finite mass condition.

Parachutes also operate in the infinite mass condition during inflation for certain applications. For example, when a parachute is used for stabilization purposes, the velocity of the airflow over the canopy remains constant during inflation. The deceleration of the system due to the drag force of the stabilization canopy is small and can be neglected and therefore infinite mass conditions can be assumed.

Talyor (1963) performed early experiments using parachutes as air brakes for landing aircraft. Future studies involved investigating the inflation time of parachute canopies. Müller and others conducted experiments which concluded that for geometrically similar canopies, the distance over which the canopy takes to inflate will be the same (Müller, 1927; French 1963; Heinrich, 1969; Heinrich & Noreen, 1970; Heinrich, 1972). French (1963) attempted to correlate the peak opening forces and the opening times of various parachute geometries. These theories helped designers determine the amount of time it takes a canopy to inflate. The initial theories measured the drag force on the canopy using Newton's second law. The equations used both steady and unsteady mass terms to describe the drag force on the canopy during inflation.

Finite-Mass Equation of Motion (French)

$$F = ma = mg\sin\theta - \frac{1}{2}\rho v^2 C_D \pi r^2 \quad (1)$$

Equation of Motion (Heinrich)

$$\left(\frac{d}{dt}\right)\left[\left(m_s + m_p + m_i + m_a\right)V\right] = \left(W_s + W_p\right)\sin\alpha - D_s - D_{pc} \quad (2)$$

When the following assumptions are used:

- suspended weight is much greater than the weight of the parachute canopy
  - $W_s >> W_p$
- drag of the parachute canopy is much greater than the drag of the suspended weight
  - $D_{pc} >> D_s$
- and when the angle to the horizontal is either zero or perpendicular
  - $\alpha = 0$ or $\alpha = \pi/2$

The equation of motion simplifies to:

$$F = m_s \frac{dV}{dt} = m_s g - \frac{\rho}{2} C_D S V^2 - V\left(\frac{dm_i}{dt} + \frac{dm_a}{dt}\right) - \left(m_p + m_i + m_a\right)\frac{dV}{dt} \quad (3)$$

The infinite mass condition is approximated by setting $m_s/(m_p+m_i+m_a)=100$

W_s =supsended weight	m_s =mass of suspended weight
W_p =weight of parachute canopy	m_p =mass of parachute
D_{pc} =drag of parachute canopy	m_i = mass of included air
D_s =drag of suspended weight	m_a =apparent mass
ρ =density	V =velocity
S = canopy projected area	C_D =drag coefficient
v =instantaneous velocity	r = instantaneous max. projected radius

Additionally, investigations aimed at describing the mass of the flow around a parachute canopy were conducted for finite mass inflation conditions (Ibrahim, 1967; Eaton, 1983; Yavuz, 1989). Much of this research has focused on using experimental data and analytical theories to predict important design parameters such as opening time and maximum opening force (French, 1964; Knacke, 1992). However, these theories used simplifications to avoid dealing with the complex fluid dynamics in the flow field near the canopy. Computational models of parachute canopies have been created to study flow around fully inflated canopies (Stein, 1999; Stein et al., 1999; Stein et al., 2000). Additionally, experiments have been conducted to determine drag coefficients for a number of bluff body objects. For example, Hoerner (1958), among others, has experimentally determined drag coefficients for a number of objects including shapes similar to those of an inflating parachute canopy such as disks, cylinders and cups. Other recent research related to the relationship between forces on the canopies and the surrounding flow field includes investigations into the study of flow in the near wake of a parachute canopy (Johari, et al., 2001; Desabrais, 2002)

It is evident that there has been a sustained interest in understanding the dynamics of parachute systems for almost a century. Since 1964, parachute researchers have gathered at the biennial AIAA (American Institute of Aeronautics and Astronautics) Aerodynamic Decelerator Systems Technology Conference to present and discuss developments in this field.

Successful parachute design requires tailoring important performance parameters to meet the mission requirements or design specifications. In the design of a parachute canopy, the most significant parameters are parachute stability, peak opening force, opening (or filling) time, and steady-state drag. “These parameters are typically obtained from full-scale testing of parachute prototypes. Full-scale testing for design purposes is time consuming and not cost effective.”

(Johari, 2003) “Because of the complexity of the fluid dynamics involved, advances in parachute technology rely heavily on experimentation.” Recent parachute research efforts have focused on gaining a better understanding of the parameters affecting parachute dynamics under inflation and fully inflated conditions. Driving this research is the desire to reduce the time, development costs and uncertainties associated with the design of new parachute systems.

At the present time, few studies have taken a comprehensive look at the aerodynamic forces on a parachute canopy and their relationship to the canopy shape. An investigation of the relationship between canopy shape and the aerodynamics on an inflating round parachute canopy may provide results useful to the effort aimed at enhancing how new parachute systems are designed.

1.2 Objective

The objective of this project was to experimentally study the connection between the shape of a parachute canopy during inflation and the aerodynamic forces on the canopy by comparing the aerodynamics of a series of rigid parachute models, which are similar in shape to the flexible inflating parachute, against unsteady aerodynamics of the flexible parachute during inflation.

To accomplish this objective, solid models of a round parachute canopy at different stages of inflation were designed, manufactured and tested to see if the drag forces on rigid models are comparable to the flexible canopy model loads during inflation.

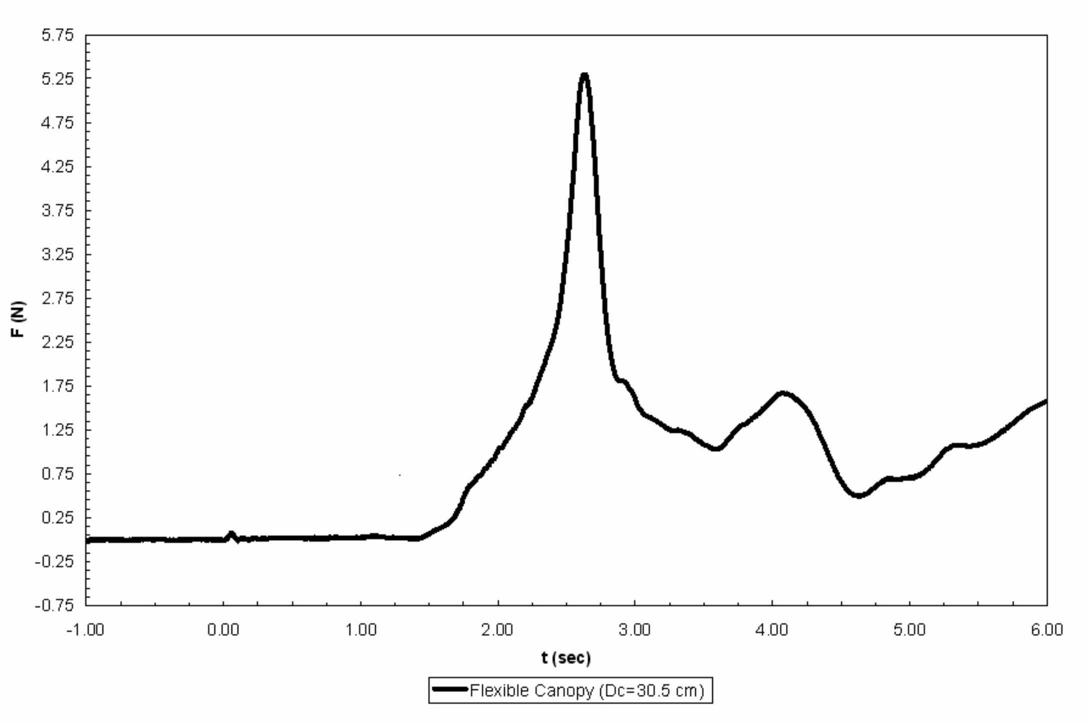

Figure 1 - Drag force vs. time graph of a flexible canopy (constructed diameter = 30.5 cm) tested in a water tunnel with a freestream velocity of 20 cm/s.

This investigation will help determine whether the drag forces on a round parachute canopy are related to the actual shape of the canopy or if they are related to other factors such as the time rate of change of the canopy's shape during inflation.

1.3 Parachute Analysis

In the study of parachute aerodynamics, certain parameters are used to characterize the environment in which the parachute is operating and the resultant forces on the canopy. The Reynolds number is a parameter correlating the viscous behavior of Newtonian fluids. Newtonian fluids exhibit a linear relationship between applied shear force and viscosity. The

Reynolds number is non-dimensional with a density, viscosity, velocity, and length scale parameter.

$$\mathrm{Re}_{D\max} = \frac{\rho U_{\infty} L}{\mu} \tag{4}$$

The drag force on a bluff body such as a parachute canopy is usually normalized with dynamic pressure and a characteristic area for comparison purposes. This value is defined as a drag coefficient C_D.

$$C_D = \frac{D}{qA} \tag{5}$$

$$q = \frac{1}{2}\rho U^2 \tag{6}$$

Drag coefficients for bluff bodies similar in shape to those of an inflating round parachute canopy include disks, cones, and cups. Hoerner reported drag measurements on a wide variety of bluff bodies. In his book *Fluid-Dynamic Drag*, Hoerner lists experimentally determined drag coefficients for 2-D and 3-D objects such as for caps, cones, cups and cylinders in flow characterized by Reynolds numbers between 10^4 and 10^6. The shape of an inflating parachute canopy is similar to these shapes at different stages during the inflation process. There is a drag curve for 3-D sheet-metal "caps" for varying C_D for Re numbers between 10^5 to 10^6. These Reynolds numbers are scaled using the diameter of the cap, d.

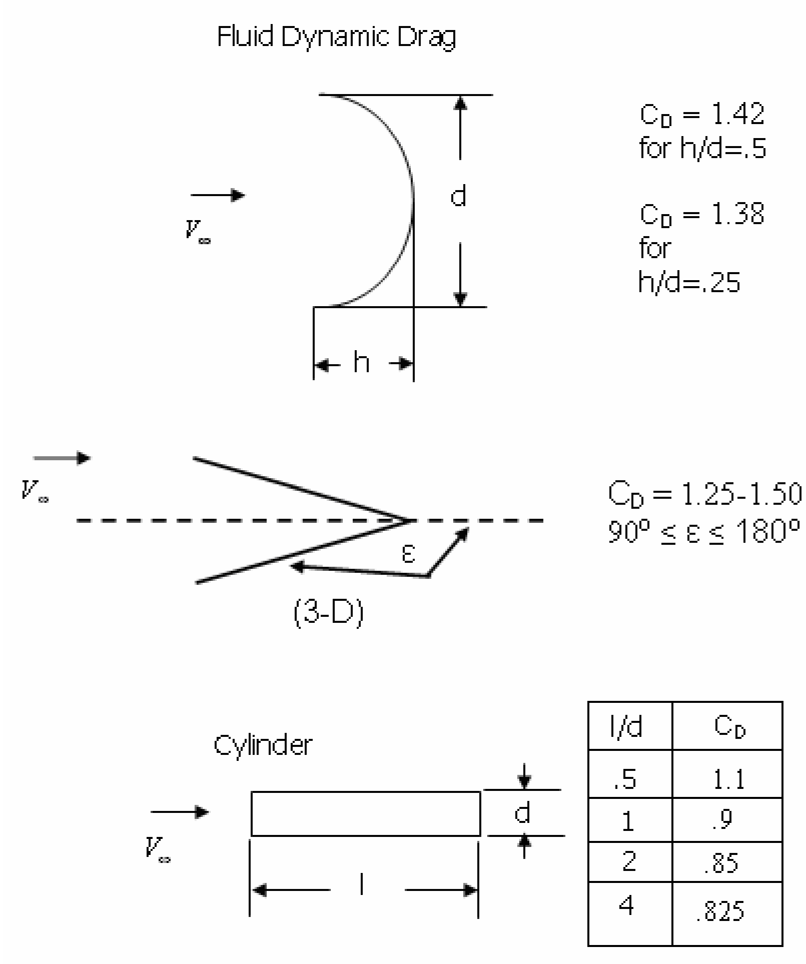

Figure 2 - Fluid Dynamic Drag Summary

According to Hoerner, in this Reynolds number range, variations in drag coefficient values depend much more heavily on the ratio of height to diameter of the cup or cap than it does on the precise Re number value. These shapes also experience separated flow and as a result of the negative pressure on the side opposite to the freestream flow, drag coefficients are noticeably higher when the concave surface meets the freestream flow as opposed to having the convex surface placed normal to the flow. In addition to caps, Hoerner has drag coefficient data for cones.

In his dissertation entitled, Velocity Field Measurement in the Near Wake of a Parachute Canopy, Desabrais (2002) tested small circular parachute models in a water tunnel. Typically, parachutes are constructed by sewing individual panels (gores) together to form a circular geometry (Knacke, 1992). It was decided that constructing scale models this way would make the canopies too stiff. For Desabrais' experiments, two different size canopies were constructed from a circular sheet of 1.1 oz/yd^2 rip-stop nylon. The single sheet of nylon cut in the shape of a circle forms the canopy. Two different canopy sizes were used in these experiments. Twenty-four suspension lines were then attached at evenly spaced intervals along the edge of the circular sheets.

Data from Desabrais' dissertation experiments contain image sets and corresponding drag data for canopies with constructed diameters of both 15.2 cm and 30.5 cm. Data collected for these canopies during inflation at 19.6 cm/s freestream water tunnel velocity over a time interval of approximately 10 seconds consists of 293 images and 2250 drag force measurements. The Reynolds number corresponding to the 15.2 cm canopy was 29,800 scaled to the canopy constructed diameter and Re = 55,900 for the 30.5 cm canopy. The force versus time plots for both the 15.2 cm and 30.5 cm constructed diameter canopies share similar characteristics.

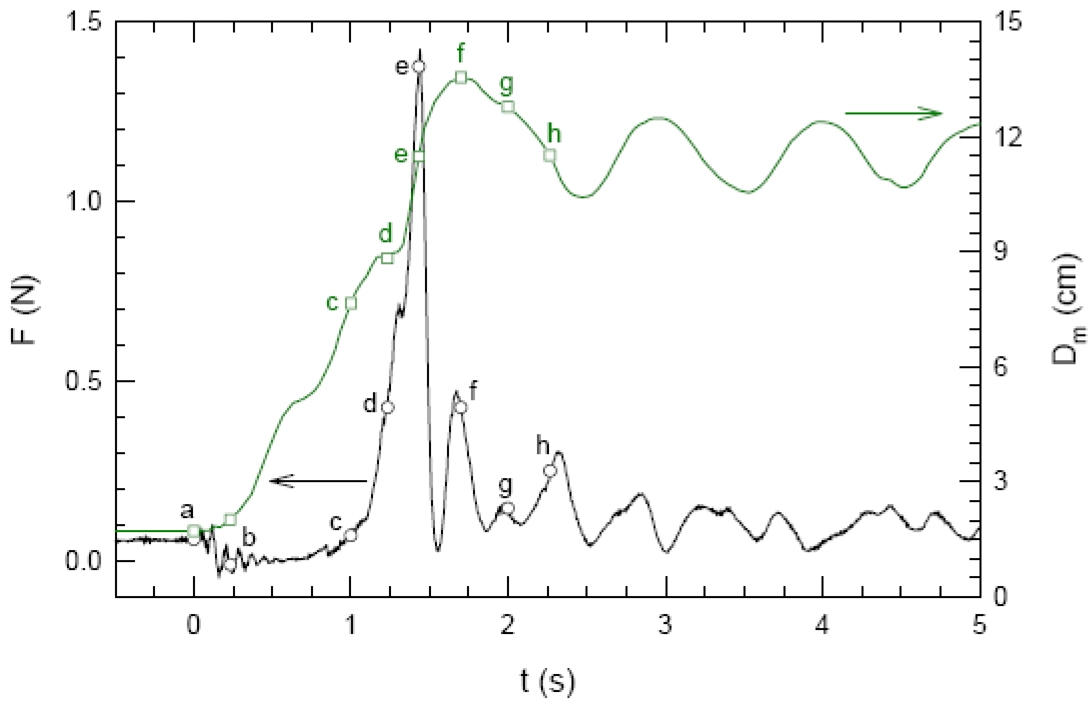

Figure 3 - Opening force and diameter for a 15 cm canopy with freestream velocity of 20 cm/s in a water tunnel.

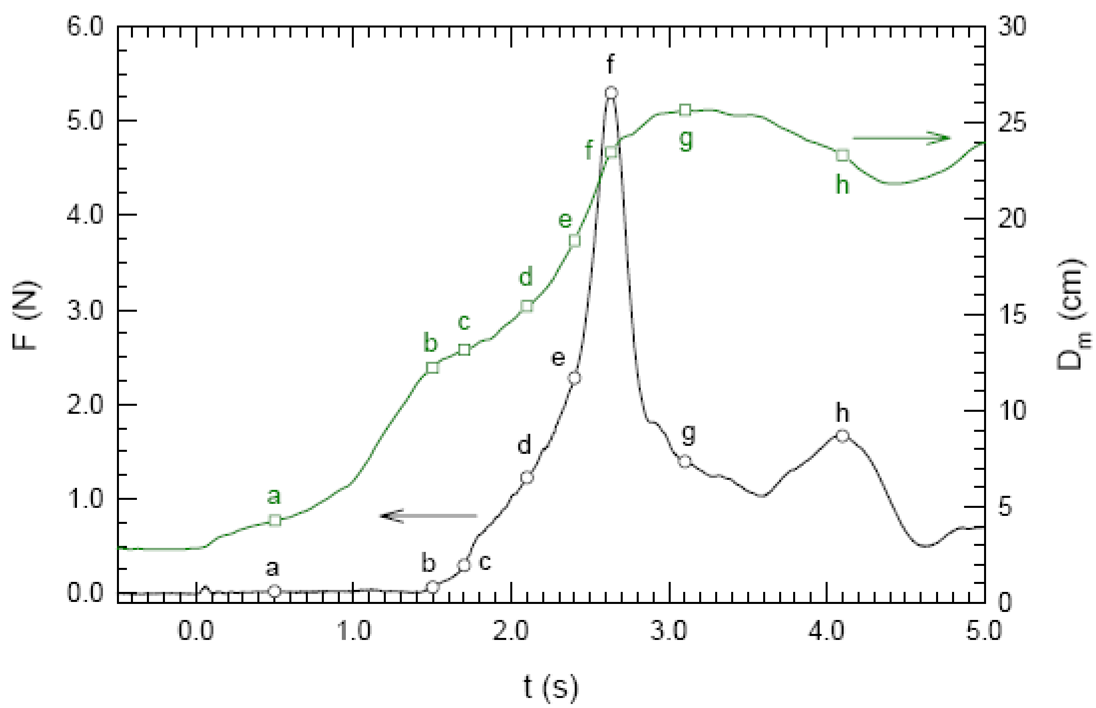

Figure 4 - Opening force and diameter for a 30 cm canopy with freestream velocity of 20 cm/s in a water tunnel.

For a direct comparison of drag forces on the proposed rigid parachute models to the drag forces on the flexible canopy models tested by Desabrais, it would be necessary to test models under dynamically similar conditions to the flexible water tunnel models. There are limitations imposed on this drag force comparison by testing in a wind tunnel as opposed to a water tunnel. First, in order to compare data, conditions must be dynamically similar. This similarity depends on Reynolds number, since Reynolds number is a characteristic of the flow. As long as Reynolds numbers are of the same order, a direct comparison of normalized drag data can be considered reasonable.

In studies of drag on rigid bluff bodies by Hoerner, it is seen that drag coefficients for bluff bodies can be quite different depending on Reynolds number. For example, a plot of experimental drag coefficients against Reynolds number for a sphere (and other objects) shows that there are transitional points where the drag coefficient can change value rapidly. For a sphere, one very noticeable transition occurs at $Re_d \approx 4.7 \times 10^5 - 5.5 \times 10^5$ where C_D drops from .8 to .2. Therefore, if the Reynolds number ranges of two different experiments differ, it must be assumed that there could be a possible Re range between these two experimental sets where drag coefficient could drastically change. Caution must be exercised when comparing two sets of experimental data when a gap exists.

Due to equipment availability at WPI, it was decided that the solid parachute canopy models would be tested in a closed-loop (full-return) wind tunnel. Closed-loop wind tunnels are generally considered best suited for obtaining aerodynamic data since the velocity distribution in the test section stays more uniform (Knacke, 1992). Drag forces would be measured by a linear displacement transducer dynamometer.

When testing in a wind tunnel, the amount of test section blockage generated by the test article must be taken into consideration when analyzing test data. In an unrestricted test section with no test article, flow is uniform ignoring boundary layer interactions at the walls. When a test article is placed in the test section, flow streamlines are deflected around the test body. However, the deflected flow is constricted by the test section walls, which interferes with the flow around the test body (Macha & Buffington, 1989). As a result, the data must be corrected to account for this wall interaction.

As tunnel blockage increases, the effects due to the change in the streamlines and properties of the flow field can produce questionable test data. In order to avoid these effects, it is suggested that the test article not block more than 6% of the test section cross-sectional area (Knacke, 1992). However, a study published in 1989 from Sandia Labs suggests that it is possible to correct test data for parachutes tested in a wind tunnel with blockage ratios up to 30% (Macha & Buffington, 1989).

According to this study, the results are believed to be applicable to any circular parachute. The results provide blockage correction factors based on Maskell correction methods for three-dimensional, non-lifting bluff bodies. According to Maskell, the effective increase in dynamic pressure due to blockage is given by

$$\frac{q}{q_u} = 1 + K_M + \frac{C_D S_u}{C} \tag{7}$$

with C being the tunnel cross-sectional area, $C_D S_u$ being the model drag area (D/q), K_M being the Maskell bluff-body blockage factor, and q being the freestream dynamic pressure. The subscript u denotes an uncorrected value. This correction factor is based on the frontal area normal to the freestream flow.

2. Canopy Model Design Process

2.1 Canopy Model Design Constraints

It was previously mentioned that the purpose of this project was to compare the drag characteristics of solid canopy models to the drag characteristics of the Desabrais (2002) flexible parachute canopies. To accomplish this task, two-dimensional digital images provided by Desabrais needed to be converted into solid models using imaging software, computer aided design software, and computer aided manufacturing software packages. Throughout this process, the design was constrained by the capabilities of the wind tunnel and drag force measurement equipment. These constraints were wind tunnel test section blockage, drag force measurement capabilities, and wind tunnel testing velocity. All design considerations needed to take into account the implications that they had on these three constraints.

The first constraint, wind tunnel test section blockage, is the ratio of the projected area of the model and the cross sectional area of the wind tunnel test section. It was known that any sized test article placed in a wind tunnel creates blockage effects that induce flow disturbances. This is a result of the flow going around the model and interfering with the test section walls. Ideally, tunnel blockage should be chosen to be less than five to six percent (Knacke, 1992). However, although tunnel correction methods have been shown to accurately correct data for blockages up to 30%, Macha suggests that tunnel blockage be no more than 10% to ensure reliability when using this method (Macha & Buffington, 1989). Therefore, this constraint limited the projected area of the model to 10% of the wind tunnel test section cross sectional area. In this case, the 2 ft X 2 ft test section had a cross-sectional area of 4 ft^2 resulting in a maximum model projected area of 0.4 ft^2, or a maximum canopy diameter of 8.56 in. Due to the fact that both drag coefficient and Reynolds number are calculated using the diameter of the canopy, this limitation would have direct affects on those constraints as well.

The second constraint was the magnitude of drag that could be accurately measured by the dynamometer. After referencing the instruction manual for the dynamometer, it was found that the maximum drag force that could be measured without damage to the instrumentation was 7 lbf. It was also ascertained that it could accurately read $1/20^{th}$ of that maximum drag force, a value of 0.35 lbf. Therefore, the drag force measurement instrumentation could not be subjected to forces outside the range of 0.35 – 7 lbf for accurate readings. This constraint also limited the size of the model, due to the fact that drag force is calculated using the projected area.

The final constraint on the model designs was the wind tunnel testing velocity. It was known that cup shaped bluff bodies tend to vibrate due to vortex shedding when subjected to the freestream. These shedding cycles tend to become more violent as the freestream velocity is increased. Therefore, to avoid damage to the models and wind tunnel equipment due to model or dynamometer failure, the wind tunnel velocity needed to be monitored. Changes in wind tunnel velocity directly affect the drag force measurements and Reynolds number calculations.

It can be seen that these three constraints are interrelated. A change in design to compensate for one limitation will directly affect one or both of the other restrictions. Therefore, this design progression was an iterative process, meaning that the sizing of the models was modified until all design boundaries were satisfied.

2.2 Drag Force Time History Curve Representation

With the constraints outlined, a method for creating three-dimensional models from the two-dimensional images could be formulated. The first design consideration was how to accurately represent the drag force time history plot using solid models. It was known that the curve was created from approximately 1,500 data points. To attempt to recreate the curve perfectly would require the production of 1,500 rigid models. This would prove to be an impossible task given the time constraints.

Therefore, it became necessary to determine a means for representing the complex curve by creating a feasible number of rigid models. One possible method for representing this curve was to create models at specific data point intervals. This would effectively reduce the number of rigid models. Another option was to choose points on the time history that, when plotted separately, could accurately reflect the dynamic nature of the inflating canopy. One final way to accurately reflect this curve was to create single models that could represent more than one data point on the time history plot. This could be accomplished by making each model adjustable in some way.

The problem with selecting models based upon data point intervals is that they may not accurately capture the key points on the time history plot. For example, if models were made at each second during the canopy inflation, the opening shock peak that can be seen at about 2.5 seconds would not be represented. The drawback of the second method was the number of models needed to represent the curve. Visual inspection of the curve determined that approximately 50 models would be needed. Lastly, the complexity of designing an adjustable rigid canopy model that accurately reflected the flexible canopy at different inflation times was deemed impractical. This was due to the fact that the design process of this single model would take more effort than simply making a greater quantity of simpler models. Also, given the fact that no previous attempts have been made to manufacture such a model, it was unknown if it could accurately represent each canopy model as well as a set of rigid models could.

With these options exhausted, the research team decided it was important to highlight critical changes in drag during the inflation process. These critical changes were identified to be the beginning of inflation when the canopy experienced relatively constant drag forces, the opening shock peak, the point of canopy overexpansion, and the fully inflated region. These four points became the basis for rigid canopy models.

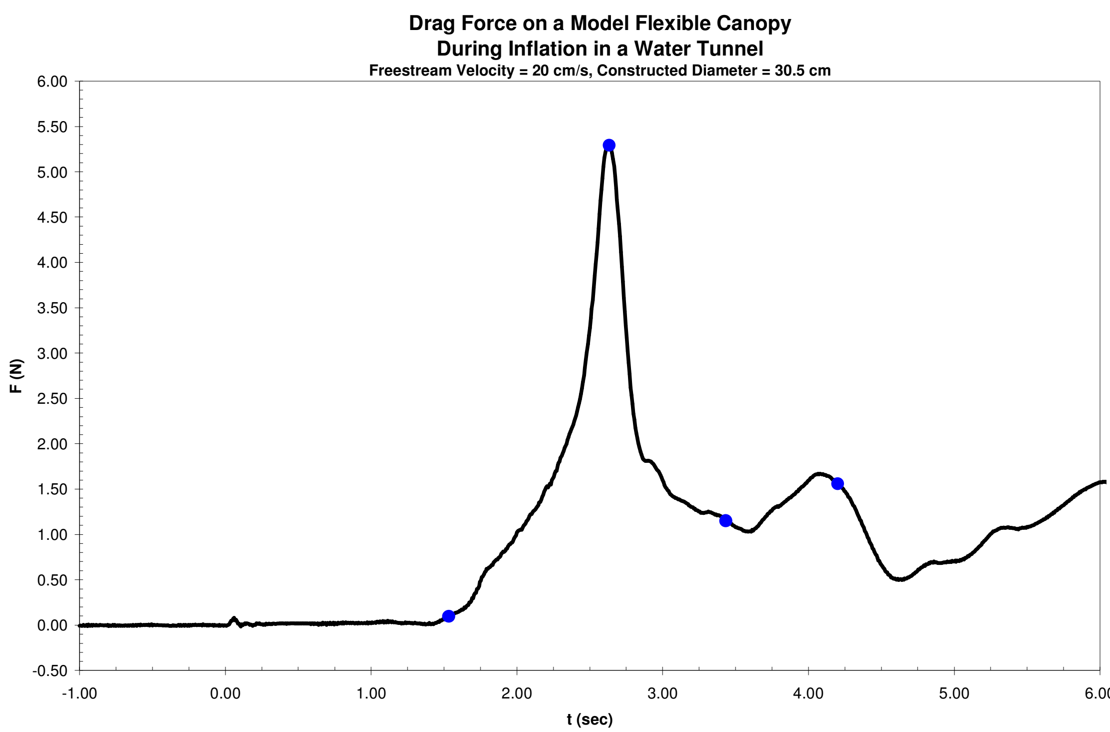

Figure 5- Four points critical in representing the force time history curve (points: just as canopy starts to inflate, peak force, over expanded, steady-state)

With the four points of greatest interest accounted for, it became necessary to determine the number of additional models that could be made to replicate the other parts of the curve.

Upon further inspection of the force time history, it was determined that a much better curve representation could be achieved using just four more points. One point was chosen in the region where the canopy has not begun to inflate, two additional points were selected before the peak force as the opening force is increasing, and one other point was selected after the peak force as the opening force is decreasing. It is important to note that the points chosen immediately before and after the peak force experience the same drag value. These points are shown in Figure 6.

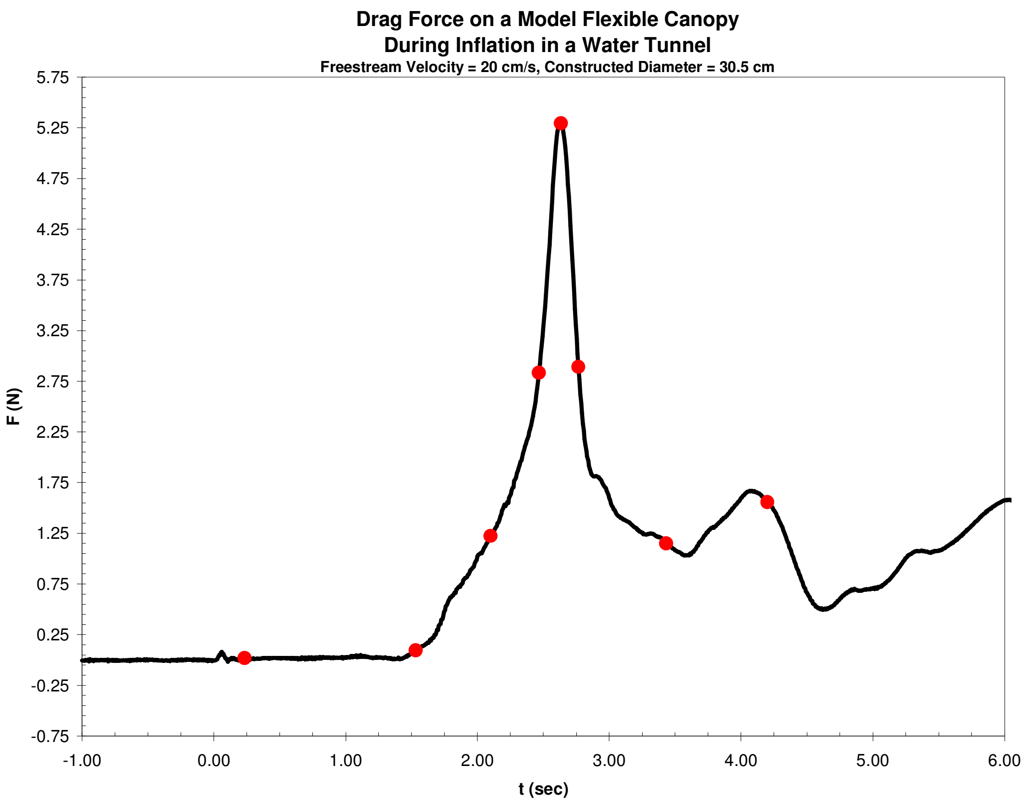

Figure 6- Points selected for model creation along the force time history plot.

These eight points captured the main features of the force time history of the inflating flexible canopy. Clearly, more points could be used for a better approximation. However, this analysis showed that the main features of the force time history could be captured using at a minimum of eight points.

2.3 Canopy Curve Estimation Using Digital Images

As mentioned earlier, two-dimensional digital images were provided to the research team. These digital images were instantaneous photographs of the canopy during the inflation process. Each digital image included the shape of the canopy, the time into the opening process, and the location of this time on the opening force time history graph. With the time and location of each image on the drag force time history plot known, it was possible to obtain the canopy image for each of the points chosen above. These images became the starting point for solid model generation, and the corresponding canopy shapes can be seen in Figure 7.

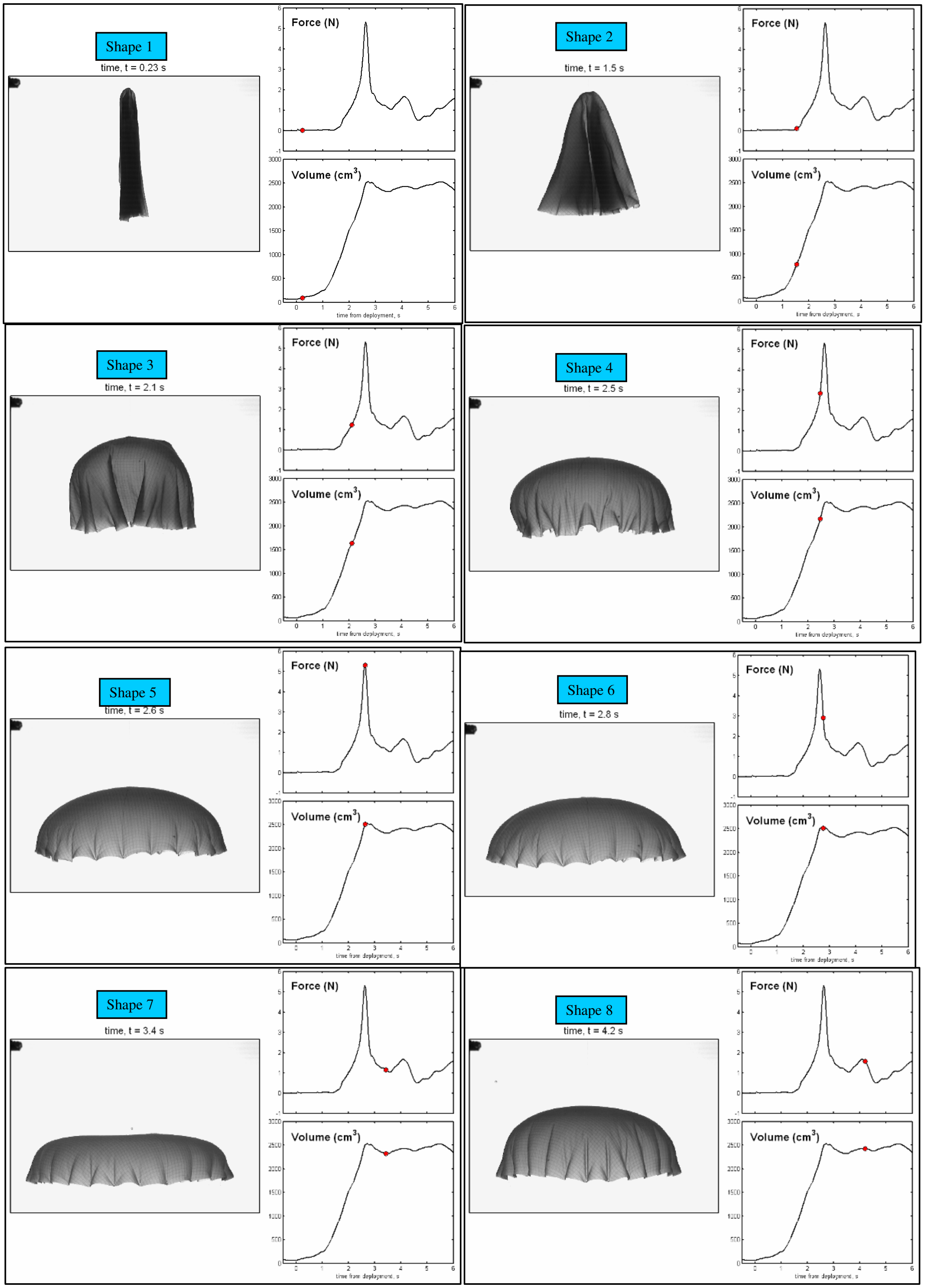

Figure 7 – Digital images of the canopy shapes chosen and their location on the drag force time history plot.

The method of creating these three-dimensional models from the images, however, presented another design challenge due to the fact that each picture only depicted an instantaneous image of one side of the canopy. Additionally, the gores on the canopy were not uniform, and the images only showed the curves for two of the twenty-four gores. It was also unknown if the gores depicted were offset from the visual plane.

Due to the complexity of the folding, and the lack of a 360° view for each canopy shape, a method to approximate these gore curves was needed. With no imagery of the backside of each canopy, it was impossible to know exactly how the gores were shaped all around the parachute. Using the images available, the best approximation of the gore curves was to consider them symmetric, evenly spaced and planar with the images. This resulted in a canopy consisting of twenty-four symmetric gores spaced 15° from midpoint to midpoint. Even if the centers of the gores depicted were not perfectly planar with the images, the maximum the centers could be offset was 7.5°. Considering that the canopy gores change at each time instance during the inflation process, the gores are never exactly the same shape. Therefore, any offsets are negligible because of the variation of each gore shape.

Further work with the digital images required the selection of an image software package. Various software packages allow the user to retrieve information about pixels in digital images. These include Microsoft Paint, Adobe Photoshop, and MATLAB.

After experimentation with each of the aforementioned software packages, Microsoft Paint was chosen for its ease of use and well-suited coordinate system, a characteristic not shared by the other, more cumbersome, software packages. The images could be aligned with an X-Y origin, allowing the X-Y coordinates of any pixel to be recorded. The X direction was in the radial direction, and the Y direction was in the axial direction. Each canopy outline was traced one half at a time with a high zoom percentage to see the exact edge of the shape. The curves of the canopy were determined by finding the X coordinates of points using predetermined Y coordinates. Due to the inconsistency of the curve from the right side to the left side, the two sets of points were averaged to create one smooth curve for the parachute canopy. This smooth curve was necessary for solid modeling using a computer aided design (CAD) package and for a better approximation of the gore shape. In total, each canopy shape was determined by finding approximately 135 points for each outside curve.

A similar procedure was used to estimate the inside curves resulting from the canopy gores. The transparency of the canopy fabric allowed for the determination of the depth of the gore folds. The image below shows a line transposed onto the image estimating the gore folding. The points of these curves were recorded, and once more averaged over each side of the canopy. Again, these gores were estimated using the same assumptions as the outside gore curves.

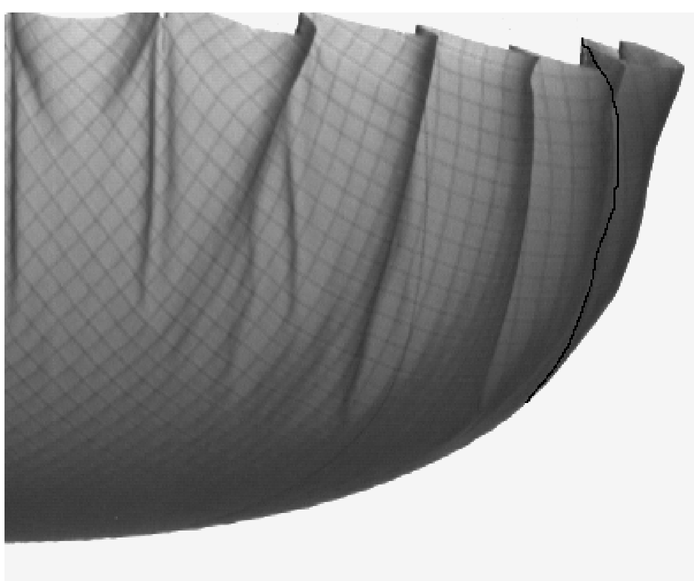

Figure 8 - Digital image of canopy 8 showing outside curve and gore curve

2.4 Sizing and Scaling of Canopies from Curve Estimations

With the pixel coordinates for each canopy curve determined, it became necessary to convert them into length coordinates. The length scale chosen determined the size of the models. Several interrelated design considerations were then encountered. As previously mentioned, the size of the models directly affected the wind tunnel blockage, the drag force measurements, and the Reynolds number calculations. This is because each of these factors is based on the frontal area. The scaling of these models was bounded by 10% tunnel blockage, 0.35 – 7.0 lbf drag measurements, and wind tunnel velocities suitable for testing.

To reduce the adverse effects of tunnel blockage on collected data, reduce the need for larger amounts of correction thereby maximizing the reliability of drag force data, the project team first attempted to scale the parachute models to five percent tunnel blockage. This meant that the projected area of the largest model could not exceed five percent of the test section area. This resulted in a maximum projected diameter of 6.056 in. for the largest model. In this case, model seven had the largest diameter. Using the X-Y coordinates determined earlier, the largest value of X was found, and scaled to 6.056 in. This scaling factor was used for the rest of the points on shape seven, and also for all of the points of the remaining seven models.

With model seven scaled to five percent tunnel blockage and the other models scaled accordingly, the expected drag force measurements and corresponding velocities could be calculated for each model. This analysis was performed using Equation (4) and Equation (5) to determine estimated drag forces on each canopy for the range of possible tunnel testing velocities and a range of possible drag coefficients. Using Equation (4) for a given range of Reynolds numbers, the kinematic viscosity for air, and the scaled maximum projected diameter of each model, the freestream velocity could be calculated. Once the freestream velocity was known, drag force was found using Equation (5) and values for estimated canopy drag coefficients, the calculated freestream velocity, projected area, and the density of air.

It was found from this analysis that scaling the models to five percent tunnel blockage resulted in extremely small drag forces for the smaller projected diameter models. The freestream tunnel velocity required to achieve measurable forces for these models needed to exceed 70 m/s. This speed is much greater than the tunnel speeds deemed safe for testing bluff bodies in the wind tunnel. Therefore, scaling to five percent tunnel blockage was not feasible.

A maximum tunnel blockage of ten percent for the rigid models was then investigated. Although not ideal, correction methods for blockages of ten percent or less exist and have been proven to successfully correct for tunnel blockage flow disturbances (Knacke, 1992). Applying the same analysis methods described above, it was determined that measurable drag force could be obtained for seven of the eight models using tunnel speeds between 15 and 30 m/s. Scaling the models to ten percent blockage resulted in a test velocity range of 15 to 25 m/s, and measurable drag forces for all but the smallest model. Shape one was chosen very early in the opening process, resulting in a relatively small projected area. This small projected area, in turn, produced little drag force at reasonable tunnel speeds. The tunnel blockage could be increased to include this model, however, it was decided not to do so because historically, tunnel blockages greater than ten percent have resulted in unacceptable flow disturbances (Knacke 1992). Although there are proven correction methods for flexible parachute canopies having tunnel blockages greater than 10%, the accuracy achieved by applying these methods to rigid canopy models could not be guaranteed (Macha & Buffington, 1989). See Appendix C for the estimated drag force analysis.

2.5 Computer Aided Design of Scaled Models

Once the scaled estimations of the canopy curves were determined, solid modeling of the shapes could begin. Pro/ENGINEER Wildfire 2.0 solid modeling software was utilized due to its availability on campus, and the project team's familiarity with its operation.

To create the solid model, the scaled X-Y coordinates of the outside curve were imported. These points were used to create a datum curve. Next, the scaled inner curve X-Y coordinates were imported, and used to create a datum curve rotated 7.5° along the center axis from the previous curve. The outside datum curve was then mirrored on the other side of the inside curve.

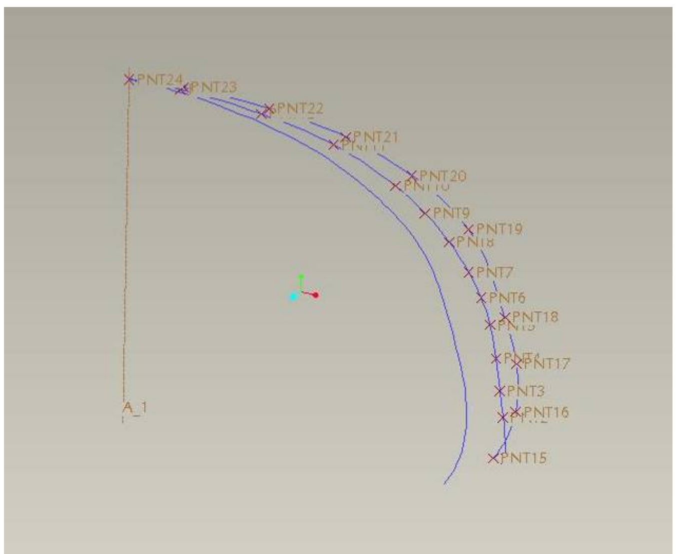

Figure 9 - Pro/E Datum Curves

This created the 15° quilt of one gore section.

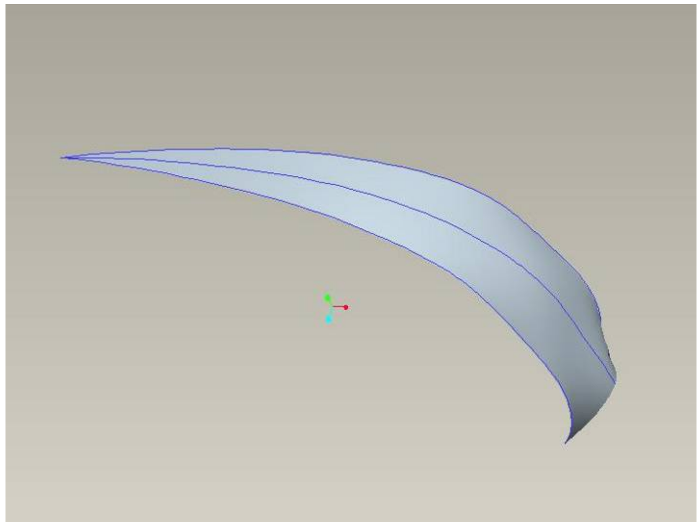

Figure 10 - Pro/E Drawing of Gore

This gore was revolved 360° to form the round canopies. The 24 separate gore quilts were then merged together forming one quilt. The quilt was then thickened to 0.05 in., the desired thickness for the canopy models. This thickness was chosen, because it is the thinnest that the Computer Numeric Control (CNC) machines can machine without damaging the model according to Dr. William Weir (personal communication, November, 2005). The model was then solidified to create a solid model.

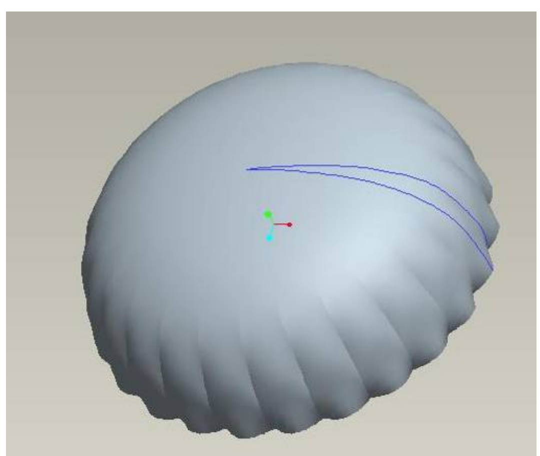

Figure 11 - Pro/E Solid Canopy

Keeping in mind that machining was a likely method of construction, in addition to modeling the canopy shape, a fixture was needed for holding the model during machining. To reduce flow disturbance caused by fixtures, it was decided to attach the canopy to the dynamometer at its center on the apex of the canopy. Additionally, it was decided to mount the parachute model in front of the dynamometer, to reduce flow disturbance created by the dynamometer structures.

Next, an investigation into feasible holding methods was conducted. This investigation concluded that a cylindrical boss extending from the top of the parachute with a smooth round to the canopy outer curve would be the strongest holding method that would minimize changes in canopy aerodynamics for drag testing. After investigating the collet holders available in the WPI Washburn machine shop for work holding, a diameter of one inch was chosen for the boss. One-inch collets were available on all of the lathes and mills, allowing smooth transfer from one machine to another during manufacturing. Bosses were then modeled and added to the Pro/E canopies.

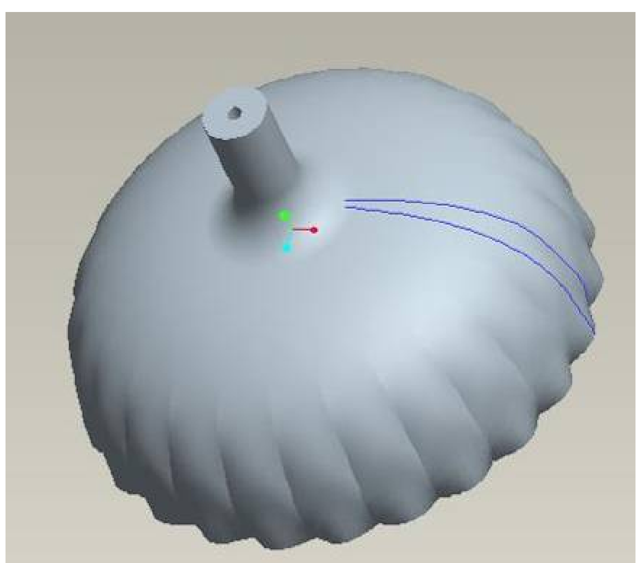

Figure 12 - Pro/E Solid Canopy with Boss

2.5 Dynamometer Sting Design

With the final solid models completed for each canopy shape, various analyses could be performed within Pro/ENGINEER to determine the models' masses, and centers of gravity. This information was needed for the sting design. The weight of the model hanging on the sting and the drag force on the model during testing created a moment about the dynamometer. To ensure the sensitive electronics within the dynamometer were not damaged, an analysis of induced moments would be needed.

The weight of the model could be found by multiplying its mass by gravity. The moment arm was calculated by choosing a sting length from the dynamometer to the top of the boss, and then adding the distance from the top of the boss to the center of gravity. Sting lengths of one inch to twelve inches were investigated for each model. An oscillatory moment was accounted for in these calculations due to expected vortex shedding. This moment was estimated to be an additional one third of the total drag force on the model (Johari, personal communication, 2005). Maximum moments found for aluminum and acetal when oscillatory forces are included were 6.13 ft-lbs and 6.28 ft-lbs, respectively. These calculations can be found in Appendix A. The manufacturer of the dynamometer was then contacted to determine if these moments were too great for the dynamometer to withstand. According to Kurt Banaszynski at Engineering Laboratory Design (personal communication, 2005), the moments expected in this experiment were insignificant relative to the capabilities of the dynamometer.

The only remaining design criteria to determine were the diameter, threading, length, and material of the sting. Because weight was not determined to be an issue, a steel rod was used due to its strength. Later physical tests with the heaviest model showed that the diameter of the rod for shapes two through eight should be no less than 5/16 in. to maintain sting rigidity. A larger sting diameter could be used to reduce vibrations, but in the interest of causing the least flow disturbance, the 5/16 in. rod was selected. Model one was light enough to only require a 1/4 in. rod. One end of the rod was threaded with 1.5 inches of 1/4-20 in. thread for the dynamometer, and the other was threaded with one inch of 5/16-18 in. thread for the model bosses. Three stings were made from 5/16 in. rod for models 2-8 with varying lengths. The lengths of the non-threaded part of these stings were 2 in., 5 in., and 8 in.

Hardware required for mounting the sting to the model boss and dynamometer were one 5/16-18 nut, one 5/16 in. lock washer, two 1/4-20 in. nuts, and two 1/4 in. lock washers. The 5/16-18 in nut and 5/16 in. lock washer were used to tighten against the boss, reducing the chances of the model vibrating off of the threads. Similarly, the two 1/4-20in. nuts and 1/4 in. lock washers were required to prevent the sting from unthreading from the dynamometer. The completed sting design can be seen in Figure 13.

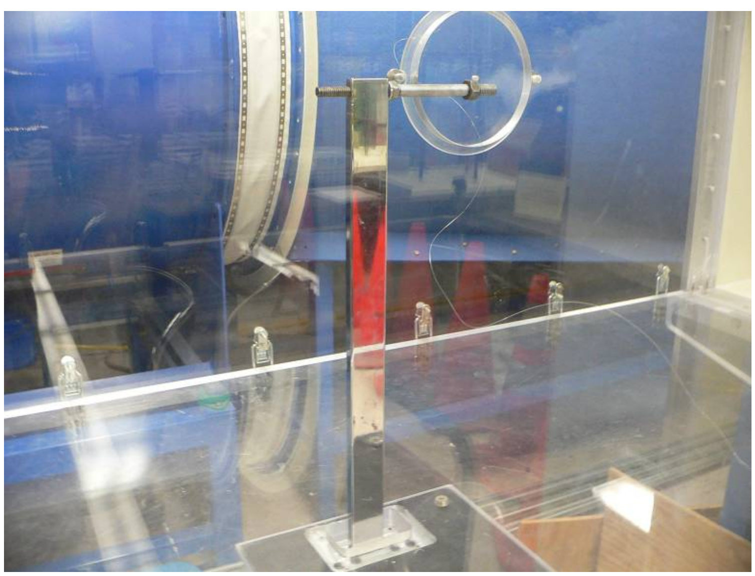

Figure 13: Completed sting design mounted to dynamometer.

3. Construction

3.1 Construction Options

There were a number of construction methods available for building the rigid parachute models. The selection criteria for choosing a construction method was based on facility availability, quality of construction, ease of manufacturing, construction cost, and manufacturing time. Construction methods considered included CNC (computer numeric control) machining, rapid prototyping, fiberglass construction using machined molds and MonoKote covered wire frames. The construction method was chosen based on these criteria.

The construction methods of CNC machining and stereolithography rapid prototyping use 3-D CAD (computer aided design) models to machine or prototype physical models. The CNC machining would involve cutting models out of large pieces of stock to create models while stereolithography prototypes are created layer by layer with a photosensitive resin. The creation of molds to create fiberglass models would also be achieved through a CAD model. Molds would then be made by a CNC machine or through stereolithography and then used to shape the fiberglass. Another construction method considered was building models using frames covered in MonoKote, a durable heat shrinkable film. The frame could be machined from a solid piece of material or assembled from individually machined parts.

The first criterion for choosing a construction method was facility availability. CNC machining facilities in the WPI Washburn Shops and mold making facilities in the Metals Processing Institute were available for student use. Also, the shops had well qualified staff and professional machinists. In addition, the Natick Soldier Center (NSC) Air Drop/Aerial Delivery Group had access to an in-house rapid prototyping facility. All construction options except for stereolithography could be done at WPI facilities. Therefore, facility availability would not be an obstacle in the construction of the rigid parachute models.

The next consideration was the quality of construction. With CNC machining and stereolithography, the models would be directly based on the generated CAD models. These manufacturing methods can easily hold tolerances to a few thousandths of an inch. Under conditions where part vibration is held to a minimum, a smooth surface finish can be achieved using machine tools. With stereolithography, it is relatively simple to obtain a polished or paintable surface finish (SLA Finish Levels, 2005). If molds were used to shape fiberglass, it would be difficult to hold the tolerances achieved through CNC machining or stereolithography. The molding process could leave an imprecise shape around the canopy skirt. In addition, the complex canopy geometries would require a two piece mold to allow the finished model to be separated after forming. When the frame method was analyzed, it was also determined that it would be very difficult to design a frame that could mimic a parachute canopy's complex geometry as accurately as the project specifications required.

In terms of manufacturability, the preliminary estimates for creating a mold showed that it would take almost the same amount of time to machine a mold as it would to machine an actual model. Again, manufacturing time estimates showed that it would probably take more time to machine a skeleton frame from a piece of solid stock than it would to machine an actual model. If instead, individual parts of the frame were machined and then put together, this would require building an assembly jig for each model. After this initial comparison, CNC machining and stereolithography rapid prototyping appeared to be the best manufacturing options when compared to forming fiberglass in molds or using MonoKote covered frames.

In terms of ease and convenience of manufacturing, the use of CNC machining was considered to be less desirable than stereolithography due to the intricate geometry of the parachute models. This complex model geometry would require multiple nonstandard part orientations, intricate machine setup and specialized tooling. There would also be problems associated with holding stock material in the CNC machines to minimize part vibrations during the cutting process.

Also, project specifications required that the model walls be as thin as possible. When machining a part, the less material there is to support the cutting surface, the more prone it becomes to vibrations and cracking. As a result, tailoring CNC G-Code and/or designing fixtures to hold and support thin, nonstandard shapes in order to minimize vibrations becomes a major manufacturing consideration. Trying to modify a CNC program to minimize vibrations for these complex model shapes is difficult for even experienced machinists. Creating fixturing to support these complex shapes is another design project in and of itself.

Therefore, to avoid the costly and time intensive process of designing and building support fixtures, it was realized that manufacturing these parachute models would require a machinist's attention while the CNC programs were running. This monitoring was necessary to make slight adjustments in cutter speeds and feed-rates.

Stereolithography is used to create a three-dimensional part directly from a CAD file. The only intermediate process is converting the CAD file to a .STL file. In Pro/E, this is a simple "save as" option. This file breaks the CAD model into slices.

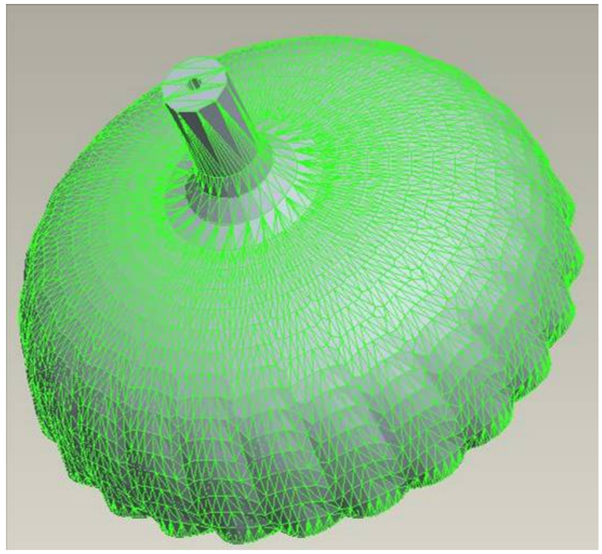

Figure 14 - Pro/E Converted STL model

This file is then used by the stereolithography machine to build the model. Although the models would not be extremely durable, construction time was estimated to be about three weeks. The autonomy of a stereolithography machine and the speed at which it could build these models makes it a better choice than CNC machining. The simplicity of stereolithography however, comes with a sacrifice. The cost of a single model using stereolithography at the NSC was estimated to be $750-$1000 (personal communication Lee, 2005). The research budget allocated for this project could not cover this expense.

Based on ease of manufacturing, construction time, quality of construction, and facility availability, stereolithography was determined to be the best manufacturing method for meeting project design objectives and schedule requirements. However, project budget restrictions prevented the use of this ideal manufacturing option. Based on selection criteria, the next best option was to use CNC machining to build the eight rigid parachute models.

3.2 Material Selection

With the manufacturing method chosen, it was necessary to choose a stock material. The model material was selected based on availability, cost, cut time and material properties including achievable surface finish, durability and strength.

Commonly machined materials include metals and plastics. Aluminum is the most commonly machined metal. Compared to steel, it is light weight, costs less and is easy to machine. After speaking with machinists and material supply companies, it was determined that a type of plastic called acetal, a commonly machined plastic, could satisfy the parachute model thin wall requirements while maintaining structural rigidity. Acetal is more commonly known by the brand name Delrin, a trademark of the DuPont Company. These materials were also chosen because the machinists in the Washburn Shops had experience machining these materials.

Design requirements dictated that the selected material be able to withstand aerodynamic and dynamometer (sting) attachment forces during wind tunnel testing. The density of the material would also have to be considered, as the weight of the parachute must not damage the transducers within the dynamometer. Based upon the previous force and moment analysis and contact with Kurt Banaszynski of Engineering Laboratory Design Inc., the manufacturer of the dynamometer and the wind tunnel, it was confirmed that using either material would not damage the transducers within the dynamometer (personal communication, 2005). This analysis can be found in Appendix A.

Next, the cost of using acetal versus aluminum was assessed. After obtaining quotes from Yarde Metals, Tri Star Plastics and Plastics Unlimited, the total estimated material cost for eight models using aluminum was approximately $1,300 and for acetal, $1,600 (Yarde Metals personal communication, 2005; TriStar Plastics personal communication, 2005; Plastics

Unlimited personal communication, 2005) Refer to Appendix E for stock sizes and pricing quotes.

With a limited amount of manufacturing time and the complex nature of the CNC machining processes, selecting a material with the shortest cut time was a major consideration. Upon consultation with Steve Derosier and Matt Munyon at the Washburn Shops, it was determined that the cut time for aluminum would be at a minimum four times that of the cut time for acetal.

Although aluminum is stronger and costs less than acetal, it is approximately twice as heavy as acetal. With a much faster cut time and suitable strength and rigidity properties, acetal was chosen as the material for the solid parachute models.

3.3 Construction Economic Considerations

The cost of construction became the most significant factor driving construction method choice. If the budget for this project had been able to support stereolithography manufacturing, models could have been made in approximately three weeks as opposed to six months. In addition, models could have been made without the boss required for holding the model during machining.

Cost also played a significant role in material selection. However, the other factors mentioned above superseded cost when it came to choosing a stock material. From the construction method decision analysis, it is seen that economic and time constraints make significant contributions when determining how to meet design requirements and project objectives.

4. Manufacturing

4.1 Design of Manufacturing Process

With a manufacturing method chosen, it was necessary to develop a machining process to make the rigid models. Preliminary discussions with machinists and manufacturing experts at WPI showed that their experience was limited making parts with the complex rounded geometries and thin walls present in the canopy models.

The part most similar to these rigid canopy models which was manufactured at the Washburn Shops was a smaller simplified parachute model that lacked the feature of the canopy curving back into itself. That machining was done by clamping a single block of aluminum to the worktable of a vertical CNC mill and surfacing the entire inside of the canopy as if it were upside down. After that process, the piece was flipped right side up and fitted onto a spherical mount for support and vibration suppression during the surfacing operation of the outer side of the canopy.

Some of the rigid models designed for this research have a skirt diameter that is less than the maximum parachute diameter. This feature is necessary to accurately represent the flexible canopy shape, however, it creates difficulties for interior machining operations. These difficulties were not encountered by the Washburn Shop when they made the smaller parachute model. In addition, the method used by the shop to make the small parachute model required making complicated custom fixturing. In order to make the rigid canopy models, the method the shop used either needed to be adapted or rethought completely.

In an effort to reduce the amount of custom fixturing needed to machine the models, it was determined that a method had to be found for removing as much stock material as possible without the use of custom fixturing. The round geometry of the canopies made using a CNC lathe the ideal choice for removing the bulk of the stock material. The CNC lathe would be able to remove a majority of the stock material on the outside of the canopy as well as bore out a majority of the stock material inside the models. Although lathe operations were adequate for making models 1 and 2, the gore geometry could not be created with the lathe.

This problem was solved by combining both lathe and milling operations. It was also determined that the addition of a fourth and fifth axis for the CNC mill would allow the machining of the canopies where the skirt curves back into the middle of the model.

The milling processes required for creating the exterior and interior gore geometry involved multiple part orientations. One orientation needed was to align the canopy model so that its central axis would be horizontal and the mill would be able to surface the top outer gores. The fifth axis would then index the piece about its central axis to enable further surfacing of the outer gores. The surfacing operation for the inside of the canopy models would entail the rotation of the fourth axis to stand the canopy upside down with its leading edge pointed upward. The surfacing operation would then proceed. If the model contained the inner curve back feature, the fourth axis would be rotated so the piece is at a 45° angle. This would allow room for the tools to move about within the canopy. The combination of the lathe and mill processes as well as the addition of the fifth axis made the manufacturing of these models a possibility.

4.2 Manufacturing Procedure

The HAAS CNC machines in the Washburn Shops are controlled using G-Code. GibbsCAM software was used to generate the G-Code needed to machine the parachute models. For models 1 and 2, only the lathe processes were need due to their simple shape. Only two GibbsCAM G-Code programs were needed to make models 1 and 2. For models 3 through 8, the lathe and mill processes required using four different GibbsCAM G-Code programs to make each model. Each time a new G-Code program was used, machine fixturing had to be adjusted, the G-Code file had to be loaded, and work piece and tool offsets had to be set.

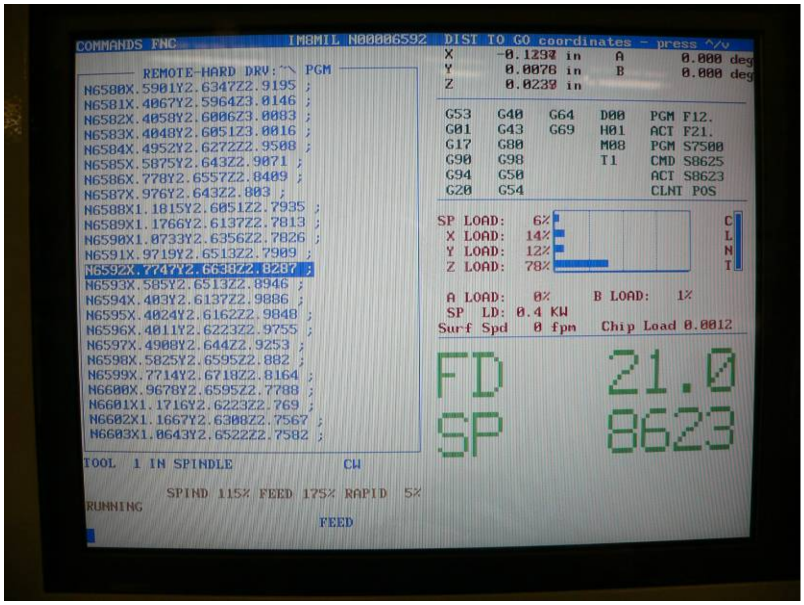

Figure 15 - Example of G-Code on VF-4

The first step in making a model was cutting the needed material from the lengths of acetal stock. This was done on the horizontal band saw. The next step was to turn the stock to the rough outside shape of the parachute model on the HAAS TL-1 tool room lathe. G-Code for this process was produced in GibbsCAM by telling the lathe to follow the outer curve to a tolerance of .001 inches. The turning of the outer curve took approximately a half hour for model 1, 1 hour for model 2 and 1.5-3 hours for models 3-8. These fast cut times were achieved because the stock was supported at both ends. This made the part stiff and eliminated noticeable vibration, which produced a clean cut. Once outside turning was complete, the turned piece was cut away from the remaining stock.

Next, the boss on the turned model was clamped into the manual lathe and a 2 inch diameter hole was drilled into the model. The depth of this hole was determined based on the distance the boring bar in the second machining operation was required to go inside the model.

The second process again used the TL-1, but this time, a boring bar was used to remove material from the inside of the parachute model. G-Code for this process was produced in GibbsCAM by telling the lathe to follow the inner curve to a tolerance of .001 inch. Because the entire model was now only being held at one end by the boss, structural rigidity was reduced and severe vibrations began to occur in all models. As a result, this operation required constant monitoring. Vibrations were minimized by careful manipulation of feed and spindle rates. These adjustments induced a higher chip load, which helped stabilize the work piece. Although these adjustments were necessary, they also increased the amount of time it took to bore out the inside of each model. Cut time for the inside of models 2-8 varied from 4-9 hours.

After these two lathe processes, models 1 & 2 were complete. Models 3-8 required milling work to create gore details on the outside, inside and skirt edge surfaces.

Figure 16 - Model 5 in TL-1 Interior Boring Operation

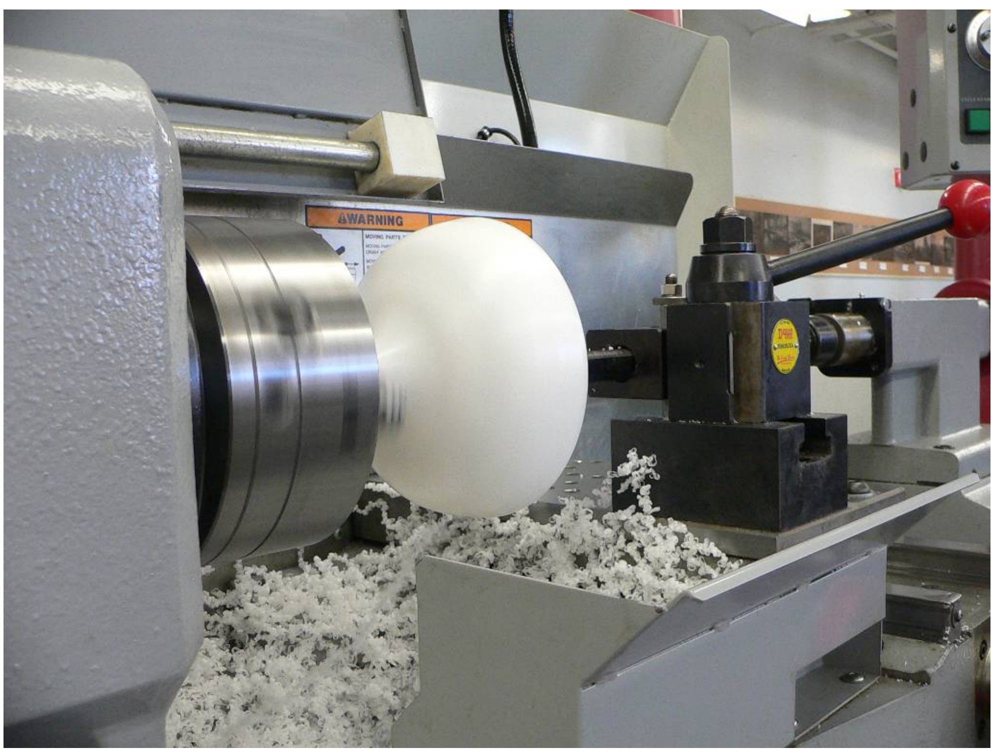

Figure 17 - Model 5 in TL-1

Figure 18 - Close-up of Interior Boring

Milling operations were done on the HAAS VF-4, 5-axis vertical milling station. For models 3-8, the third G-Code process consisted of creating the outside gores and shaping the skirt edge surfaces. Due to unique model geometry, turned models were held in the TC-5 fifth axis using a one inch diameter compressed air collet clamp system. The fourth and fifth axes were used to index and rotate the model for the outside and inside surfacing operation.

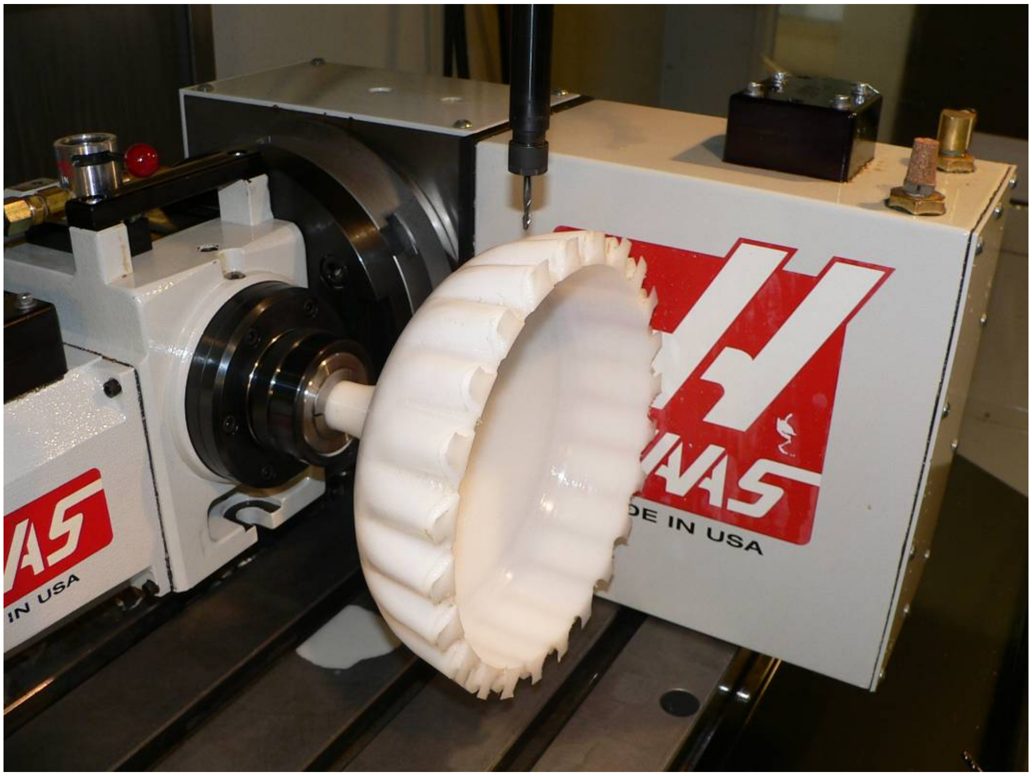

Figure 19 - Model 5 in VF-4 Work Holding Setup

To begin the outside surfacing operations, the turned piece was placed in the collet clamp and probed to set tool and work piece offsets. The G-Code for this process was written so that three gores would be surfaced at a time, after which the machine would cut the skirt shape on these three gores. Cutting more than three gores at a time made the ball endmill cut into the finished portion of the model. The 5th axis was then manually indexed 45°, and three more gores would be surfaced. This process was repeated seven more times until all twenty-four gores were completed.

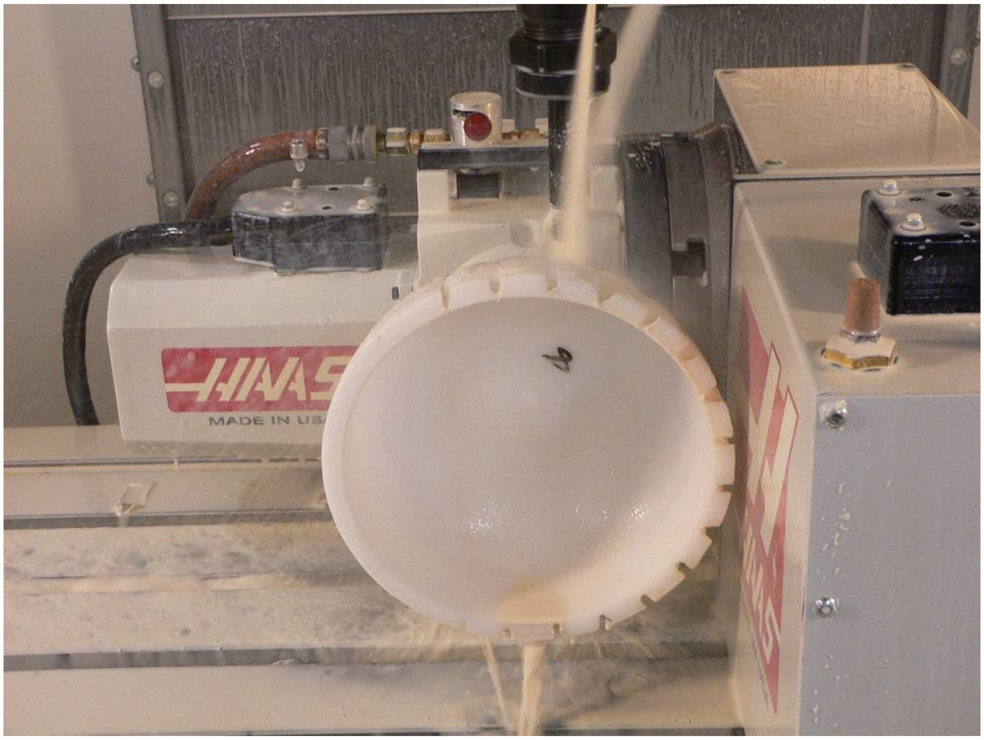

Figure 20 - Model 8 Outer Surfacing Operation and Indexing

The fourth process involved surfacing the inside of the parachute model. For models that did not have interior geometry that curved back on itself interior milling operations could be conducted with the piece rotated as shown in Figure 22.

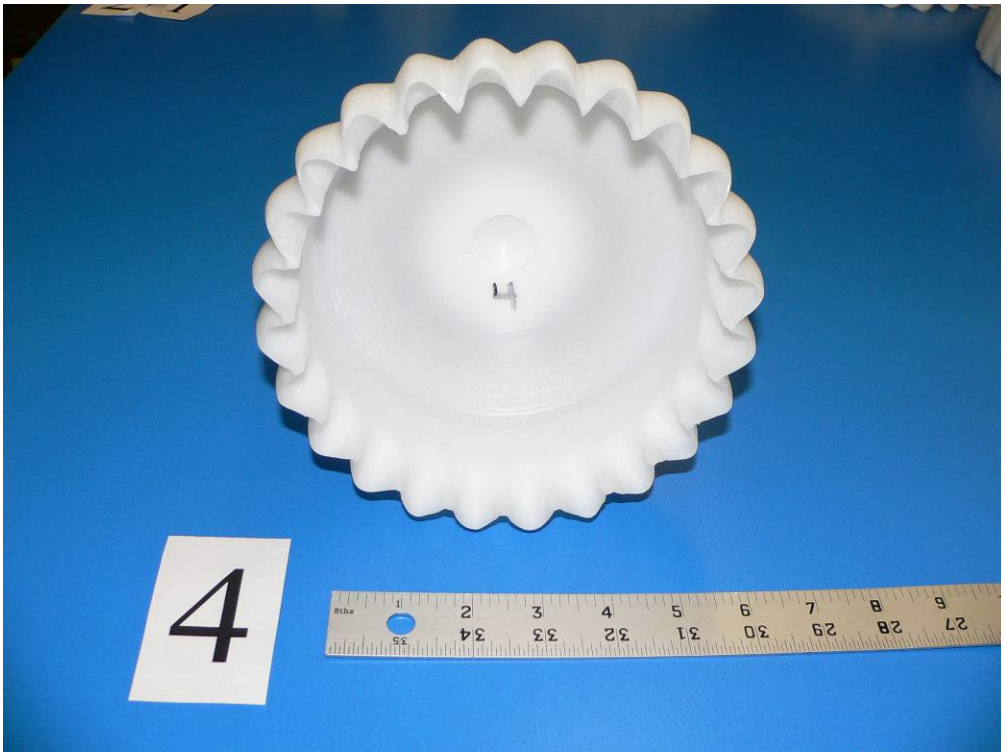

Figure 21 - Model 4 Example of Interior Curve

As seen in Figure 22, the piece was rotated up to a vertical position, with the open cup pointed straight up. Pieces which had gores that curved back into the piece needed to be set at a 45° angle to cut the interior curve from the skirt to the apex. Figure 21 shows an example of a model with gores curving back toward the centerline of the canopy. However, probing these canopy models tilted at a 45º angle to set CNC machine coordinates and offsets could not be done precisely. Therefore, the CNC machine was programmed to cut the inside of the canopy with the part oriented in the vertical position. As a result, the inside milling operation only surfaced a thin lip at the edges to keep the pieces from becoming too thin and losing their stiffness and strength and also to prevent the finished portions of the model from being cut away due to lack of tool clearance. If too thin and subjected to too strong of a cutting force, the piece would become more susceptible to breaking apart. Therefore, this operation also needed constant monitoring to ensure that the change in model structure from removing material did not induce vibrations that could break the model. Including setup time, the third and fourth operations took approximately 15 hours each.

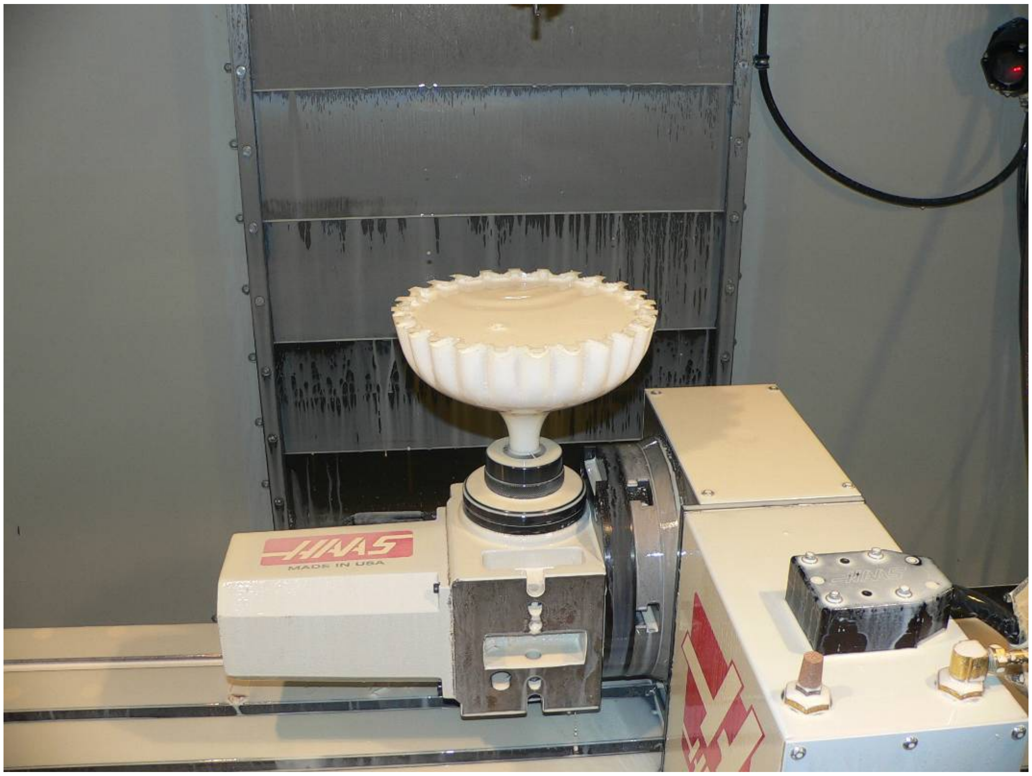

Figure 22 - Model 5 in Vertical Position

The models were then hand finished using a Dremel rotary tool and 500-grit sandpaper to remove slight imperfections in the surface finish. The boss on each model was also drilled and tapped to accept the sting allowing for attachment to the dynamometer in the wind tunnel.

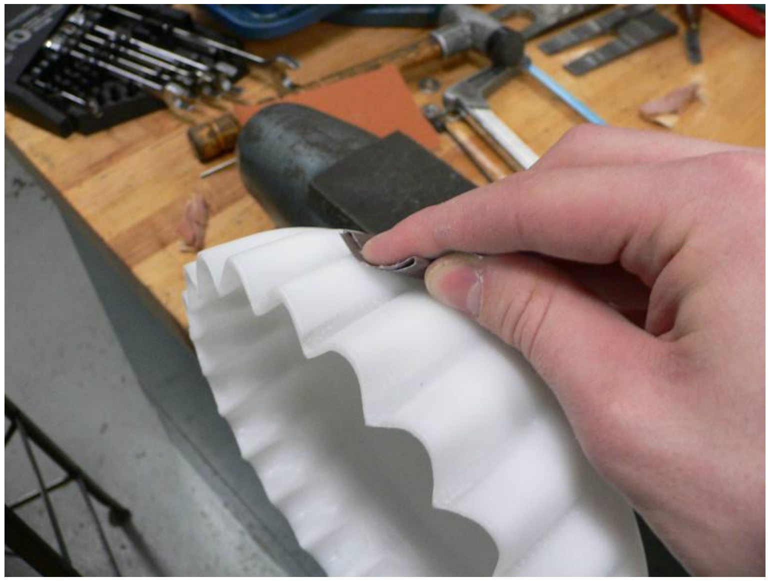

Figure 23 - Hand Sanding

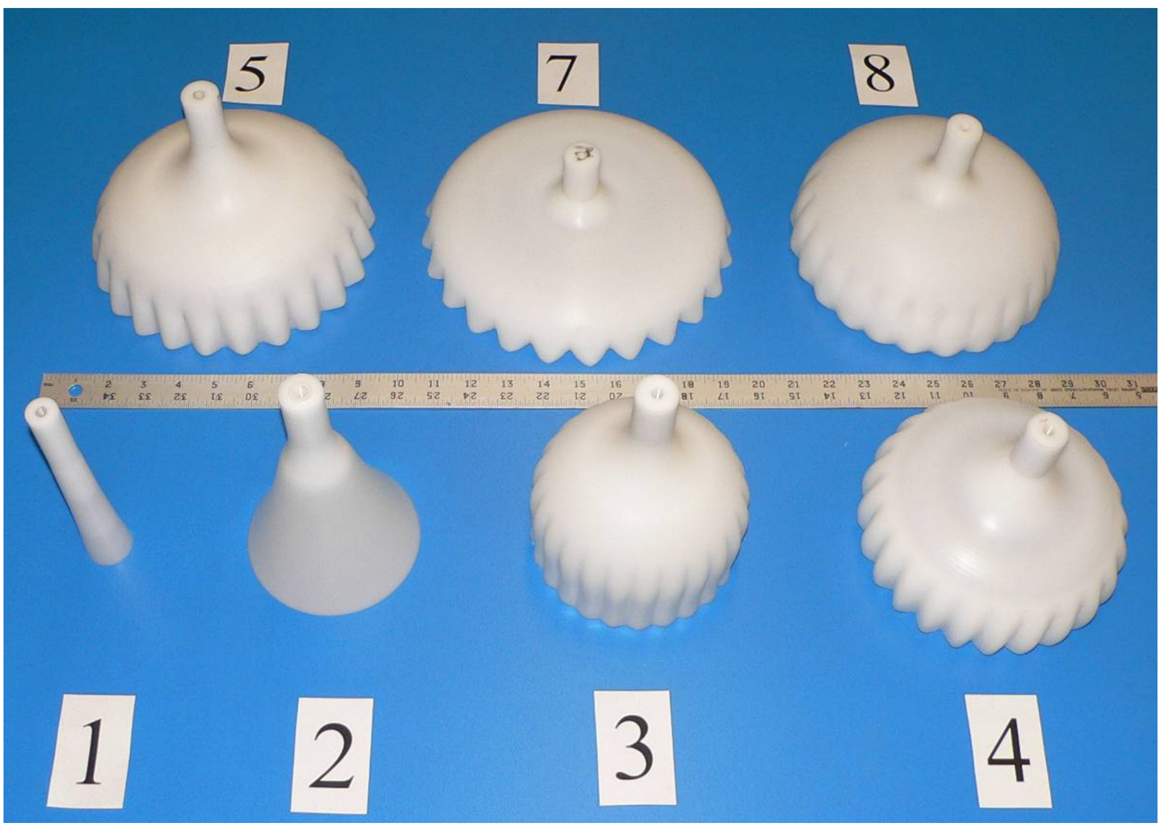

Figure 24 - Final Models

Figure 25 - All Models (Excluding 6) Side by Side

Due to time constraints and machine workspace limitations, the manufacturing of model six was not completed. As a result, the milling processes were not finished on this model.

4.3 Economic Considerations

The price of the manufacturing these eight models at the Washburn shops was considerably less than the price of using the rapid prototyping method at NSC. This is because WPI covers the cost of student project teams using the Washburn Shop CNC machines. However, if these models were machined at an outside machine shop, completion of the models would take approximately two months to complete (Munyon personal communication, 2006). The average hourly rate for CNC machining in the United States is $70.00 per hour (Derosier personal communication, 2006). It was estimated that for models 3-8, a highly qualified machinist could make one model in 40 hours. For models 1 and 2, it would take an experienced machinist about 15 hours to make a model. This includes G-code generation using a software tool such as GibbsCAM, machine setup time, cut time, and finishing processes. This would be $2,800 each for models 3-8 and $1,050 each for models 1 and 2. This is a total of $18,900 for all models. This does not include the cost of materials. Although the machining costs associated with using the WPI Washburn Shops are not directly charged to this project, the total cost of

CNC machining at an outside machine shop, including materials, is at least four times the cost of using the Natick Soldier Center stereolithography facilities.

5. Testing Procedure

5.1 Facilities and Equipment Used

The wind tunnel used for this research was a 2 x 2 x 8 ft test section, re-circulating wind tunnel manufactured by Engineering Laboratory Design Inc. Data acquisition was performed with an ELD Inc. dynamometer and Digital Readout.

Figure 26 - ELD Digital Readout

LabVIEW 7.1 software in conjunction with a National Instruments DAQ-PAD USB 6020-E were used to read dynamometer voltages from the analog output on the ELD Digital Readout Box. These voltages vary linearly with the force on the dynamometer. This linearity was verified during dynamometer calibration. A LabVIEW VI was created to capture the voltage readings from the dynamometer analog output readout box. Shown below are the front panel and the block diagram of the LabVIEW VI.

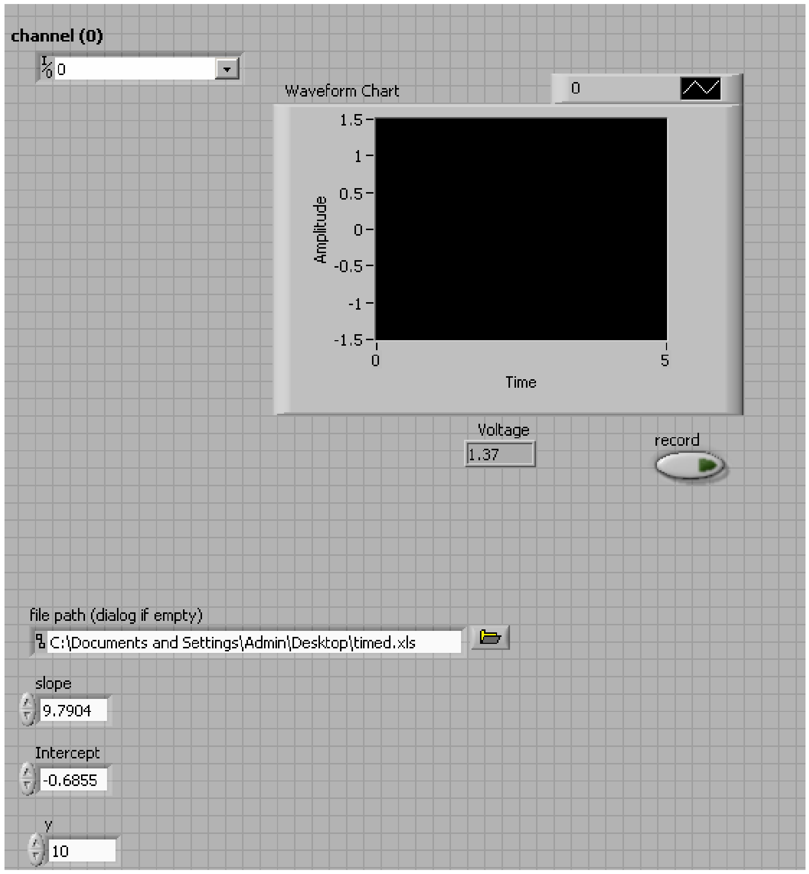

Figure 27 - LabVIEW VI Front Panel.

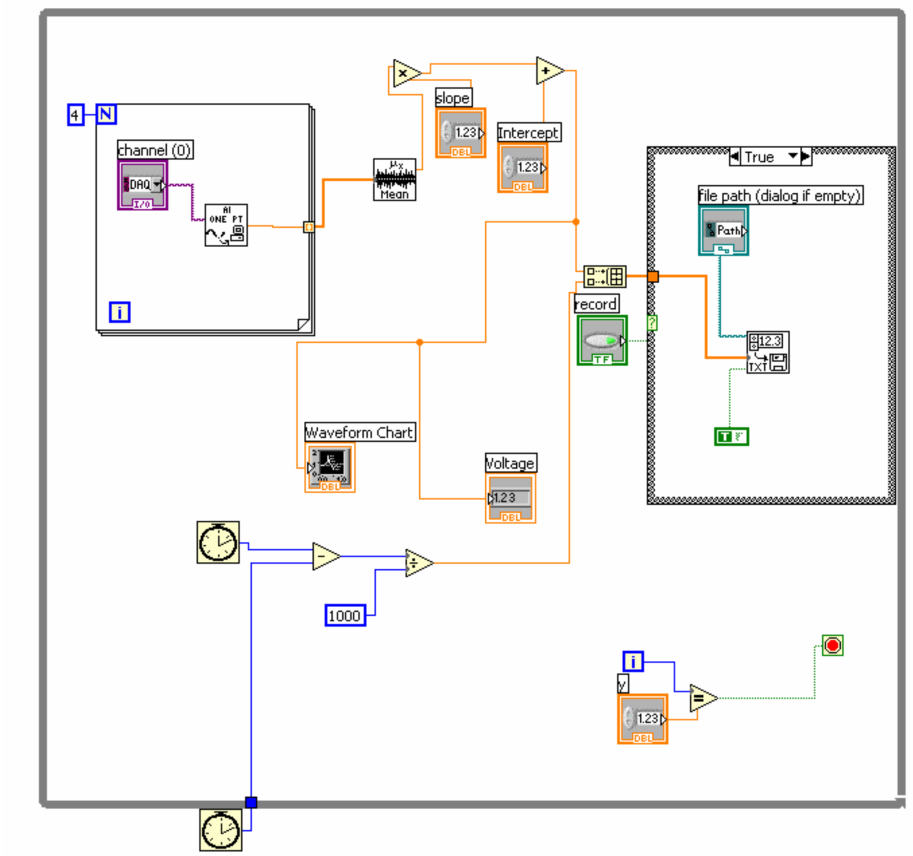

Figure 28: LabVIEW VI Block Diagram.

It can be seen from the VI block diagram that data is averaged, displayed on a waveform chart, and exported to a spreadsheet along with the real time of data acquisition. The control in the bottom right of the while loop sets the number of times the VI will iterate. This allows the user to control the number of data points acquired. Due to the linearity of the voltages to corresponding weight values, the averaged data was multiplied by a slope and summed with an intercept. This was done to scale the voltage values to a weight value. The slope and intercept values input into LabVIEW were obtained using a dynamometer calibration procedure described in the following section. The calibration procedure was used to find the relationship between known weights and the dynamometer output voltages. The slope and intercept could be input into the VI front panel. This was all designed to save time later when analyzing and reducing the data points. It also allowed the user to directly compare force measurements between the VI and the ELD digital readout box in real time.

Voltage data coming into the VI was averaged using a For loop and the mean function. This combination was used to remove signal noise from the system. The For loop was programmed to execute four times, meaning that four data points were collected. Those four data points were then sent to the mean function, where they were averaged. This process continued until the condition of the while loop became false i.e. after the programmed number of iterations. Due to the fact that all of the drag force measurements were averaged later on using Excel, this method of averaging does not corrupt the data. The data points would have been averaged eventually; however, this allowed the project team to read more stable drag values for direct comparison with the ELD digital readout box. The block diagram for the mean function can be seen below.

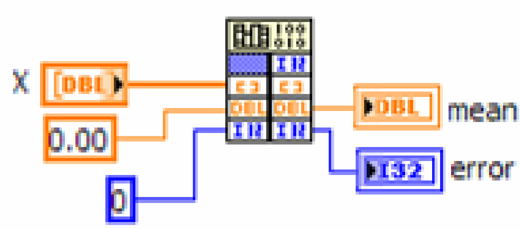

Figure 29: Block Diagram of the Mean Function

Inputs were placed within the VI to collect a variety of information. An “append to file” function was used to export the dynamometer forces calculated by the VI from the voltages to an Excel file. The temperature of the wind tunnel test section, pitot static pressure, and the time of each sample were also exported to this excel sheet. One data spreadsheet was generated for each model at each test velocity. With each spreadsheet generated, various calculations were made to process the data. The drag force measurements were averaged and converted to pounds of force. It is important to note that this calculation was also completed for the dynamometer and sting structure with no model attached. The average drag force for the dynamometer and sting attachment was subtracted from all of the other averages to determine the drag on the models alone. The standard deviation of each set of drag force measurements was calculated, and used to calculate error. A sample of these processed data spreadsheets can be found in Appendix D. The error calculations are summarized in the results section of this document.

5.2 Dynamometer Calibration

Before wind tunnel testing could begin, it was necessary to calibrate the wind tunnel dynamometer and ELD data readout system and LabVIEW VI. To do this, the dynamometer was first taken out of the wind tunnel test section, and clamped to a workbench. Preliminary investigation showed that the dynamometer was set to read drag forces in kilograms. The potentiometers on the digital readout were zeroed and a known weight of 0.5 kg was hung from the end of the dynamometer. The span of the potentiometers was then adjusted to display 0.5 kg on the dynamometer box digital readout. This process was repeated using weight values of 0.1 kg, 1 kg, and 1.5 kg. This procedure ensured that the ELD readout box and corresponding output voltages were calibrated properly.

Next, the slope and intercept values needed to calibrate the LabVIEW VI were determined. For each mass (.1 kg, .5 kg, 1 kg, 1.5 kg), the VI was run and set to record 100 voltage data points. The voltage data points and the known masses were exported to a spreadsheet. Once these tests were complete, the masses were plotted as a function of voltage. A linear trend-line was added to determine the slope and intercept of the data. A least squares value was also calculated to determine the accuracy of the trend-line. The calibration curve used during wind tunnel testing on 2/23/06 is shown in Figure 30.

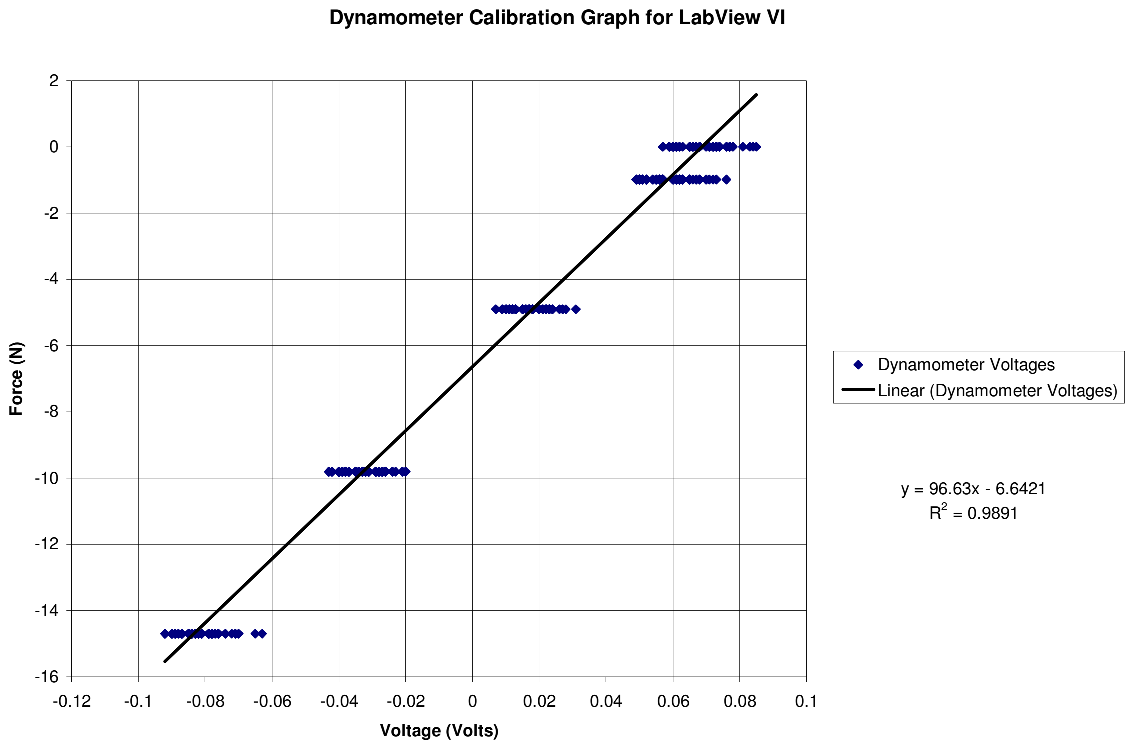

Figure 30 - Calibration curve used to convert voltages from the dynamometer readout to force for rigid model testing on 2/23/06. The linear curve fit trend line for the calibration data has an R^2 value of .99.

Using a least squares test, it was shown that the linear trend was a very good fit for the data. It is also seen that for a constant force on the dynamometer, the variation in voltages recorded by the virtual instrument was on the order of only a few millivolts. With a slope and intercept value input into the VI front panel, the readouts from the VI and ELD readout box were again checked using all four weights to verify that they were both reading the same force values.

Once the calibration was determined to be satisfactory, the dynamometer was mounted in the wind tunnel test section.

5.3 Pressure Calibration

The freestream stagnation pressure within the test section was required to verify the freestream velocity in the wind tunnel. To determine the pressure, a pitot tube was placed in the test section. The pitot tube measured the difference between the stagnation pressure in the freestream and the static pressure inside the test section. This pressure measurement was recorded using the pressure transducer in the ELD readout box.

The pressure value on the readout box was set by ELD to read pressure in inches of water. It was calibrated by first placing the pitot probe a quarter of the way down into the test section from the top of the tunnel. The pressure readout was then zeroed. With only the dynamometer in the test section, the tunnel fan was set to run at 12.8 Hz. This fan speed corresponds to a freestream velocity of 10 m/s according to the wind tunnel manual (ELD, 1998). Using Equation (8), the pressure difference was calculated to be 0.241 in-H_20. The potentiometer span on the digital readout was then adjusted to read this value.

$$\Delta h = \frac{.5\rho_{air} U_{\infty}^{2}}{\rho_{H_2O}\, g} \tag{8}$$

This calculation was repeated at tunnel speeds of 18 m/s and 25 m/s, resulting in values of 0.782 and 1.505 in-H_20. The wind tunnel fan was then set to the frequency corresponding to each of these velocities to be sure that the pressure readouts matched their respective calculated values. The values did in fact match, resulting in a calibrated pressure measurement system.

As mentioned earlier, the pitot tube was essential for verifying the freestream velocity in the wind tunnel test section. This is due to the fact that the addition of a parachute model inside the wind tunnel test section constricts the flow within the wind tunnel. This creates a pressure difference, which in turn results in varying freestream velocities around the canopy depending on the size of the model for a set wind tunnel fan frequency. Rather than using the wind tunnel fan frequency to set the freestream velocity, the pressure reading was used. In doing so, freestream velocities could be matched to the three standard test velocities regardless of the size of the model.

The three velocities were based on earlier calculations of the expected drag forces that each model would experience at different drag coefficients and tunnel velocities within the range of forces the dynamometer could accurately measure. They were also chosen to make the Reynolds number range as broad as possible. The speeds selected were 10 m/s, 18 m/s, and 25 m/s. The velocity of 10 m/s was chosen because it was the slowest speed where measurable drag forces could be recorded. The velocity of 18 m/s was selected because it was the fastest velocity for which it was expected that all models could be accurately measured by the dynamometer for a range of possible drag coefficients with magnitudes from 0.5 to 3. Lastly, the velocity of 25 m/s was selected because it was anticipated that drag coefficients of two or more were unrealistic, allowing for greater freestream velocities than 18 m/s. The tables used for determining these velocity ranges can be seen in Appendix C.

5.4 Drag Measurements

The wind tunnel and data acquisition system was set up as shown in the schematic shown below.

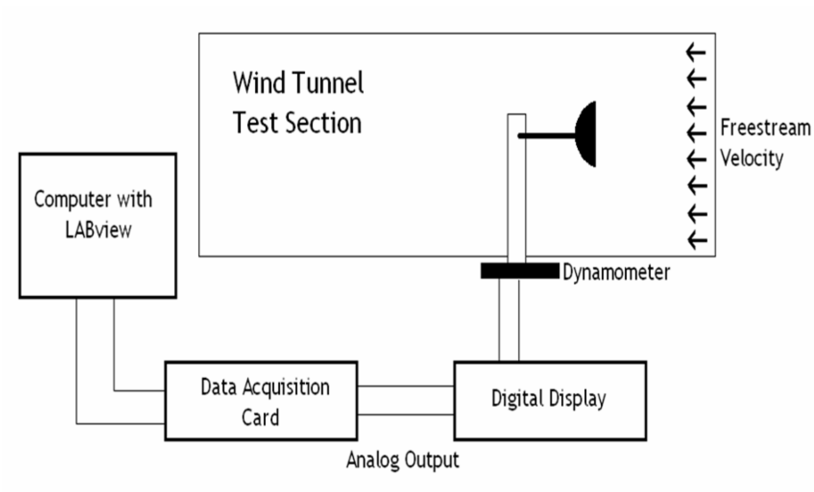

Figure 31 - Wind Tunnel Schematic

The data acquisition system was set up as shown in the picture below.

Figure 32 - Data Acquisition System

A model was attached to the sting through its boss and then placed on the dynamometer. This configuration is seen in the photo below.

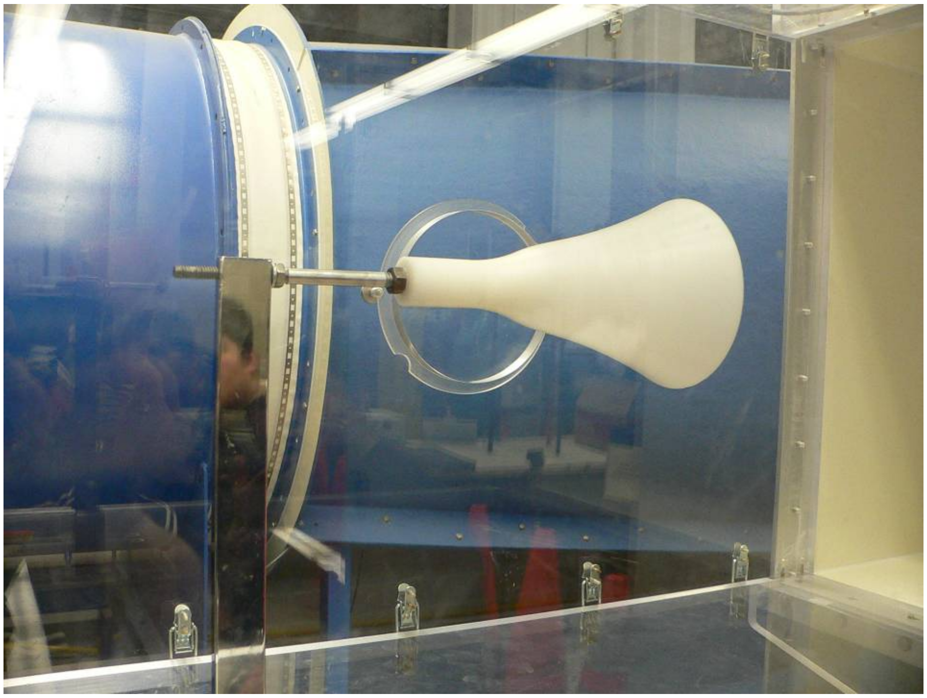

Figure 33 - Testing Configuration (model 2 shown)

The wind tunnel fan was then adjusted until the pressure required for the desired freestream velocity was achieved. Upon reaching this freestream velocity, one minute was allowed to pass before recording data to make sure that any effects from ramping the tunnel speed had dissipated. Two hundred data points were then recorded at a sample rate of approximately 2 Hz. The pressure was then adjusted to reach the next freestream velocity. Again, approximately one minute after stabilization, the data acquisition procedure was repeated. Finally, this same procedure was used for the last freestream velocity. This completed the testing procedure for one model. Each of the remaining models followed the same procedure.

6. Results

The seven rigid canopy models were tested in one day following the testing procedure outlined above. Testing all models in one day had the benefits of using a single calibration, relatively constant atmospheric conditions, and minimized the error introduced by varying set-ups from day to day. These experiments were completed on February 23, 2006. This particular day was cloudy with intermittent showers. The atmospheric pressure was obtained from the Worcester Regional Airport at hourly intervals. Throughout this experiment this measurement remained constant at 404.454 in-H_2O.

It was noted that each model behaved differently under the same testing conditions. Due to the blunt shape of these models, vibrations were a serious concern. To determine the upper bound of freestream velocity, each model was placed in the wind tunnel to observe stability. The most unstable models were found to be models 5, 7 and 8. After preliminary testing of these models at varying tunnel speeds, it was determined that a freestream velocity of 25 m/s was indeed a satisfactory upper bound velocity that the models could be safely tested without inducing serious vibrations.

At 10 m/s, vibrations were not visually noticeable for any model. Force variations, however, could be seen on the dynamometer output, and within the virtual instrument. This may be due to the fact that, at such a slow speed, vortex shedding is not present. It may also mean that the vortex shedding that is present is not strong enough to induce visually noticeable vibrations.

At a freestream velocity of 18 m/s, vibrations were more noticeable for models 3-8. The model movement tended to be horizontal rather than vertical or in a circular motion. Estimated deflections were approximately ¼ inch maximum at this speed. This motion is most likely due to the interaction of vortex shedding cycles with the canopy model. Models 1 and 2 remained relatively stable, most likely due to the fact that they were the least blunt of all the models. It was noticed that the onset of vibration was a gradual process. If the vibrations were stopped by hand, they could be seen slowly building up to a maximum once again. Depending on model shape, the time to reach maximum vibration was approximately 2-10 seconds.

Similarly, for a freestream velocity of 25 m/s, oscillatory vibrations were seen in model 2 and became increasingly noticeable for models 3-8. At this velocity, the model movement tended to be in both the horizontal and vertical directions. Estimated maximum deflections from the model centerlines were approximately 1/2 inch for models 4, 5, 7 and 8 and ¼ inch for models 2 and 3. Model one remained relatively steady. Again, the onset of these oscillatory vibrations was gradual; however, the time it took for these models to reach maximum vibrations was reduced to about 1-5 seconds depending on model.

The oscillations and vortex shedding caused by flow separation created variation in the drag measurements. This could be seen both on the dynamometer output and the virtual instrument as recorded values did not stay constant. Analysis of the data collected quantified this variation in the form of percent error.

Table 1 summarizes the testing conditions, and results from processed test data.

Table 1 - Test Conditions and Data Summary

Model	Freestream Velocity (m/s)	Tunnel Frequency (Hz)	Temperature (ºF)	Atmospheric Pressure (in H_20)	Pressure (P_o-P_{static}) (in H_20)	Average Drag (lbs)	Standard Deviation (lbs)	Total Percent Error of Drag Calculations
1	10	14.6	79	404.454	0.241	0.0295	0.1327	137.38
	18	25.1	80	404.454	0.782	0.1222	0.1376	85.35
	25	34.2	83	404.454	1.505	0.2691	0.1317	24.45
2	10	14	73	404.454	0.241	0.2307	0.1420	10.22
	18	24.5	75	404.454	0.782	0.8106	0.1487	3.22
	25	33.5	77	404.454	1.505	1.6007	0.1601	1.74
3	10	14.3	79	404.454	0.241	0.3832	0.1233	6.29
	18	24.6	79	404.454	0.782	1.2292	0.1579	2.35
	25	33.5	82	404.454	1.505	2.4182	0.2925	1.97
4	10	13.9	76	404.454	0.241	0.5379	0.1229	5.31
	18	23.9	77	404.454	0.782	1.7311	0.2222	2.31
	25	32.8	81	404.454	1.505	3.5613	1.9355	8.15
5	10	13.5	76	404.454	0.241	0.8360	0.1209	4.63
	18	23.2	76	404.454	0.782	2.7390	0.1876	1.63
	25	31.8	78	404.454	1.505	5.2392	0.6097	1.83
7	10	12.9	79	404.454	0.241	0.9735	0.1162	4.47
	18	22.9	80	404.454	0.782	3.4272	0.2244	1.60
	25	30.1	81	404.454	1.505	5.9788	0.1527	0.76
8	10	13.7	80	404.454	0.241	0.8372	0.1308	4.71
	18	23.3	80	404.454	0.782	2.5853	0.1697	1.60
	25	32	82	404.454	1.505	5.0371	0.2068	0.90

The results in Table 1 show that the percent error is larger for the smaller models. It is believed that this is due to the relatively low drag force measurements for these models. There was a small amount of "noise" within the system when no measurements were being taken. This could be seen on the digital readout when the tunnel was not running. This noise was estimated to be approximately +/- 0.02 kg. Average drag measurements for model one ranged from 0.013 to 0.122 kg. Although this noise was averaged out within the virtual instrument, it still accounted for a great percent of the drag readout for the smaller models. This explains the large percent error for the small models.

The same reasoning explains why the percent error decreased as the freestream velocity increased. Slower freestream velocities again resulted in lower drag forces, which were more influenced by system noise. Faster freestream velocities resulted in higher drag forces, which were more able to overwhelm the system noise, resulting in less error.

Plots of the measured drag force on each model at 10 m/s, 18 m/s and 25 m/s are shown in Figure 34, Figure 35, and Figure 36. Table 2 summarizes drag forces obtained at each freestream test velocity. These results show that drag force is directly proportional to the model area normal to the freestream flow in the wind tunnel test section.

Table 2 - Measured Drag Forces

Model Number	Frontal Area (m^2)	Model Drag (lb) 10 m/s	Model Drag (lb) 18 m/s	Model Drag (lb) 25 m/s
1	0.00083	0.0137	0.0228	0.0762
2	0.01021	0.2148	0.7112	1.4078
3	0.01523	0.3674	1.1297	2.2254
4	0.02577	0.5221	1.6317	3.3685
5	0.03658	0.8202	2.6396	5.0464
7	0.04264	0.9576	3.3277	5.7860
9	0.03390	0.8213	2.4858	4.8443

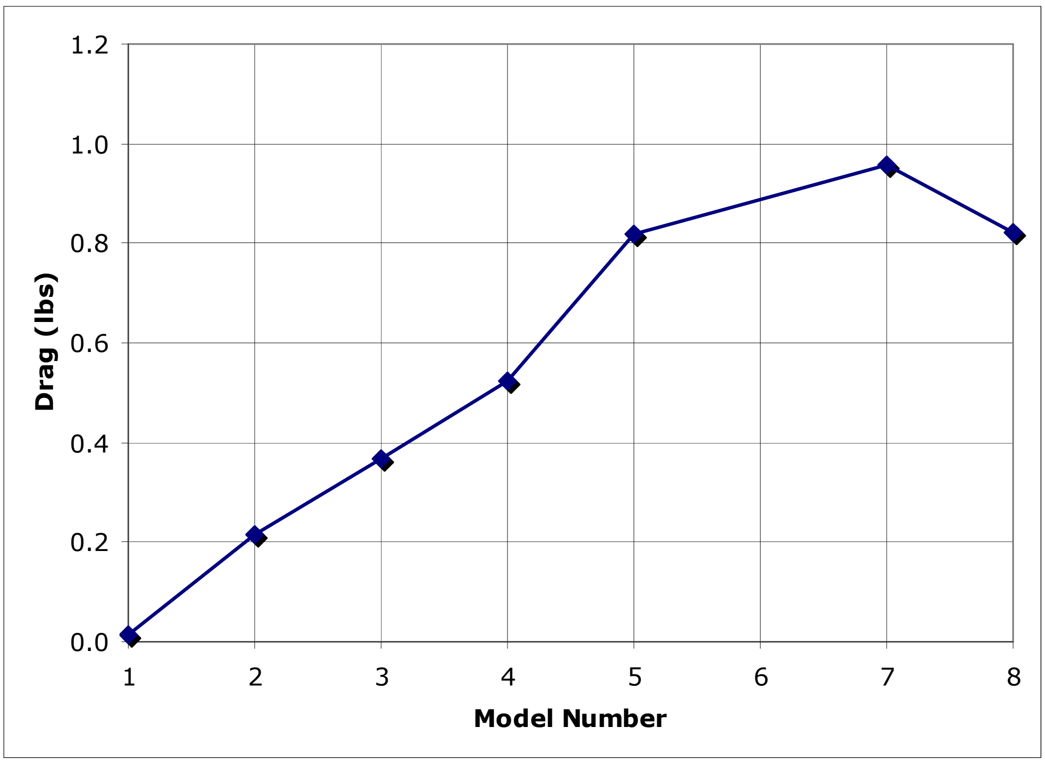

Figure 34 - Drag Force of Various Models at 10 m/s

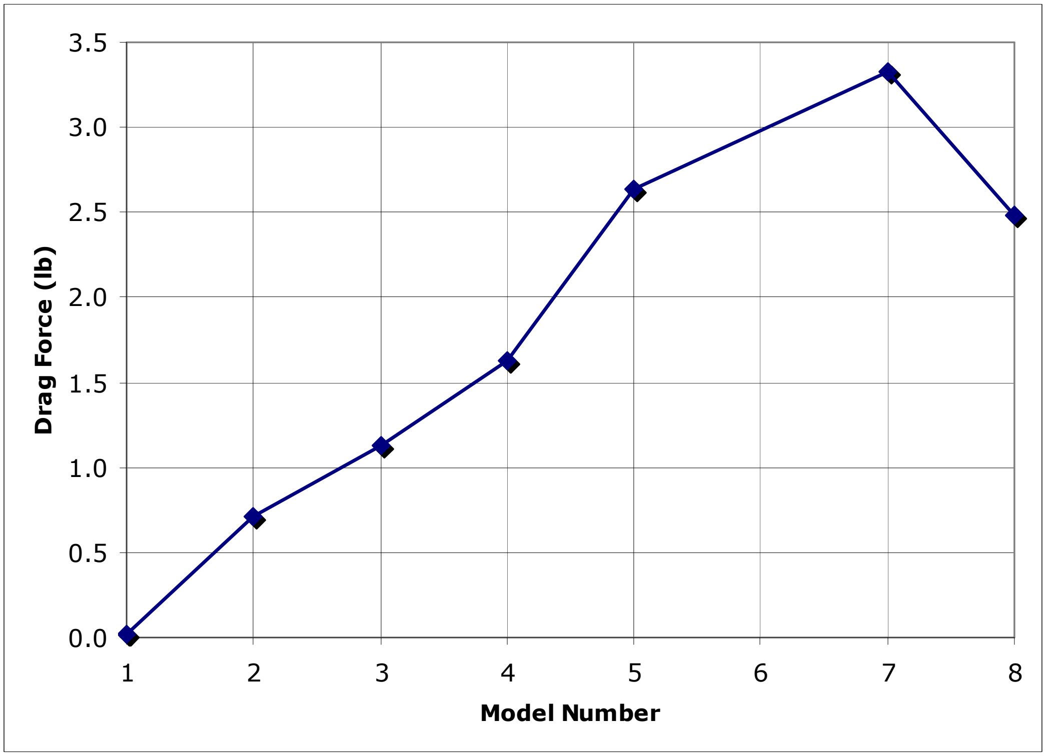

Figure 35 - Drag Force of Various Models at 18 m/s

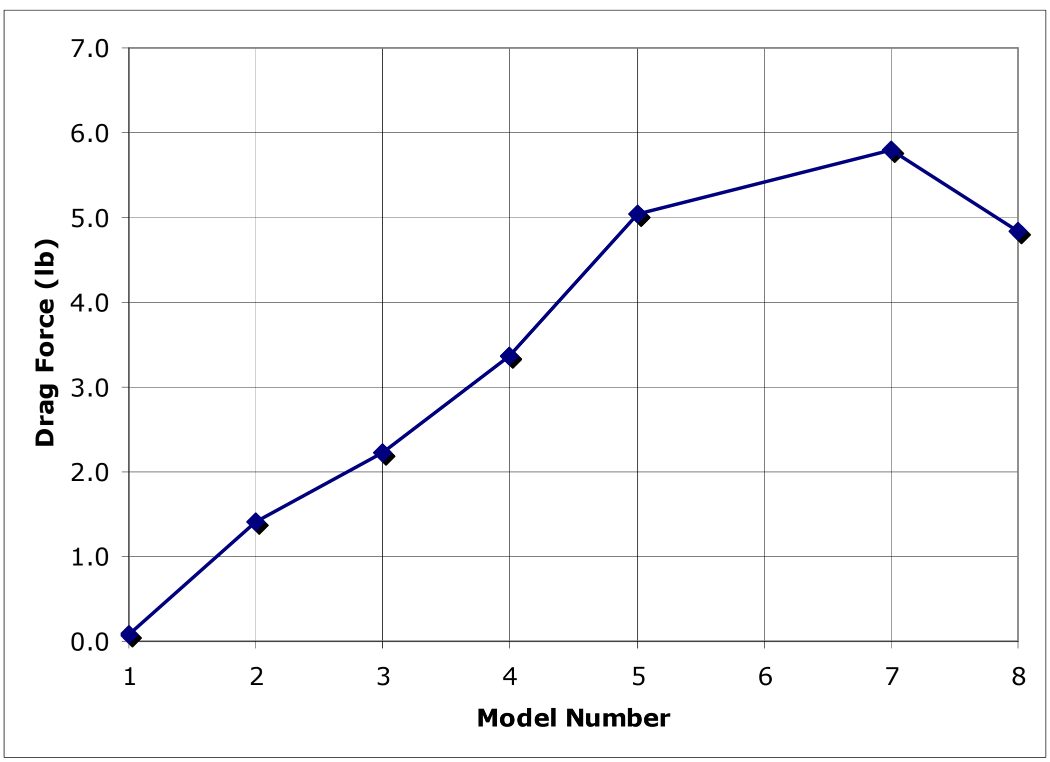

Figure 36 - Drag Force of Various Models at 25 m/s

The average drag values for each model at each freestream velocity were found by averaging the 200 drag values recorded by the virtual instrument. The standard deviation was then calculated for each of these averages.

$$StdDev = \sqrt{\frac{\sum (x - \bar{x})^2}{(n-1)}} \tag{9}$$

where $\bar{x}$ is the arithmetic mean, x is a sample point and n is the number of sample points. Uncertainty was found using the least squares uncertainty method.

$$\omega = \left[\sum \left(\frac{\partial R}{\partial x} \omega_i \right)^2 \right]^{\frac{1}{2}} \tag{10}$$

where ω is the total uncertainty, $\frac{\partial R}{\partial x}$ is the change in the results with respect to the measured variables and ω_i is the uncertainty for each result. The total error was based upon the uncertainties in pressure and drag measurements. The uncertainty for pressure was estimated to be +/- .01 inches of H_2O due to oscillations on the dynamometer digital readout. The uncertainty for drag was calculated using the standard deviation for the drag measurements, using the following formula.

$$\omega = \frac{2StdDev}{\sqrt{n}} \tag{11}$$

To calculate percent error, the uncertainty is divided by the results.

$$PercentError = \frac{\omega}{R} \times 100 \tag{12}$$

Uncorrected drag coefficients were then calculated based upon the average drag, freestream dynamic pressure and maximum projected frontal area using Equation (5) and Equation (6). Drag coefficients using this average drag data were calculated for each model at each tunnel test speed. These results are summarized in the table below.

Table 3 - Uncorrected Drag Coefficients and Reynolds Number for Rigid Models

Model	Freestream Velocity (m/s)	Uncorrected C_D	Reynolds Number
1	10	1.219	21637
	18	0.628	38946
	25	1.088	54092
2	10	1.553	76006
	18	1.586	136811
	25	1.628	190015
3	10	1.779	92835
	18	1.689	167102
	25	1.725	232086
4	10	1.495	120759
	18	1.442	217366
	25	1.543	301897
5	10	1.654	143875
	18	1.643	258975
	25	1.628	359688
7	10	1.657	149053
	18	1.777	268296
	25	1.602	372633
8	10	1.787	155341
	18	1.669	279613
	25	1.686	388352

These uncorrected drag coefficients do not account for wall interference effects within the wind tunnel. As a result, the values of the drag coefficients were larger than they should be. Recall that the pressure increases around the model due to the flow constriction. This effect must be accounted for within the drag coefficient by correcting the dynamic pressure.

The method used for correcting tunnel data for wall interference effects was the Maskell Correction method for bluff bodies adapted by Macha and Buffington for circular parachutes under test in a closed-loop wind tunnel. Using test-section cross sectional area C, the model drag area $C_D S_u$ and the freestream dynamic pressure q_u, the adapted Maskell equation for the dynamic pressure correction at the model is

$$\frac{q}{q_u} = 1 + K_M + \frac{C_D S_u}{C} \tag{7}$$

The results of Macha and Buffington's experiments provide blockage correction factors based on Maskell correction methods for three-dimensional, non-lifting bluff bodies. According to these experiments, Macha and Buffington determined that for a single round parachute canopy, a Maskell bluff-body blockage factor of 1.85 accurately accounts for the effective increase in dynamic pressure due to the presence of a round parachute canopy in the tunnel. It was also found that this correction factor is independent of canopy porosity and can be applied to circular canopies in general (Macha & Buffington, 1989). See Appendix B for correction calculations.

This correction method was applied to the calculated drag coefficients. Since the correction method accounts for the increase in velocity around the model, the corrected dynamic pressure will increase. As a result, the values of the drag coefficients will decrease. The corrected drag coefficients and corresponding Reynolds numbers are shown in the following table.

Table 4 - Corrected Drag Coefficients and Reynolds Numbers for Rigid Models

Model	Freestream Velocity (m/s)	Corrected C_D	Reynolds Number
1	10	1.213	21691
	18	0.626	38996
	25	1.083	54213
2	10	1.439	78947
	18	1.468	142218
	25	1.504	197718
3	10	1.568	98899
	18	1.497	18567
	25	1.525	246794
4	10	1.254	131829
	18	1.217	36228
	25	1.288	330427
5	10	1.271	164119
	18	1.265	295185
	25	1.256	409558
7	10	1.226	173292
	18	1.290	314855
	25	1.195	431350
8	10	1.373	177226
	18	1.302	316564
	25	1.313	440167

Table 5 - Corrected Drag Coefficients and Reynolds Numbers for the Flexible Canopy

Flexible Canopy - Water Tunnel (C_D based on frontal area and corrected for wall interference)					
Corresponding Solid Model	D (cm)	F (N)	C_D	F (lbs)	RE #
1	3.62	0.0193	0.9762	0.0043	6886
2	12.51	0.0966	0.4091	0.0217	24191
3	15.44	1.2243	3.4039	0.2752	29547
4	20.05	2.8345	4.6732	0.6372	38435
5	23.46	5.2926	6.3738	1.1898	45792
6	24.36	2.8909	3.2289	0.6499	47440
7	25.36	1.1512	1.1864	0.2588	49441
8	22.61	1.5585	2.0206	0.3504	44085

With drag coefficients corrected for wall interference effects, it was necessary to determine how these drag coefficients varied over the range of tunnel test velocities. For each model, the three experimentally determined drag coefficients were plotted against corresponding Reynolds number. Error bars were included for each point based on the percent error from drag and pressure measurements. The average of the three experimentally determined drag coefficients for each model was then calculated. Plots of this data are shown below.

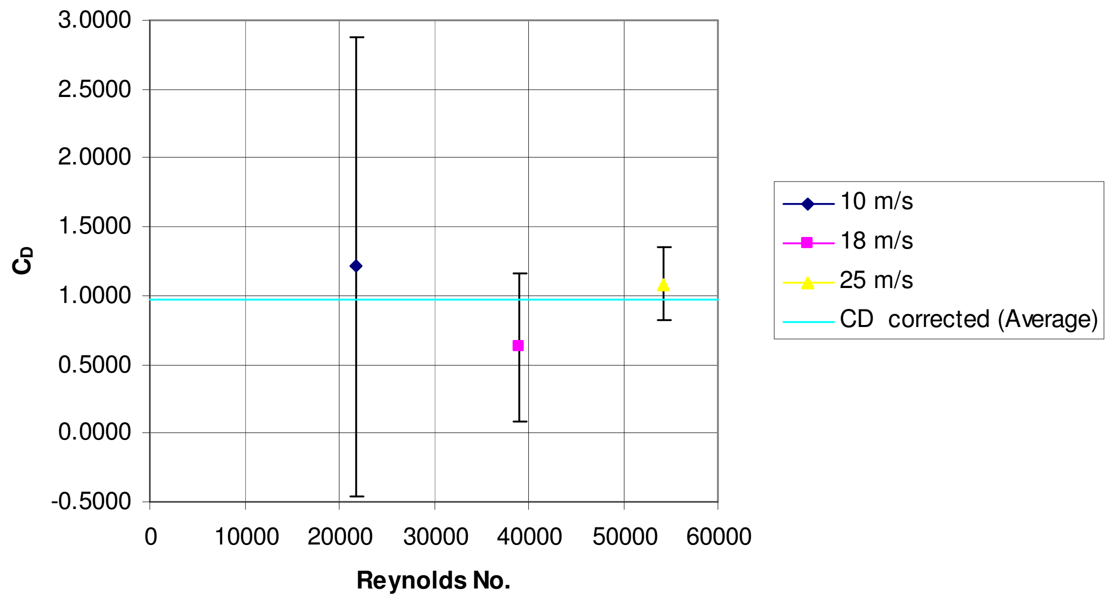

Figure 37 - C_D vs. Re: Model 1

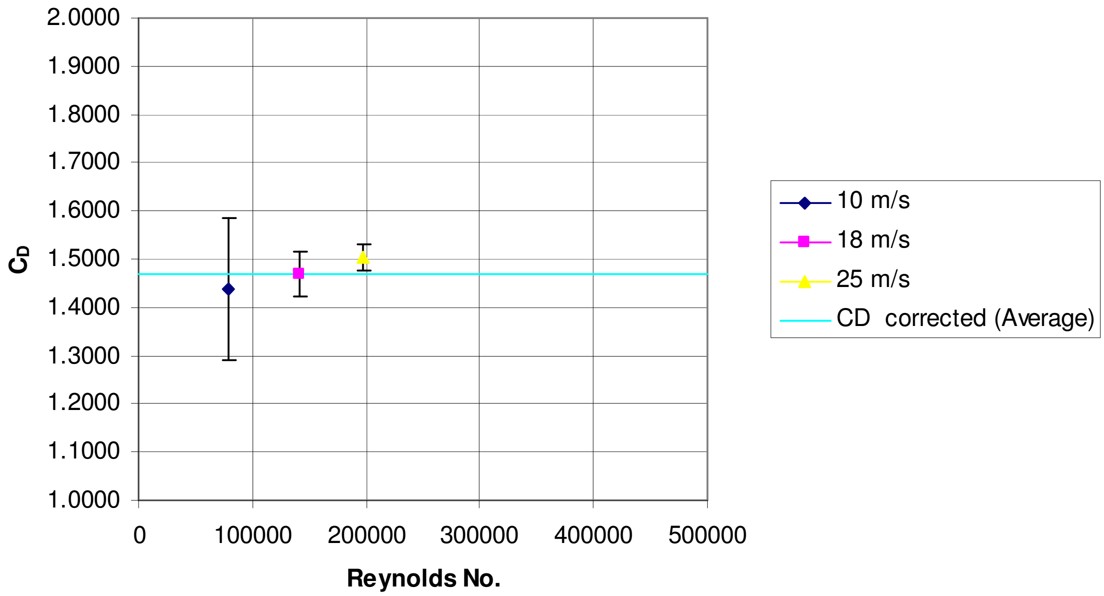

Figure 38 - C_D vs. Re: Model 2

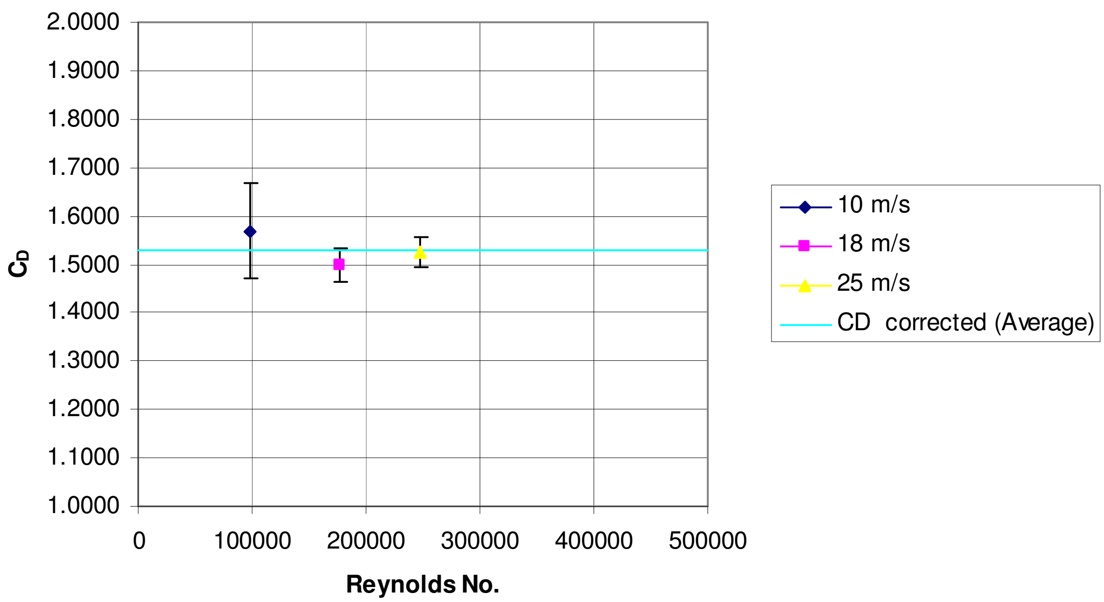

Figure 39 - C_D vs. Re: Model 3

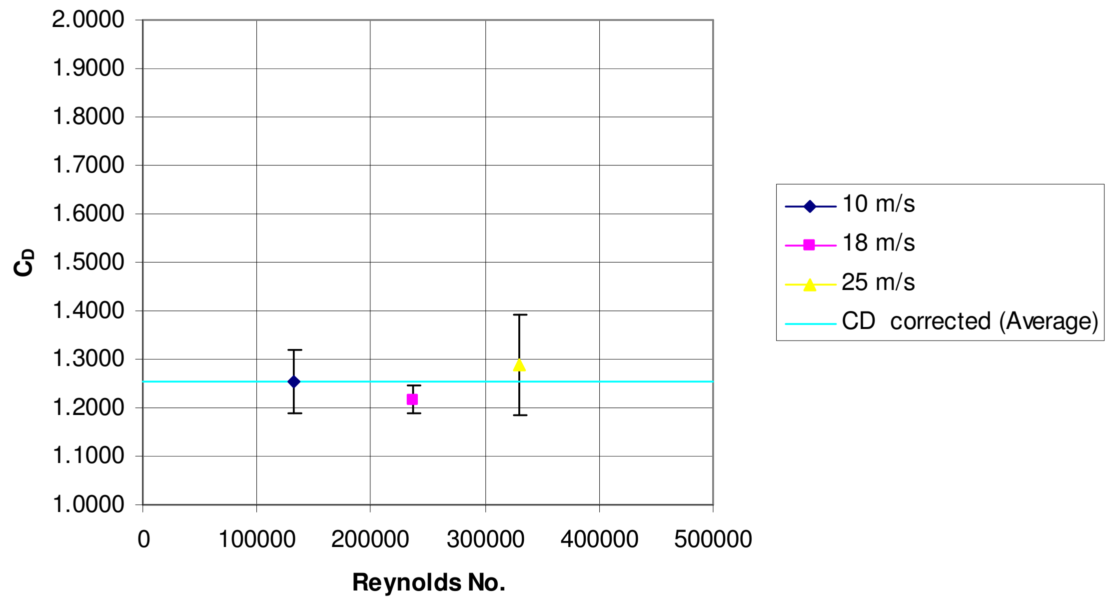

Figure 40 - C_D vs. Re: Model 4

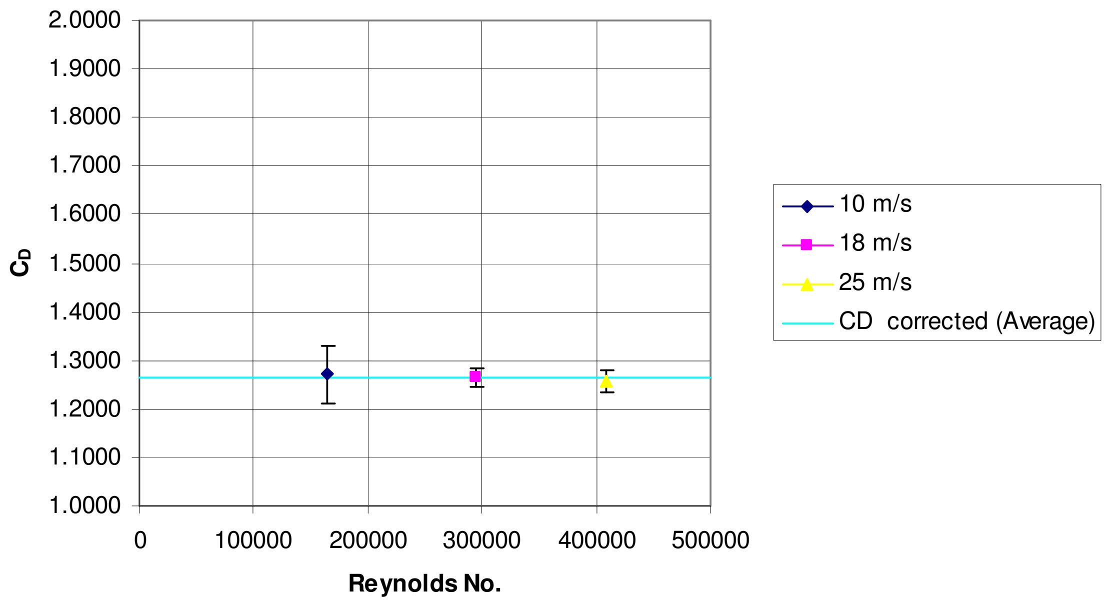

Figure 41 - C_D vs. Re: Model 5

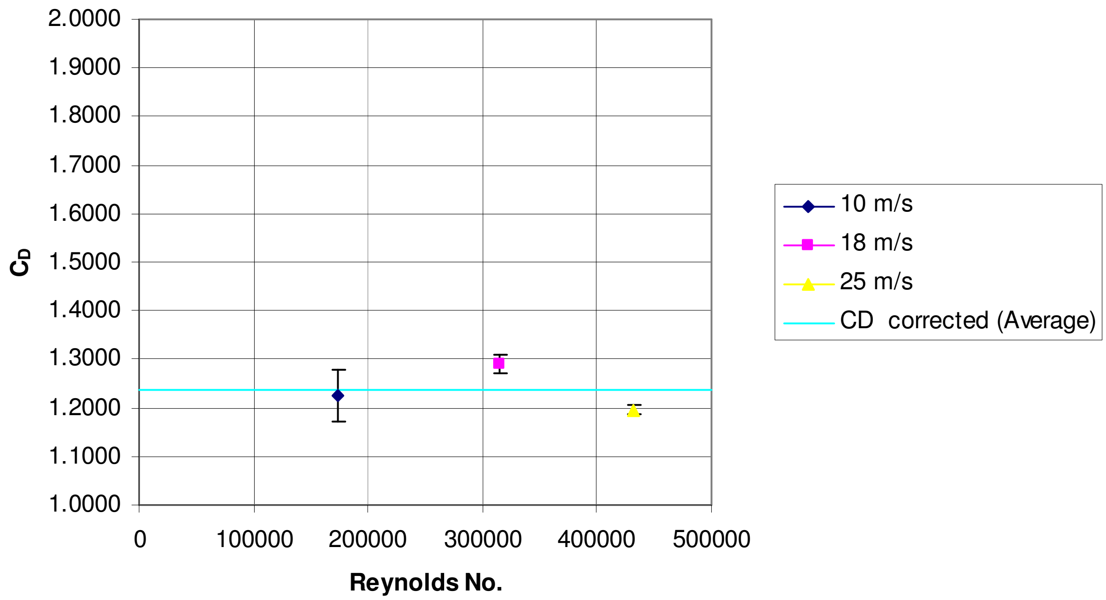

Figure 42 - C_D vs. Re: Model 7

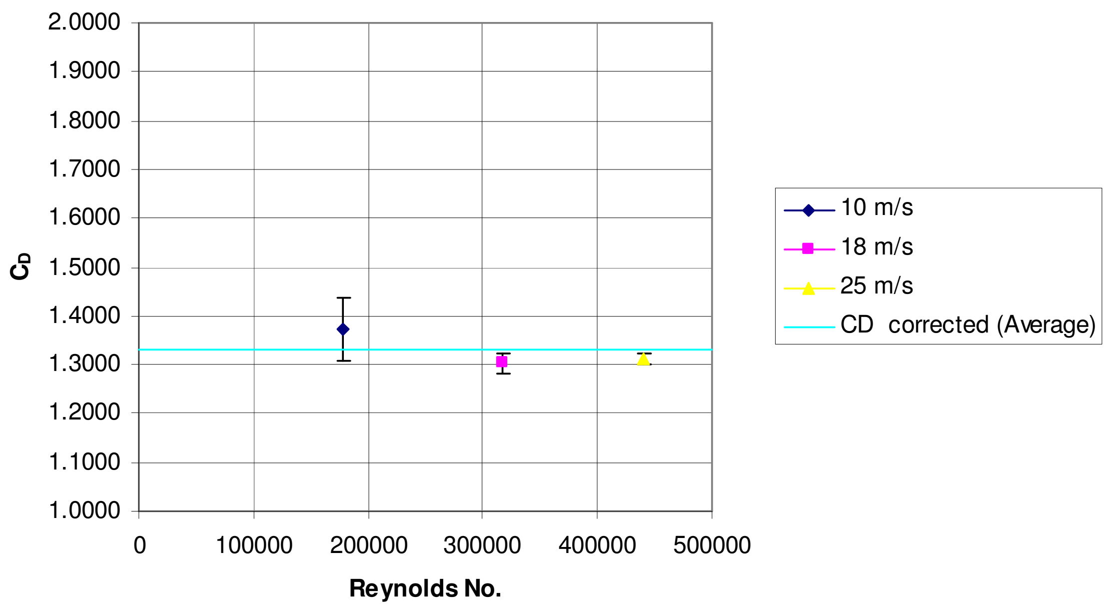

Figure 43 - C_D vs. Re: Model 8

It is clear that the calculated drag coefficient for each model remains relatively constant over the range of Reynolds numbers achieved during testing. The averaged drag coefficient falls within the range of error or very near to the range of error for all models. Transitions in flow characteristics causing the drag coefficient to drastically change are not noticed in this Reynolds number range.

After determining that the averaged C_D values for each model appropriately represented the C_D values for the range of Reynolds numbers seen during this testing, these values were plotted against C_D values from the flexible canopy model tested in a water tunnel. The Reynolds number range under which the 30.5 cm constructed diameter flexible canopy water tunnel test was conducted are not the same as the Reynolds numbers achieved with wind tunnel testing for this research.

Reynolds numbers for the flexible canopy tests were on the order of 10^4 whereas the Reynolds numbers for the solid model tests were on the order of 10^5. Although this difference is only one order of magnitude, a direct comparison of these separate results can only be made if it known that the slope of the drag coefficient vs. Reynolds number plot is relatively constant in and between these two Reynolds number ranges.

A direct comparison of flexible canopy and solid model test data can be done with confidence for two reasons. First, a comparison of drag coefficient data for shapes similar to the flexible canopy and solid models showed that for these Reynolds number ranges, the slope of the drag coefficient with Reynolds number curve is very small and remains constant (Hoerner, 1958). Therefore, it is not expected that an abrupt change in slope of the drag coefficient will occur in the experimental data between the flexible and solid canopy model data. Secondly, it is seen in Figure 44 that the drag coefficients for models 1 and 8 are nearly equal to the drag coefficients calculated for the flexible canopy. Therefore, since both these models represent steady-state conditions, this result again helps validate this comparison.

The results suggest that the opening force on the flexible canopy is not directly related to the shape of the canopy. Therefore, other factors, such as the dynamic time rate of change of the canopy shape, must contribute to the drag forces seen during inflation. In the charts that follow, drag coefficients for the 30.5 cm flexible canopy model are plotted against normalized time. Also plotted are the drag coefficients for the solid models that correspond to the shape of the flexible canopy at times corresponding to specific points of interest on the force vs. time graph for the flexible canopy. The Reynolds numbers are scaled to the model's projected area normal to the freestream flow.

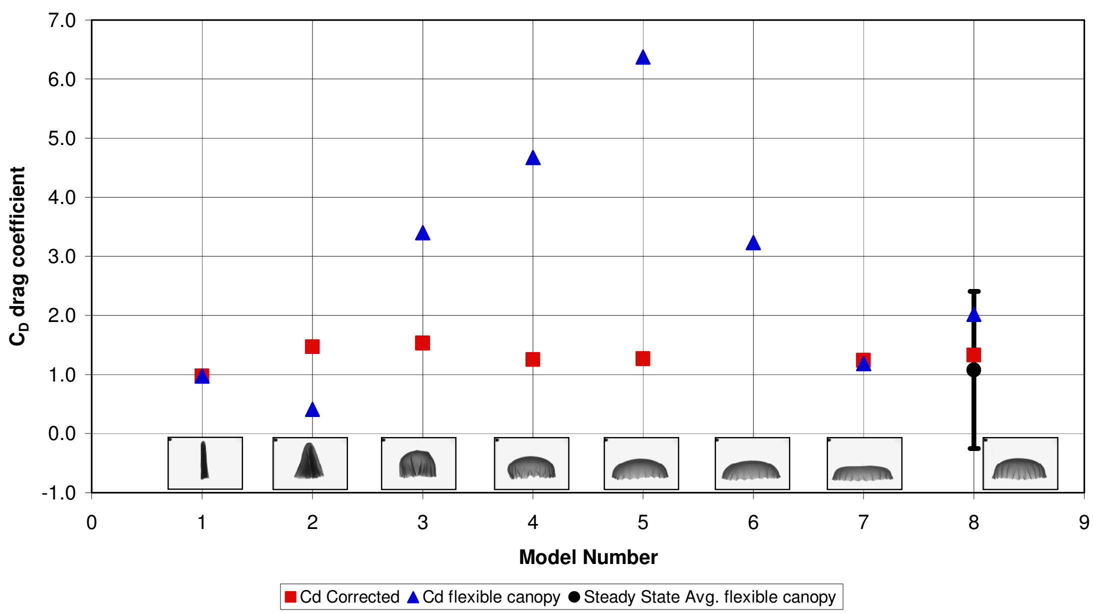

Figure 44 - Calculated drag coefficients (C_D) of rigid models (red) and the flexible canopy model (blue). The time average drag coefficient (black) and corresponding drag coefficient range (black range bar) for the flexible canopy model under steady-state conditions is also shown

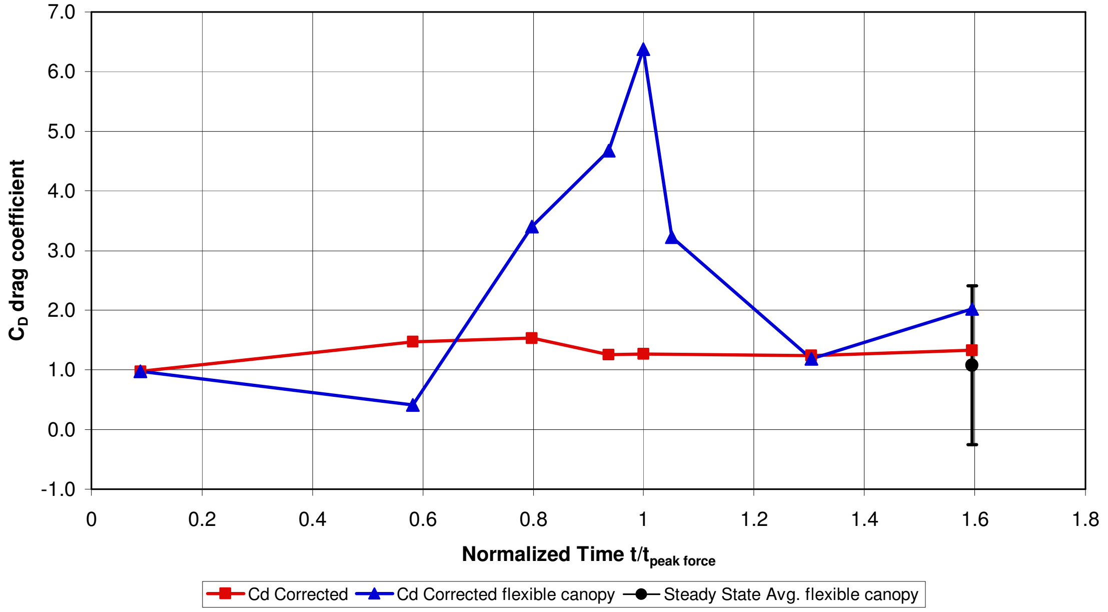

Figure 45 - Calculated drag coefficients of rigid models (red) and the flexible canopy model (blue) against normalized time. The average drag coefficient (black) and corresponding drag coefficient range (black range bar) for the flexible canopy model under steady-state conditions is also shown

It can be seen in the figure above that the C_D values for models 1, 2, 7 and 8 are relatively close to the C_D values of the flexible canopy models. The other models, however, do not compare with the flexible canopy. It is important to note that the flexible canopy C_D for model number 8 can fall within the error bar depicted in the graph. Due to the breathing cycle of the canopy in steady state, the projected area is constantly changing. This area change directly affects the C_D value. Therefore, based on the time chosen during steady state, the C_D will vary slightly. It can be seen that the results from this experiment fall within the error bar for the flexible canopy as well.

7. Conclusions

Based upon the data presented in this report, several conclusions can be drawn. First, it was shown that the drag coefficients for each model remained relatively constant over the range of Reynolds numbers tested.

Table 6- Reynolds Number Ranges for Rigid Parachute Models

Experimental Reynolds Number Ranges For Each Model							
Model Number	1	2	3	4	5	7	8
Reynolds Number Range (Re x 10^3)	**21 - 54**	**78 - 197**	**98 - 246**	**131 - 330**	**164 - 409**	**173 - 431**	**177 - 440**

Secondly, it was determined that the drag coefficients calculated in this experiment for models 2-7 do not match the drag coefficients found for a flexible model parachute canopy in the water tunnel even though the geometries are nearly identical. The fact that the drag coefficients for each model at each freestream velocity were found to be constant within a narrow margin of error shows very good experimental technique.

The variation in drag coefficient values between the flexible parachute canopy and the solid canopy models suggest that factors other than canopy geometry are related to the drag forces measured. The drag coefficients in this experiment remained relatively constant on the order of 1-1.4. The drag coefficients for the flexible canopy, however, ranged from about 0.4-6.4, with a sharp spike at models 4, 5, and 6. This spike is perhaps due to the time rate of change of the canopy opening.

8. Recommendations

This research project was the culmination of four years of education, encompassing a broad range of engineering topics. The design, construction, and testing procedures used in this experiment came both from prior experience, as well as hands-on trial and error. By no means was this group expert in all of these areas. Throughout the course of this project, many new concepts were learned. From learning new software, to becoming CNC machine operators, this project has welcomed many new experiences. From these experiences, this project group has recommendations to ease the creation and testing of similar models.

To begin, the machining of these models was incredibly difficult. The models needed to be very thin, yet precise. There is really no ideal material for this situation. Aluminum would have been more stable during the machining process, but it would have taken at least four times as long to cut compared to acetal. Due to the fact that acetal took nearly 45 hours per model to cut, this would be a substantial time investment. It is important to note that this is strictly cut time. This estimate does not consider the amount of time required to write the code, design the work holding, or set-up the machines, each of which was a very experimental process. Acetal also had its problems, as it became very unstable during machining. The consequence was broken models and/or tools resulting in lost time and money.

Due to this extreme difficulty, this project team recommends using stereolithography. Although in this academic setting, the availability of labor and machining facilities at no cost to the project budget made the use stereolithography uneconomical, it would have been much more cost effective and a wiser use of resources to use stereolithography if this project was done in a commercial setting. Using rapid prototyping, models can be constructed much more quickly, with very thin and accurate surfaces. At an estimated cost of $750-$1000 per model, the final investment would be less than half of what was predicted for CNC machining in local machine shops.

However, if future models with thin walls and complex geometry are to be made using CNC machining, this project team has recommendations to make the process slightly more streamlined. To begin, be sure that the material stock ordered can fit and be held within all machines used in the manufacturing process. In several instances, unforeseen machine set-up configurations resulted in machine clearances that would not accept the size of stock ordered. This resulted in large time investments to alter the stock and/or become creative in the work holding techniques.

Secondly, the procedure outlined in the construction section of this document worked very well, provided someone could monitor the CNC machines at all times. Spindle speeds and feed rates needed constant monitoring due to extreme model vibrations, as the acetal became thinner and thinner. Contrary to normal convention, *increasing* the feed rate by 30 to 40% reduced vibrations at the same spindle speeds. It was found that this was due to increasing the chip load, giving the tool less chance of chattering out of the material.

Also, it is recommended to work very closely with the professional machinists. Countless hours were spent by the staff in the WPI machine shop helping this project team learn CAM (Computer Aided Machining) software, and teaching the operation of the CNC machines. By listening carefully, checking for machine availability, being responsible, cleaning the work area and following the rules, trust can be earned from the staff. Such work ethic earned this team great respect in the machine shop, allowing for increased CNC machine privileges with less direct supervision. This is essential when approaching deadlines need to be met.

It is also recommended that when testing in the WPI closed-loop wind tunnel, great attention be paid to the drag measurement readouts taken from the tunnel dynamometer. During preliminary testing of the dynamometer setup, it was noticed that the adjustment mechanism on the drag transducer can be moved to touch the inside of the transducer. When this happens, the transducer does not function properly and fails to accurately measure drag forces. Therefore, it is suggested that after the drag adjustment wheel is fine-tuned and secured with the set screw, it is checked to make sure that the adjustable part of the transducer is not touching the inside of the main transducer body. Also, it should be checked again after the dynamometer is installed in the test section.

9. Recommendations for Future Study

Great care was taken to ensure that the canopy models in this project accurately reflected the shape of the flexible canopy models at each time instance chosen. From the imaging and design, to the manufacturing and finishing processes, many hours were spent making sure that every detail was as accurate as possible. Therefore, these models should serve as the basis for future projects related to rigid canopy models.

These models would be an excellent starting point for the study of vortex shedding on solid models. This phenomenon was witnessed by the project team, both visually and quantitatively through the use of the LabVIEW VI. Flow characteristics surrounding each shape could also be analyzed to determine what wake effects may exist. These experiments would be even further validated by the fact that the canopy models were designed so that no mounting apparatus is subjected to the freestream flow in front of the model.

The data presented in this report could also be used as a comparison for flexible canopy experiments within the wind tunnel. The flexible canopy could be scaled to match the size of the models used here, and run at the same Reynolds numbers to double check the findings on differing drag coefficients for solid versus flexible canopies.

References

Desabrais, K.J., *Velocity Field Measurements in the Near Wake of a Parachute Canopy*, Ph.D. thesis, Mechanical Engineering Department, Worcester Polytechnic Institute, Worcester, MA, April 2002.

Eaton, J.A., "Added Fluid Mass and the Equations of Motion of a Parachute," *Aeronautical Quarterly*, Vol. 34, Aug. 1983, pp. 226-242.

ELD Wind Tunnel Manual. Engineering Laboratory Design, Inc. July 1998.

French, K.E., "Inflation of a Parachute," *AIAA Journal*, Vol. 1, No. 11, Nov., 1963, pp. 2615-2617.

French, K.E., "Model Law for Parachute Opening Shock," *AIAA Journal*, Vol. 2, No. 12, Dec., 1964, pp. 2226-2228.

Heinrich, H.G., "Opening Time of Parachutes Under Infinite-Mass Conditions," *Journal of Aircraft*, Vol. 6, No. 3, May-June, 1969, pp. 268-272.

Heinrich, H.G., "A Linearised Theory of Parachute Opening Dynamics," *Aeronautical Journal*, Dec., 1972, pp. 723-731.

Heinrich, H.G. and Noreen, R.A., "Analysis of Parachute Opening Dynamics with Supporting Wind-Tunnel Experiments," *Journal of Aircraft*, Vol. 7, No. 4, July- Aug., 1970, pp. 341-347.

Hoerner, S. F., *Fluid Dynamic Drag,* S. F. Hoerner, New Jersey: Midland Park, 1958

Ibrahim, S.K., "Potential Flowfield and Added Mass of the Idealized Hemispherical Parachute," *Journal of Aircraft*, Vol. 4, No. 2, Mar.-Apr., 1967, pp. 96-100.

Johari, H., Stein, K., Tezduyar, T., "Impulsively Started Flow About a Rigid Parachute Canopy," *Journal of Aircraft*, Vol. 38, No. 6, 2001, pp. 1102-1109

Johari, H. & Desabrais, K. J., "Stiffness scaling for solid cloth parachutes," *Journal of Aircraft*, Vol. 40, No. 4, 2003, pp. 631-638

Knacke, T.W., Parachute Recovery Systems Design Manual, Para Publishing, 1992.

Macha, Michael J. and Robert J. Buffington. "Wall-Interference Corrections for Parachutes in a Closed Wind Tunnel." *Journal of Aircraft*, Vol 27 No. 4, 1989.

Müller, W., "Parachutes for Aircraft," National Advisory Committee for Aeronautics, Technical Memorandums, No. 450, October 28, 1927.

O'Hara, F., "Notes on the Opening Behavior and the Opening Forces of Parachutes," *Journal of the Royal Aeronautical Society*, Vol. 53, Nov., 1949, pp. 1053-1062.

SLA Finish Levels. 2004. Protogenic, Inc. 2005. < http://www.protogenic.com/Finish_Levels.aspx>

Stein, K.R., "Simulation and Modeling Techniques for Parachute Fluid-Structure Interactions," Ph.D. dissertation, Department of Aerospace Engineering, University of Minnesota, December 1999.

Stein, K., Benney, R., Tezduyar, T., Kalro, V., Leonard, J., and Accorsi, M., "3-D Computation of Parachute Fluid-Structure Interactions: Performance and Control," 15th CEAS/AIAA Aerodynamic Deceleration Systems Technology Conference, Toulouse, France, June 8-11, 1999, AIAA Paper 99-1714.

Stein, K., Benney, R., Kalro, V., Tezduyar, T.E., Leonard, J., and Accorsi, M., "Parachute Fluid-Structure Interactions: 3-D Computation," *Computer Methods in Applied Mechanics and Engineering*, Vol. 190, 2000, pp. 373-386.

Taylor, G.I., "On the Shape of Parachutes," The Scientific Papers of Sir Geoffrey Ingram Taylor, Volume III, Aerodynamics and The Mechanics of Projectiles and Explosions, edit. Batchelor, G.K., 1963, pp. 26-37.

Yavuz, T., "Determining and Accounting for a Parachute Virtual Mass," *Journal of Aircraft*, Vol. 26, No. 5, May, 1989, pp. 432-437.

Appendices

Appendix A: Estimated dynamometer moment calculations.

ALUMINUM

DENSITY=0.0975 (LB/IN^3)

Model	Weight (lbs)	CG from boss (in)
1	0.415	3.741
2	0.301	3.490
3	0.830	3.620
4	1.010	3.356
5	1.250	3.725
6	1.099	3.221
7	1.190	2.377
8	0.968	3.128

Model	Drag Force (lbs)
1	0.131
2	1.62
3	2.46
4	4.08
5	5.802
6	6.227
7	6.29
8	5.378

Worst Case Values: Expected Drag Force on models taken at 28 m/s assuming a Cd of 1.5 for all models. 28 m/s is the highest tunnel velocity where expected drag forces on all models are less than 7 lbs, the maximum drag force the dynamometer is able to measure

MOMENTS ABOUT DYNAMOMETER DISPLACEMENT TRANSDUCER

Sting Length inches	1	2	3	4	5	6	7	8	9	10	11	12
Model	Torque in-lbs											
1	0.396	0.811	1.226	1.641	2.056	2.471	2.886	3.301	3.716	4.131	4.546	4.961
2	18.089	17.788	17.487	17.186	16.885	16.584	16.283	15.982	15.681	15.380	15.079	14.778
3	25.685	24.855	24.025	23.195	22.365	21.535	20.705	19.875	19.045	18.215	17.385	16.555
4	44.560	43.550	42.540	41.530	40.520	39.510	38.500	37.490	36.480	35.470	34.460	33.450
5	63.718	62.468	61.218	59.968	58.718	57.468	56.218	54.968	53.718	52.468	51.218	49.968
6	70.085	68.986	67.887	66.788	65.689	64.590	63.491	62.392	61.293	60.194	59.095	57.996
7	71.461	70.271	69.081	67.891	66.701	65.511	64.321	63.131	61.941	60.751	59.561	58.371
8	60.540	59.572	58.604	57.636	56.668	55.700	54.732	53.764	52.796	51.828	50.860	49.892
Sting Length inches	1	2	3	4	5	6	7	8	9	10	11	12
Model	Torque ft-lbs											
1	0.033	0.068	0.102	0.137	0.171	0.206	0.240	0.275	0.310	0.344	0.379	0.413
2	1.507	1.482	1.457	1.432	1.407	1.382	1.357	1.332	1.307	1.282	1.257	1.231
3	2.140	2.071	2.002	1.933	1.864	1.795	1.725	1.656	1.587	1.518	1.449	1.380
4	3.713	3.629	3.545	3.461	3.377	3.293	3.208	3.124	3.040	2.956	2.872	2.788
5	5.310	5.206	5.101	4.997	4.893	4.789	4.685	4.581	4.476	4.372	4.268	4.164
6	5.840	5.749	5.657	5.566	5.474	5.383	5.291	5.199	5.108	5.016	4.925	4.833
7	5.955	5.856	5.757	5.658	5.558	5.459	5.360	5.261	5.162	5.063	4.963	4.864
8	5.045	4.964	4.884	4.803	4.722	4.642	4.561	4.480	4.400	4.319	4.238	4.158

Max Torque in-lb
71.461
Max Torque ft-lb
5.955

ALUMINUM

DENSITY=0.0975 (LB/IN^3)

Model	Weight (lbs)	CG from boss (in)
1	0.415	3.741
2	0.301	3.490
3	0.830	3.620
4	1.010	3.356
5	1.250	3.725
6	1.099	3.221
7	1.190	2.377
8	0.968	3.128

Model	Drag Force (lbs)
1	0.131
2	1.62
3	2.46
4	4.08
5	5.802
6	6.227
7	6.29
8	5.378

Worst Case Values: Expected Drag Force on models taken at 28 m/s assuming a Cd of 1.5 for all models. 28 m/s is the highest tunnel velocity where expected drag forces on all models are less than 7 lbs, the maximum drag force the dynamometer is able to measure

MOMENTS ABOUT DYNAMOMETER DISPLACEMENT TRANSDUCER
INCLUDES OSCILLATING MOMENT EFFECTS

Sting Length inches	1	2	3	4	5	6	7	8	9	10	11	12
Model	Torque in-lbs											
1	0.352	0.767	1.182	1.597	2.012	2.427	2.842	3.257	3.672	4.087	4.502	4.917
2	18.629	18.328	18.027	17.726	17.425	17.124	16.823	16.522	16.221	15.920	15.619	15.318
3	26.505	25.675	24.845	24.015	23.185	22.355	21.525	20.695	19.865	19.035	18.205	17.375
4	45.920	44.910	43.900	42.890	41.880	40.870	39.860	38.850	37.840	36.830	35.820	34.810
5	65.652	64.402	63.152	61.902	60.652	59.402	58.152	56.902	55.652	54.402	53.152	51.902
6	72.161	71.062	69.963	68.864	67.765	66.666	65.567	64.468	63.369	62.270	61.171	60.072
7	73.558	72.368	71.178	69.988	68.798	67.608	66.418	65.228	64.038	62.848	61.658	60.468
8	62.333	61.365	60.397	59.429	58.461	57.493	56.525	55.557	54.589	53.621	52.653	51.685
Sting Length inches	1	2	3	4	5	6	7	8	9	10	11	12
Model	Torque ft-lbs											
1	0.029	0.064	0.098	0.133	0.168	0.202	0.237	0.271	0.306	0.341	0.375	0.410
2	1.552	1.527	1.502	1.477	1.452	1.427	1.402	1.377	1.352	1.327	1.302	1.276
3	2.209	2.140	2.070	2.001	1.932	1.863	1.794	1.725	1.655	1.586	1.517	1.448
4	3.827	3.743	3.658	3.574	3.490	3.406	3.322	3.238	3.153	3.069	2.985	2.901
5	5.471	5.367	5.263	5.158	5.054	4.950	4.846	4.742	4.638	4.533	4.429	4.325
6	6.013	5.922	5.830	5.739	5.647	5.555	5.464	5.372	5.281	5.189	5.098	5.006
7	6.130	6.031	5.932	5.832	5.733	5.634	5.535	5.436	5.337	5.237	5.138	5.039
8	5.194	5.114	5.033	4.952	4.872	4.791	4.710	4.630	4.549	4.468	4.388	4.307

Max Torque in-lb
73.558
Max Torque ft-lb
6.130

DELRIN

DENSITY=0.0513 (LB/IN^3)

Model	Weight (lbs)	CG from boss (in)
1	0.218	3.741
2	0.260	3.490
3	0.436	3.620
4	0.530	3.356
5	0.658	3.725
6	0.578	3.221
7	0.627	2.377
8	0.509	3.128

Model	Drag Force (lbs)
1	0.131
2	1.62
3	2.46
4	4.08
5	5.802
6	6.227
7	6.29
8	5.378

Worst Case Values: Expected Drag Force on models taken at 28 m/s assuming a Cd of 1.5 for all models. 28 m/s is the highest tunnel velocity where expected drag forces on all models are less than 7 lbs, the maximum drag force the dynamometer is able to measure

MOMENTS ABOUT DYNAMOMETER DISPLACEMENT TRANSDUCER

Sting Length inches	1	2	3	4	5	6	7	8	9	10	11	12
Model	**Torque in-lbs**											
1	0.538	0.320	0.102	0.116	0.334	0.552	0.770	0.988	1.206	1.424	1.642	1.860
2	18.273	18.013	17.753	17.493	17.233	16.973	16.713	16.453	16.193	15.933	15.673	15.413
3	27.506	27.070	26.634	26.198	25.762	25.326	24.890	24.454	24.018	23.582	23.146	22.710
4	46.651	46.121	45.591	45.061	44.531	44.001	43.471	42.941	42.411	41.881	41.351	40.821
5	66.515	65.857	65.199	64.541	63.883	63.225	62.567	61.909	61.251	60.593	59.935	59.277
6	72.284	71.706	71.128	70.550	69.972	69.394	68.816	68.238	67.660	67.082	66.504	65.926
7	73.363	72.736	72.109	71.482	70.855	70.228	69.601	68.974	68.347	67.720	67.093	66.466
8	62.435	61.926	61.417	60.908	60.399	59.890	59.381	58.872	58.363	57.854	57.345	56.836
Sting Length inches	**1**	**2**	**3**	**4**	**5**	**6**	**7**	**8**	**9**	**10**	**11**	**12**
Model	**Torque ft-lbs**											
1	0.045	0.027	0.009	0.010	0.028	0.046	0.064	0.082	0.100	0.119	0.137	0.155
2	1.523	1.501	1.479	1.458	1.436	1.414	1.393	1.371	1.349	1.328	1.306	1.284
3	2.292	2.256	2.219	2.183	2.147	2.110	2.074	2.038	2.001	1.965	1.929	1.892
4	3.888	3.843	3.799	3.755	3.711	3.667	3.623	3.578	3.534	3.490	3.446	3.402
5	5.543	5.488	5.433	5.378	5.324	5.269	5.214	5.159	5.104	5.049	4.995	4.940
6	6.024	5.976	5.927	5.879	5.831	5.783	5.735	5.687	5.638	5.590	5.542	5.494
7	6.114	6.061	6.009	5.957	5.905	5.852	5.800	5.748	5.696	5.643	5.591	5.539
8	5.203	5.160	5.118	5.076	5.033	4.991	4.948	4.906	4.864	4.821	4.779	4.736

Max Torque in-lb
73.363
Max Torque ft-lb
6.114

DELRIN

DENSITY=0.0513 (LB/IN^3)

Model	Weight (lbs)	CG from boss (in)
1	0.218	3.741
2	0.260	3.490
3	0.436	3.620
4	0.530	3.356
5	0.658	3.725
6	0.578	3.221
7	0.627	2.377
8	0.509	3.128

Model	Drag Force (lbs)
1	0.131
2	1.62
3	2.46
4	4.08
5	5.802
6	6.227
7	6.29
8	5.378

Worst Case Values: Expected Drag Force on models taken at 28 m/s assuming a Cd of 1.5 for all models. 28 m/s is the highest tunnel velocity where expected drag forces on all models are less than 7 lbs, the maximum drag force the dynamometer is able to measure

MOMENTS ABOUT DYNAMOMETER DISPLACEMENT TRANSDUCER
INCLUDES OSCILLATING MOMENT EFFECTS

Sting Length inches	1	2	3	4	5	6	7	8	9	10	11
Model	**Torque in-lbs**										
1	0.582	0.364	0.146	0.072	0.290	0.508	0.726	0.944	1.162	1.380	1.598
2	18.813	18.553	18.293	18.033	17.773	17.513	17.253	16.993	16.733	16.473	16.213
3	28.326	27.890	27.454	27.018	26.582	26.146	25.710	25.274	24.838	24.402	23.966
4	48.011	47.481	46.951	46.421	45.891	45.361	44.831	44.301	43.771	43.241	42.711
5	68.449	67.791	67.133	66.475	65.817	65.159	64.501	63.843	63.185	62.527	61.869
6	74.360	73.782	73.204	72.626	72.048	71.470	70.892	70.314	69.736	69.158	68.580
7	75.459	74.832	74.205	73.578	72.951	72.324	71.697	71.070	70.443	69.816	69.189
8	64.228	63.719	63.210	62.701	62.192	61.683	61.174	60.665	60.156	59.647	59.138
Sting Length inches	**1**	**2**	**3**	**4**	**5**	**6**	**7**	**8**	**9**	**10**	**11**
Model	**Torque ft-lbs**										
1	0.049	0.030	0.012	0.006	0.024	0.042	0.060	0.079	0.097	0.115	0.133
2	1.568	1.546	1.524	1.503	1.481	1.459	1.438	1.416	1.394	1.373	1.351
3	2.360	2.324	2.288	2.251	2.215	2.179	2.142	2.106	2.070	2.033	1.997
4	4.001	3.957	3.913	3.868	3.824	3.780	3.736	3.692	3.648	3.603	3.559
5	5.704	5.649	5.594	5.540	5.485	5.430	5.375	5.320	5.265	5.211	5.156
6	6.197	6.148	6.100	6.052	6.004	5.956	5.908	5.859	5.811	5.763	5.715
7	6.288	6.236	6.184	6.132	6.079	6.027	5.975	5.923	5.870	5.818	5.766
8	5.352	5.310	5.267	5.225	5.183	5.140	5.098	5.055	5.013	4.971	4.928

Max Torque in-lb
75.459
Max Torque ft-lb
6.288

Appendix B: Wall Interference Correction Calculations

METHOD OF WALL CORRECTIONS
Macha & Buffington (AIAA Journal of Aircraft 1989)

Wall-Interference Corrections for Parachutes in Closed Wind Tunnel
"The results are believed to be applicable to any parachute or circular or conical constructions"

Maskell Correction Method for Bluff Bodies

$$\frac{q}{q_u} = 1 + K_M \frac{C_D S_u}{C}$$

Nomenclature

C	tunnel cross-sectional area
$C_D S$	model drag area D/q
K_M	Maskell bluff-body blockage factor
q	freestream dynamic pressure

subscript

u	uncorrected for wall interference

Method of Wall Correction
SINGLE PARACHUTE

K_M	Description
1.85	parachute (independent of porosity)
2.8	nonporous disk

approx C_D of parachutes tested by Macha
1.35 corrected drag coefficient based on solid frontal area of inflated canopy

MODEL 1
WALL CORRECTIONS

Model 7: Frontal Area	0.00083	m^2

Freestream Velocity:	**10 m/s**	
Model 1		Units
C	4	ft^2
D = Drag Force	0.0137	lbs
q_u	1.2594	lb/ft^2
K_M	1.85	
C_DS	0.0109	ft^2
q	**1.2657**	lb/ft^2
Resultant Tunnel Velocity (above model)	**10.0251**	m/s
ΔV	0.0251	m/s
C_D uncorrected	**1.2192**	
C_D corrected	**1.2131**	

RE #
21636.74
21690.98

K_M	q (lb/ft^2)	V (m/s)	ΔV (m/s)	% change
1	1.26	10.01	0.01	0.1
1.5	1.26	10.02	0.02	0.2
1.85	1.27	10.03	0.03	0.3
2	1.27	10.03	0.03	0.3
3	1.27	10.04	0.04	0.4

Freestream Velocity:	**18 m/s**	
Model 1		Units
C	4	ft^2
D = Drag Force	0.0228	lbs
q_u	4.0804	lb/ft^2
K_M	1.85	
C_DS	0.0056	ft^2
q	**4.0909**	lb/ft^2
Resultant Tunnel Velocity (above model)	**18.0232**	m/s
ΔV	0.0232	m/s
C_D uncorrected	**0.6276**	
C_D corrected	**0.6260**	

RE #
38946.14
38996.42

K_M	q (lb/ft^2)	V (m/s)	ΔV (m/s)	% change
1	4.09	18.01	0.01	0.1
1.5	4.09	18.02	0.02	0.1
1.85	4.09	18.02	0.02	0.1
2	4.09	18.03	0.03	0.1
3	4.10	18.04	0.04	0.2

Freestream Velocity:	**25 m/s**	
Model 1		Units
C	4	ft^2
D = Drag Force	0.0762	lbs
q_u	7.8711	lb/ft^2
K_M	1.85	
C_DS	0.0097	ft^2
q	**7.9064**	lb/ft^2
Resultant Tunnel Velocity (above model)	**25.0559**	m/s
ΔV	0.0559	m/s
C_D uncorrected	**1.0880**	
C_D corrected	**1.0832**	

RE #
54091.86
54212.88

K_M	q (lb/ft^2)	V (m/s)	ΔV (m/s)	% change
1	7.89	25.03	0.03	0.1
1.5	7.90	25.05	0.05	0.2
1.85	7.9064	25.06	0.06	0.2
2	7.91	25.06	0.06	0.2
3	7.93	25.09	0.09	0.4

$$\frac{q}{q_u} = 1 + K_M \frac{C_D S_u}{C}$$

Nomenclature

C	tunnel cross-sectional area
C_DS	model drag area D/q
K_M	Maskell bluff-body blockage factor
q	freestream dynamic pressure

subscript

u	uncorrected for wall interference

ERROR

Freestream Velocity:	**10 m/s**
Model 1	

Drag Force error +/-	0.018769449	lb
Total Error	137.3795359	%

Freestream Velocity:	**18 m/s**
Model 1	

Drag Force error +/-	0.019454502	lb
Total Error	85.35205881	%

Freestream Velocity:	**25 m/s**
Model 1	

Drag Force error +/-	0.01863147	lb
Total Error	24.44827619	%

MODEL 2
WALL CORRECTIONS

Model 2: Frontal Area	0.01021	m^2

Freestream Velocity:	**10 m/s**	
Model 2		Units
C	4	ft^2
D = Drag Force	0.2148	lbs
q_u	1.2594	lb/ft^2
K_M	1.85	
C_DS	0.1706	ft^2
q	**1.3587**	lb/ft^2
Resultant Tunnel Velocity (above model)	**10.3870**	m/s
ΔV	0.3870	m/s
C_D uncorrected	**1.5526**	
C_D corrected	**1.4391**	

RE #
76006
78947.33

K_M	q (lb/ft^2)	V (m/s)	ΔV (m/s)
1	1.31	10.21	0.21
1.5	1.34	10.31	0.31
1.85	1.36	10.39	0.39
2	1.37	10.42	0.42
3	1.42	10.62	0.62

Freestream Velocity:	**18 m/s**	
Model 2		Units
C	4	ft^2
D = Drag Force	0.7112	lbs
q_u	4.0804	lb/ft^2
K_M	1.85	
C_DS	0.1743	ft^2
q	**4.4093**	lb/ft^2
Resultant Tunnel Velocity (above model)	**18.7114**	m/s
ΔV	0.7114	m/s
C_D uncorrected	**1.5864**	
C_D corrected	**1.4680**	

RE #
136810.8
142218.1

K_M	q (lb/ft^2)	V (m/s)	ΔV (m/s)
1	4.26	18.39	0.39
1.5	4.35	18.58	0.58
1.85	4.41	18.71	0.71
2	4.44	18.77	0.77
3	4.61	19.14	1.14

Freestream Velocity:	**25 m/s**	
Model 2		Units
C	4	ft^2
D = Drag Force	1.4078	lbs
q_u	7.8711	lb/ft^2
K_M	1.85	
C_DS	0.1789	ft^2
q	**8.5222**	lb/ft^2
Resultant Tunnel Velocity (above model)	**26.0135**	m/s
ΔV	1.0135	m/s
C_D uncorrected	**1.6280**	
C_D corrected	**1.5036**	

RE #
190015
197718.1

K_M	q (lb/ft^2)	V (m/s)	ΔV (m/s)
1	8.22	25.55	0.55
1.5	8.40	25.82	0.82
1.85	8.5222	26.01	1.01
2	8.58	26.09	1.09
3	8.93	26.62	1.62

$$\frac{q}{q_u} = 1 + K_M \frac{C_D S_u}{C}$$

Nomenclature

C	tunnel cross-sectional area
C_DS	model drag area D/q
K_M	Maskell bluff-body blockage factor
q	freestream dynamic pressure

subscript

u	uncorrected for wall interference

ERROR

Freestream Velocity:	**10 m/s**
Model 2	

Drag Force error +/-	0.020086319	lb
Total Error	10.22231855	%

Freestream Velocity:	**18 m/s**
Model 2	

Drag Force error +/-	0.021034024	lb
Total Error	3.222241252	%

Freestream Velocity:	**25 m/s**
Model 2	

Drag Force error +/-	0.02263605	lb
Total Error	1.739754028	%

MODEL 3
WALL CORRECTIONS

Model 7: Frontal Area	0.01523	m^2

Freestream Velocity:	**10 m/s**	
Model 3		Units
C	4	ft^2
D = Drag Force	0.3674	lbs
q_u	1.2594	lb/ft^2
K_M	1.85	
C_DS	0.2917	ft^2
q	**1.4293**	lb/ft^2
Resultant Tunnel Velocity (above model)	**10.6532**	m/s
ΔV	0.6532	m/s
C_D uncorrected	**1.7795**	
C_D corrected	**1.5679**	

RE #
92834.58
98898.84

K_M	q (lb/ft^2)	V (m/s)	ΔV (m/s)
1	1.35	10.36	0.36
1.5	1.40	10.53	0.53
1.85	1.43	10.65	0.65
2	1.44	10.70	0.70
3	1.53	11.04	1.04

Freestream Velocity:	**18 m/s**	
Model 3		Units
C	4	ft^2
D = Drag Force	1.1297	lbs
q_u	4.0804	lb/ft^2
K_M	1.85	
C_DS	0.2769	ft^2
q	**4.6029**	lb/ft^2
Resultant Tunnel Velocity (above model)	**19.1178**	m/s
ΔV	1.1178	m/s
C_D uncorrected	**1.6890**	
C_D corrected	**1.4973**	

RE #
167102.2
177479

K_M	q (lb/ft^2)	V (m/s)	ΔV (m/s)
1	4.36	18.61	0.61
1.5	4.50	18.91	0.91
1.85	4.60	19.12	1.12
2	4.65	19.21	1.21
3	4.93	19.78	1.78

Freestream Velocity:	**25 m/s**	
Model 3		Units
C	4	ft^2
D = Drag Force	2.2254	lbs
q_u	7.8711	lb/ft^2
K_M	1.85	
C_DS	0.2827	ft^2
q	**8.9004**	lb/ft^2
Resultant Tunnel Velocity (above model)	**26.5843**	m/s
ΔV	1.5843	m/s
C_D uncorrected	**1.7247**	
C_D corrected	**1.5253**	

RE #
232086.4
246794.5

K_M	q (lb/ft^2)	V (m/s)	ΔV (m/s)
1	8.43	25.87	0.87
1.5	8.71	26.29	1.29
1.85	8.9004	26.58	1.58
2	8.98	26.71	1.71
3	9.54	27.52	2.52

$$\frac{q}{q_u} = 1 + K_M \frac{C_D S_u}{C}$$

Nomenclature

C	tunnel cross-sectional area
C_DS	model drag area D/q
K_M	Maskell bluff-body blockage factor
q	freestream dynamic pressure

subscript

u	uncorrected for wall interference

ERROR

Freestream Velocity:	**10 m/s**	
Model 3		
Drag Force error +/-	0.017431498	lb
Total Error	6.292070952	%

Freestream Velocity:	**18 m/s**	
Model 3		
Drag Force error +/-	0.022334747	lb
Total Error	2.354513841	%

Freestream Velocity:	**25 m/s**	
Model 3		
Drag Force error +/-	0.04137108	lb
Total Error	1.974223212	%

MODEL 4
WALL CORRECTIONS

Model 4: Frontal Area	0.02577	m^2

Freestream Velocity:	10 m/s	
Model 4		Units
C	4	ft^2
D = Drag Force	0.5221	lbs
q_u	1.2594	lb/ft^2
K_M	1.85	
C_DS	0.4146	ft^2
q	**1.5008**	lb/ft^2
Resultant Tunnel Velocity (above model)	**10.9167**	m/s
ΔV	0.9167	m/s
C_D uncorrected	**1.4945**	
C_D corrected	**1.2541**	

RE #
120758.9
131828.6

K_M	q (lb/ft^2)	V (m/s)	ΔV (m/s)	% change
1	1.39	10.51	0.51	5.1
1.5	1.46	10.75	0.75	7.5
1.85	1.50	10.92	0.92	9.2
2	1.52	10.99	0.99	9.9
3	1.65	11.45	1.45	14.5

Freestream Velocity:	18 m/s	
Model 4		Units
C	4	ft^2
D = Drag Force	1.6317	lbs
q_u	4.0804	lb/ft^2
K_M	1.85	
C_DS	0.3999	ft^2
q	**4.8350**	lb/ft^2
Resultant Tunnel Velocity (above model)	**19.5940**	m/s
ΔV	1.5940	m/s
C_D uncorrected	**1.4416**	
C_D corrected	**1.2166**	

RE #
217366.1
236614.7

K_M	q (lb/ft^2)	V (m/s)	ΔV (m/s)	% change
1	4.49	18.88	0.88	4.9
1.5	4.69	19.30	1.30	7.2
1.85	4.84	19.59	1.59	8.9
2	4.90	19.72	1.72	9.5
3	5.30	20.52	2.52	14.0

Freestream Velocity:	25 m/s	
Model 4		Units
C	4	ft^2
D = Drag Force	3.3685	lbs
q_u	7.8711	lb/ft^2
K_M	1.85	
C_DS	0.4280	ft^2
q	**9.4290**	lb/ft^2
Resultant Tunnel Velocity (above model)	**27.3625**	m/s
ΔV	2.3625	m/s
C_D uncorrected	**1.5428**	
C_D corrected	**1.2879**	

RE #
301897.3
330426.7

K_M	q (lb/ft^2)	V (m/s)	ΔV (m/s)	% change
1	8.71	26.30	1.30	5.2
1.5	9.13	26.93	1.93	7.7
1.85	9.4290	27.36	2.36	9.5
2	9.56	27.55	2.55	10.2
3	10.40	28.73	3.73	14.9

$$\frac{q}{q_u} = 1 + K_M \frac{C_D S_u}{C}$$

Nomenclature

C	tunnel cross-sectional area
C_DS	model drag area D/q
K_M	Maskell bluff-body blockage factor
q	freestream dynamic pressure

subscript

u	uncorrected for wall interference

ERROR

Freestream Velocity:	10 m/s
Model 4	

Drag Force error +/-	0.0173816	lb
Total Error	5.306483627	%

Freestream Velocity:	18 m/s
Model 4	

Drag Force error +/-	0.031428119	lb
Total Error	2.311941572	%

Freestream Velocity:	25 m/s
Model 4	

Drag Force error +/-	0.273717929	lb
Total Error	8.152910024	%

MODEL 5
WALL CORRECTIONS

Model 5: Frontal Area	0.03658	m^2

Freestream Velocity:	**10 m/s**	
Model 5		Units
C	4	ft^2
D = Drag Force	0.8202	lbs
q_u	1.2594	lb/ft^2
K_M	1.85	
C_DS	0.6513	ft^2
q	**1.6387**	lb/ft^2
Resultant Tunnel Velocity (above model)	**11.4070**	m/s
ΔV	1.4070	m/s
C_D uncorrected	**1.6540**	
C_D corrected	**1.2712**	

RE #
143875.1
164118.9

K_M	q (lb/ft^2)	V (m/s)	ΔV (m/s)
1	1.46	10.78	0.78
1.5	1.57	11.15	1.15
1.85	1.64	11.41	1.41
2	1.67	11.51	1.51
3	1.87	12.20	2.20

Freestream Velocity:	**18 m/s**	
Model 5		Units
C	4	ft^2
D = Drag Force	2.6396	lbs
q_u	4.0804	lb/ft^2
K_M	1.85	
C_DS	0.6469	ft^2
q	**5.3012**	lb/ft^2
Resultant Tunnel Velocity (above model)	**20.5168**	m/s
ΔV	2.5168	m/s
C_D uncorrected	**1.6430**	
C_D corrected	**1.2646**	

RE #
258975.2
295185.5

K_M	q (lb/ft^2)	V (m/s)	ΔV (m/s)
1	4.74	19.40	1.40
1.5	5.07	20.06	2.06
1.85	5.30	20.52	2.52
2	5.40	20.71	2.71
3	6.06	21.94	3.94

Freestream Velocity:	**25 m/s**	
Model 5		Units
C	4	ft^2
D = Drag Force	5.0464	lbs
q_u	7.8711	lb/ft^2
K_M	1.85	
C_DS	0.6411	ft^2
q	**10.2051**	lb/ft^2
Resultant Tunnel Velocity (above model)	**28.4662**	m/s
ΔV	3.4662	m/s
C_D uncorrected	**1.6283**	
C_D corrected	**1.2559**	

RE #
359687.8
409558.4

K_M	q (lb/ft^2)	V (m/s)	ΔV (m/s)
1	9.13	26.93	1.93
1.5	9.76	27.84	2.84
1.85	10.2051	28.47	3.47
2	10.39	28.73	3.73
3	11.66	30.42	5.42

Nomenclature

C	tunnel cross-sectional area
C_DS	model drag area D/q
K_M	Maskell bluff-body blockage factor
q	freestream dynamic pressure

subscript

u	uncorrected for wall interference

$$\frac{q}{q_u} = 1 + K_M \frac{C_D S_u}{C}$$

ERROR

Freestream Velocity:	**10 m/s**	
Model 5		
Drag Force error +/-	0.017100467	lb
Total Error	4.628441646	%

Freestream Velocity:	**18 m/s**	
Model 5		
Drag Force error +/-	0.02653258	lb
Total Error	1.626536606	%

Freestream Velocity:	**25 m/s**	
Model 5		
Drag Force error +/-	0.086218022	lb
Total Error	1.833158724	%

MODEL 7
WALL CORRECTIONS

Model 7: Frontal Area	0.04264	m^2

Freestream Velocity:	**10 m/s**	
Model 7		Units
C	4	ft^2
D = Drag Force	0.9576	lbs
q_u	1.2594	lb/ft^2
K_M	1.85	
C_DS	0.7604	ft^2
q	**1.7023**	lb/ft^2
Resultant Tunnel Velocity (above model)	**11.6262**	m/s
ΔV	1.6262	m/s
C_D uncorrected	**1.6567**	
C_D corrected	**1.2256**	

RE #
149053.1
173292.4

K_M	q (lb/ft^2)	V (m/s)	ΔV (m/s)	% change
1	1.50	10.91	0.91	9.1
1.5	1.62	11.34	1.34	13.4
1.85	1.70	11.63	1.63	16.3
2	1.74	11.75	1.75	17.5
3	1.98	12.53	2.53	25.3

Freestream Velocity:	**18 m/s**	
Model 7		Units
C	4	ft^2
D = Drag Force	3.3277	lbs
q_u	4.0804	lb/ft^2
K_M	1.85	
C_DS	0.8155	ft^2
q	**5.6195**	lb/ft^2
Resultant Tunnel Velocity (above model)	**21.1237**	m/s
ΔV	3.1237	m/s
C_D uncorrected	**1.7768**	
C_D corrected	**1.2902**	

RE #
268295.6
314854.8

K_M	q (lb/ft^2)	V (m/s)	ΔV (m/s)	% change
1	4.91	19.75	1.75	9.7
1.5	5.33	20.57	2.57	14.3
1.85	5.62	21.12	3.12	17.4
2	5.74	21.36	3.36	18.6
3	6.58	22.85	4.85	27.0

Freestream Velocity:	**25 m/s**	
Model 7		Units
C	4	ft^2
D = Drag Force	5.7860	lbs
q_u	7.8711	lb/ft^2
K_M	1.85	
C_DS	0.7351	ft^2
q	**10.5471**	lb/ft^2
Resultant Tunnel Velocity (above model)	**28.9394**	m/s
ΔV	3.9394	m/s
C_D uncorrected	**1.6015**	
C_D corrected	**1.1952**	

RE #
372632.8
431350.4

K_M	q (lb/ft^2)	V (m/s)	ΔV (m/s)	% change
1	9.32	27.20	2.20	8.8
1.5	10.04	28.24	3.24	12.9
1.85	10.5471	28.94	3.94	15.8
2	10.76	29.24	4.24	16.9
3	12.21	31.14	6.14	24.6

$$\frac{q}{q_u} = 1 + K_M \frac{C_D S_u}{C}$$

Nomenclature

C	tunnel cross-sectional area
C_DS	model drag area D/q
K_M	Maskell bluff-body blockage factor
q	freestream dynamic pressure

subscript

u	uncorrected for wall interference

ERROR

Freestream Velocity:	**10 m/s**	
Model 7		
Drag Force error +/-	0.016436322	lb
Total Error	4.474496708	%

Freestream Velocity:	**18 m/s**	
Model 7		
Drag Force error +/-	0.031732667	lb
Total Error	1.595174764	%

Freestream Velocity:	**25 m/s**	
Model 7		
Drag Force error +/-	0.021588262	lb
Total Error	0.762043227	%

MODEL 8
WALL CORRECTIONS

Model 8: Frontal Area	0.03390	m^2

Freestream Velocity:	**10 m/s**	
Model 8		Units
C	4	ft^2
D = Drag Force	0.8213	lbs
q_u	1.2594	lb/ft^2
K_M	1.85	
C_DS	0.6522	ft^2
q	**1.6392**	lb/ft^2
Resultant Tunnel Velocity (above model)	**11.4089**	m/s
ΔV	1.4089	m/s
C_D uncorrected	**1.7870**	
C_D corrected	**1.3729**	

RE #
155340.7
177226.4

K_M	q (lb/ft^2)	V (m/s)	ΔV (m/s)
1	1.46	10.78	0.78
1.5	1.57	11.16	1.16
1.85	1.64	11.41	1.41
2	1.67	11.52	1.52
3	1.88	12.20	2.20

Freestream Velocity:	**18 m/s**	
Model 8		Units
C	4	ft^2
D = Drag Force	2.4858	lbs
q_u	4.0804	lb/ft^2
K_M	1.85	
C_DS	0.6092	ft^2
q	**5.2301**	lb/ft^2
Resultant Tunnel Velocity (above model)	**20.3787**	m/s
ΔV	2.3787	m/s
C_D uncorrected	**1.6693**	
C_D corrected	**1.3024**	

RE #
279613.3
316563.9

K_M	q (lb/ft^2)	V (m/s)	ΔV (m/s)
1	4.70	19.32	1.32
1.5	5.01	19.95	1.95
1.85	5.23	20.38	2.38
2	5.32	20.56	2.56
3	5.94	21.73	3.73

Freestream Velocity:	**25 m/s**	
Model 8		Units
C	4	ft^2
D = Drag Force	4.8443	lbs
q_u	7.8711	lb/ft^2
K_M	1.85	
C_DS	0.6155	ft^2
q	**10.1116**	lb/ft^2
Resultant Tunnel Velocity (above model)	**28.3356**	m/s
ΔV	3.3356	m/s
C_D uncorrected	**1.6864**	
C_D corrected	**1.3128**	

RE #
388351.8
440166.9

K_M	q (lb/ft^2)	V (m/s)	ΔV (m/s)
1	9.08	26.85	1.85
1.5	9.69	27.74	2.74
1.85	10.1116	28.34	3.34
2	10.29	28.59	3.59
3	11.50	30.22	5.22

Nomenclature

C	tunnel cross-sectional area
C_DS	model drag area D/q
K_M	Maskell bluff-body blockage factor
q	freestream dynamic pressure

subscript

u	uncorrected for wall interference

$$\frac{q}{q_u} = 1 + K_M \frac{C_D S_u}{C}$$

ERROR

Freestream Velocity:	**10 m/s**
Model 8	

Drag Force error +/-	0.018501385	lb
Total Error	4.706347692	%

Freestream Velocity:	**18 m/s**
Model 8	

Drag Force error +/-	0.023994115	lb
Total Error	1.602168526	%

Freestream Velocity:	**25 m/s**
Model 8	

Drag Force error +/-	0.029245565	lb
Total Error	0.897753905	%

Appendix C: Estimated expected drag forces for rigid canopy models for varying tunnel speeds and drag coefficients.

DRAG FORCE CALCULATIONS FOR VARIOUS WIND TUNNEL FREESTREAM VELOCITIES AND DRAG COEFFICIENTS.

IMAGE 1

WIDTH (m)	HEIGHT (M)
0.03245	0.143135

BLOCKAGE LESS THAN 10%

Diameter Dprojected (m)	0.03245
Area Projected (m^2)	0.00083
Density (kg/m^3)	1.2
Mu ($N\text{-}s/m^2$)	1.80E-05
Kinematic Viscosity	1.50E-05

			Cd															
				0.5	0.7	0.8	0.85	0.9	1	1.1	1.2	1.3	1.4	1.5	1.6	2	2.5	3	3.5
Tunnel Speed				Force															
m/s	MPH	Hz	RE #	lbs	lbs	lbs	lbs	lbs	lbs	lbs	lbs	lbs	lbs	lbs	lbs	lbs	lbs	lbs	lbs
0	0.0		0.00E+00	0.000	0.000	0.000	0.000	0.000	0.000	0.000	0.000	0.000	0.000	0.000	0.000	0.000	0.000	0.000	0.000
1	2.2		2.16E+03	0.000	0.000	0.000	0.000	0.000	0.000	0.000	0.000	0.000	0.000	0.000	0.000	0.000	0.000	0.000	0.000
2	4.5	2	4.33E+03	0.000	0.000	0.000	0.000	0.000	0.000	0.000	0.001	0.001	0.001	0.001	0.001	0.001	0.001	0.001	0.002
3	6.7	2	6.49E+03	0.001	0.001	0.001	0.001	0.001	0.001	0.001	0.001	0.001	0.001	0.002	0.002	0.002	0.003	0.003	0.004
4	8.9	4	8.65E+03	0.001	0.001	0.001	0.002	0.002	0.002	0.002	0.002	0.002	0.002	0.003	0.003	0.004	0.004	0.005	0.006
5	11.2		1.08E+04	0.001	0.002	0.002	0.002	0.003	0.003	0.003	0.003	0.004	0.004	0.004	0.004	0.006	0.007	0.008	0.010
6	13.4		1.30E+04	0.002	0.003	0.003	0.003	0.004	0.004	0.004	0.005	0.005	0.006	0.006	0.006	0.008	0.010	0.012	0.014
7	15.7		1.51E+04	0.003	0.004	0.004	0.005	0.005	0.005	0.006	0.007	0.007	0.008	0.008	0.009	0.011	0.014	0.016	0.019
8	17.9		1.73E+04	0.004	0.005	0.006	0.006	0.006	0.007	0.008	0.009	0.009	0.010	0.011	0.011	0.014	0.018	0.021	0.025
9	20.1		1.95E+04	0.005	0.006	0.007	0.008	0.008	0.009	0.010	0.011	0.012	0.013	0.014	0.014	0.018	0.023	0.027	0.032
10	22.4		2.16E+04	0.006	0.008	0.009	0.009	0.010	0.011	0.012	0.013	0.015	0.016	0.017	0.018	0.022	0.028	0.033	0.039
11	24.6		2.38E+04	0.007	0.009	0.011	0.011	0.012	0.013	0.015	0.016	0.018	0.019	0.020	0.022	0.027	0.034	0.040	0.047
12	26.8		2.60E+04	0.008	0.011	0.013	0.014	0.014	0.016	0.018	0.019	0.021	0.022	0.024	0.026	0.032	0.040	0.048	0.056
13	29.1	15	2.81E+04	0.009	0.013	0.015	0.016	0.017	0.019	0.021	0.023	0.025	0.026	0.028	0.030	0.038	0.047	0.057	0.066
14	31.3		3.03E+04	0.011	0.015	0.017	0.019	0.020	0.022	0.024	0.026	0.028	0.031	0.033	0.035	0.044	0.055	0.066	0.077
15	33.6		3.25E+04	0.013	0.018	0.020	0.021	0.023	0.025	0.028	0.030	0.033	0.035	0.038	0.040	0.050	0.063	0.075	0.088
16	35.8		3.46E+04	0.014	0.020	0.023	0.024	0.026	0.029	0.031	0.034	0.037	0.040	0.043	0.046	0.057	0.071	0.086	0.100
17	38.0	20	3.68E+04	0.016	0.023	0.026	0.027	0.029	0.032	0.035	0.039	0.042	0.045	0.048	0.052	0.064	0.081	0.097	0.113
18	40.3		3.89E+04	0.018	0.025	0.029	0.031	0.033	0.036	0.040	0.043	0.047	0.051	0.054	0.058	0.072	0.090	0.108	0.127
19	42.5		4.11E+04	0.020	0.028	0.032	0.034	0.036	0.040	0.044	0.048	0.052	0.056	0.060	0.064	0.081	0.101	0.121	0.141
20	44.7		4.33E+04	0.022	0.031	0.036	0.038	0.040	0.045	0.049	0.054	0.058	0.062	0.067	0.071	0.089	0.112	0.134	0.156
21	47.0		4.54E+04	0.025	0.034	0.039	0.042	0.044	0.049	0.054	0.059	0.064	0.069	0.074	0.079	0.098	0.123	0.148	0.172
22	49.2	25	4.76E+04	0.027	0.038	0.043	0.046	0.049	0.054	0.059	0.065	0.070	0.076	0.081	0.086	0.108	0.135	0.162	0.189
23	51.4		4.98E+04	0.030	0.041	0.047	0.050	0.053	0.059	0.065	0.071	0.077	0.083	0.089	0.094	0.118	0.148	0.177	0.207
24	53.7		5.19E+04	0.032	0.045	0.051	0.055	0.058	0.064	0.071	0.077	0.084	0.090	0.096	0.103	0.129	0.161	0.193	0.225
25	55.9		5.41E+04	0.035	0.049	0.056	0.059	0.063	0.070	0.077	0.084	0.091	0.098	0.105	0.112	0.139	0.174	0.209	0.244
26	58.2	30	5.62E+04	0.038	0.053	0.060	0.064	0.068	0.075	0.083	0.090	0.098	0.106	0.113	0.121	0.151	0.189	0.226	0.264
27	60.4		5.84E+04	0.041	0.057	0.065	0.069	0.073	0.081	0.089	0.098	0.106	0.114	0.122	0.130	0.163	0.203	0.244	0.285
28	62.6		6.06E+04	0.044	0.061	0.070	0.074	0.079	0.087	0.096	0.105	0.114	0.122	0.131	0.140	0.175	0.219	0.262	0.306
29	64.9		6.27E+04	0.047	0.066	0.075	0.080	0.084	0.094	0.103	0.113	0.122	0.131	0.141	0.150	0.188	0.235	0.281	0.328
30	67.1		6.49E+04	0.050	0.070	0.080	0.085	0.090	0.100	0.110	0.120	0.131	0.141	0.151	0.161	0.201	0.251	0.301	0.351
31	69.3	35	6.71E+04	0.054	0.075	0.086	0.091	0.096	0.107	0.118	0.129	0.139	0.150	0.161	0.172	0.214	0.268	0.322	0.375
32	71.6		6.92E+04	0.057	0.080	0.091	0.097	0.103	0.114	0.126	0.137	0.149	0.160	0.171	0.183	0.228	0.286	0.343	0.400
33	73.8		7.14E+04	0.061	0.085	0.097	0.103	0.109	0.121	0.134	0.146	0.158	0.170	0.182	0.194	0.243	0.304	0.364	0.425
34	76.1		7.36E+04	0.064	0.090	0.103	0.110	0.116	0.129	0.142	0.155	0.168	0.181	0.193	0.206	0.258	0.322	0.387	0.451
35	78.3	40	7.57E+04	0.068	0.096	0.109	0.116	0.123	0.137	0.150	0.164	0.178	0.191	0.205	0.219	0.273	0.342	0.410	0.478
36	80.5		7.79E+04	0.072	0.101	0.116	0.123	0.130	0.145	0.159	0.173	0.188	0.202	0.217	0.231	0.289	0.361	0.434	0.506
37	82.8		8.00E+04	0.076	0.107	0.122	0.130	0.137	0.153	0.168	0.183	0.199	0.214	0.229	0.244	0.305	0.382	0.458	0.535
38	85.0		8.22E+04	0.081	0.113	0.129	0.137	0.145	0.161	0.177	0.193	0.209	0.226	0.242	0.258	0.322	0.403	0.483	0.564
39	87.2		8.44E+04	0.085	0.119	0.136	0.144	0.153	0.170	0.187	0.204	0.221	0.238	0.255	0.271	0.339	0.424	0.509	0.594
40	89.5	45	8.65E+04	0.089	0.125	0.143	0.152	0.161	0.178	0.196	0.214	0.232	0.250	0.268	0.286	0.357	0.446	0.535	0.625
41	91.7		8.87E+04	0.094	0.131	0.150	0.159	0.169	0.188	0.206	0.225	0.244	0.263	0.281	0.300	0.375	0.469	0.563	0.656
42	94.0		9.09E+04	0.098	0.138	0.157	0.167	0.177	0.197	0.216	0.236	0.256	0.275	0.295	0.315	0.394	0.492	0.590	0.689
43	96.2		9.30E+04	0.103	0.144	0.165	0.175	0.186	0.206	0.227	0.248	0.268	0.289	0.309	0.330	0.413	0.516	0.619	0.722
44	98.4	50	9.52E+04	0.108	0.151	0.173	0.184	0.194	0.216	0.238	0.259	0.281	0.302	0.324	0.346	0.432	0.540	0.648	0.756
45	100.7		9.74E+04	0.113	0.158	0.181	0.192	0.203	0.226	0.248	0.271	0.294	0.316	0.339	0.361	0.452	0.565	0.678	0.791
46	102.9		9.95E+04	0.118	0.165	0.189	0.201	0.212	0.236	0.260	0.283	0.307	0.330	0.354	0.378	0.472	0.590	0.708	0.826
47	105.1		1.02E+05	0.123	0.172	0.197	0.209	0.222	0.246	0.271	0.296	0.320	0.345	0.370	0.394	0.493	0.616	0.739	0.862
48	107.4		1.04E+05	0.129	0.180	0.206	0.218	0.231	0.257	0.283	0.308	0.334	0.360	0.386	0.411	0.514	0.643	0.771	0.900
49	109.6	55	1.06E+05	0.134	0.187	0.214	0.228	0.241	0.268	0.295	0.321	0.348	0.375	0.402	0.429	0.536	0.670	0.804	0.937
50	111.8		1.08E+05	0.139	0.195	0.223	0.237	0.251	0.279	0.307	0.335	0.363	0.390	0.418	0.446	0.558	0.697	0.837	0.976
51	114.1		1.10E+05	0.145	0.203	0.232	0.247	0.261	0.290	0.319	0.348	0.377	0.406	0.435	0.464	0.580	0.725	0.870	1.016
52	116.3		1.12E+05	0.151	0.211	0.241	0.256	0.271	0.302	0.332	0.362	0.392	0.422	0.452	0.483	0.603	0.754	0.905	1.056
53	118.6	60	1.15E+05	0.157	0.219	0.251	0.266	0.282	0.313	0.345	0.376	0.407	0.439	0.470	0.501	0.627	0.783	0.940	1.097
54	120.8		1.17E+05	0.163	0.228	0.260	0.276	0.293	0.325	0.358	0.390	0.423	0.455	0.488	0.520	0.651	0.813	0.976	1.139

DRAG FORCE CALCULATIONS FOR VARIOUS WIND TUNNEL FREESTREAM VELOCITIES AND DRAG COEFFICIENTS.

IMAGE 2

WIDTH (m)	HEIGHT (m)
0.114	0.12582

BLOCKAGE LESS THAN 10%

Diameter Dprojected (m)	0.114
Area Projected (m^2)	0.01021
Density (kg/m^3)	1.2
Mu ($N\text{-}s/m^2$)	1.80E-05
Kinematic Viscosity	1.50E-05

			Cd																
				0.5	0.7	0.8	0.85	0.9	1	1.1	1.2	1.3	1.4	1.5	1.6	2	2.5	3	3.5
Tunnel Speed				Force															
m/s	MPH	Hz	RE #	lbs	lbs	lbs	lbs	lbs	lbs	lbs	lbs	lbs	lbs	lbs	lbs	lbs	lbs	lbs	lbs
0	0.0		0.00E+00	0.000	0.000	0.000	0.000	0.000	0.000	0.000	0.000	0.000	0.000	0.000	0.000	0.000	0.000	0.000	0.000
1	2.2		7.60E+03	0.001	0.001	0.001	0.001	0.001	0.001	0.002	0.002	0.002	0.002	0.002	0.002	0.003	0.003	0.004	0.005
2	4.5	2	1.52E+04	0.003	0.004	0.004	0.005	0.005	0.006	0.006	0.007	0.007	0.008	0.008	0.009	0.011	0.014	0.017	0.019
3	6.7	2	2.28E+04	0.006	0.009	0.010	0.011	0.011	0.012	0.014	0.015	0.016	0.017	0.019	0.020	0.025	0.031	0.037	0.043
4	8.9	4	3.04E+04	0.011	0.015	0.018	0.019	0.020	0.022	0.024	0.026	0.029	0.031	0.033	0.035	0.044	0.055	0.066	0.077
5	11.2		3.80E+04	0.017	0.024	0.028	0.029	0.031	0.034	0.038	0.041	0.045	0.048	0.052	0.055	0.069	0.086	0.103	0.120
6	13.4		4.56E+04	0.025	0.035	0.040	0.042	0.045	0.050	0.055	0.059	0.064	0.069	0.074	0.079	0.099	0.124	0.149	0.173
7	15.7		5.32E+04	0.034	0.047	0.054	0.057	0.061	0.067	0.074	0.081	0.088	0.094	0.101	0.108	0.135	0.169	0.202	0.236
8	17.9		6.08E+04	0.044	0.062	0.070	0.075	0.079	0.088	0.097	0.106	0.115	0.123	0.132	0.141	0.176	0.220	0.264	0.308
9	20.1		6.84E+04	0.056	0.078	0.089	0.095	0.100	0.112	0.123	0.134	0.145	0.156	0.167	0.178	0.223	0.279	0.335	0.390
10	22.4		7.60E+04	0.069	0.096	0.110	0.117	0.124	0.138	0.151	0.165	0.179	0.193	0.207	0.220	0.275	0.344	0.413	0.482
11	24.6		8.36E+04	0.083	0.117	0.133	0.142	0.150	0.167	0.183	0.200	0.217	0.233	0.250	0.267	0.333	0.416	0.500	0.583
12	26.8		9.12E+04	0.099	0.139	0.159	0.169	0.178	0.198	0.218	0.238	0.258	0.278	0.297	0.317	0.397	0.496	0.595	0.694
13	29.1	15	9.88E+04	0.116	0.163	0.186	0.198	0.209	0.233	0.256	0.279	0.302	0.326	0.349	0.372	0.465	0.582	0.698	0.814
14	31.3		1.06E+05	0.135	0.189	0.216	0.229	0.243	0.270	0.297	0.324	0.351	0.378	0.405	0.432	0.540	0.675	0.810	0.944
15	33.6		1.14E+05	0.155	0.217	0.248	0.263	0.279	0.310	0.341	0.372	0.403	0.434	0.465	0.496	0.620	0.774	0.929	1.084
16	35.8		1.22E+05	0.176	0.247	0.282	0.300	0.317	0.352	0.388	0.423	0.458	0.493	0.529	0.564	0.705	0.881	1.057	1.234
17	38.0	20	1.29E+05	0.199	0.279	0.318	0.338	0.358	0.398	0.438	0.477	0.517	0.557	0.597	0.637	0.796	0.995	1.194	1.393
18	40.3		1.37E+05	0.223	0.312	0.357	0.379	0.401	0.446	0.491	0.535	0.580	0.625	0.669	0.714	0.892	1.115	1.338	1.561
19	42.5		1.44E+05	0.249	0.348	0.398	0.422	0.447	0.497	0.547	0.596	0.646	0.696	0.746	0.795	0.994	1.243	1.491	1.740
20	44.7		1.52E+05	0.275	0.385	0.441	0.468	0.496	0.551	0.606	0.661	0.716	0.771	0.826	0.881	1.101	1.377	1.652	1.927
21	47.0		1.60E+05	0.304	0.425	0.486	0.516	0.546	0.607	0.668	0.729	0.789	0.850	0.911	0.971	1.214	1.518	1.821	2.125
22	49.2	25	1.67E+05	0.333	0.466	0.533	0.566	0.600	0.666	0.733	0.800	0.866	0.933	1.000	1.066	1.333	1.666	1.999	2.332
23	51.4		1.75E+05	0.364	0.510	0.583	0.619	0.655	0.728	0.801	0.874	0.947	1.020	1.092	1.165	1.457	1.821	2.185	2.549
24	53.7		1.82E+05	0.397	0.555	0.634	0.674	0.714	0.793	0.872	0.952	1.031	1.110	1.190	1.269	1.586	1.983	2.379	2.776
25	55.9		1.90E+05	0.430	0.602	0.688	0.731	0.774	0.860	0.947	1.033	1.119	1.205	1.291	1.377	1.721	2.151	2.581	3.012
26	58.2	30	1.98E+05	0.465	0.651	0.745	0.791	0.838	0.931	1.024	1.117	1.210	1.303	1.396	1.489	1.861	2.327	2.792	3.257
27	60.4		2.05E+05	0.502	0.703	0.803	0.853	0.903	1.004	1.104	1.204	1.305	1.405	1.506	1.606	2.007	2.509	3.011	3.513
28	62.6		2.13E+05	0.540	0.756	0.864	0.917	0.971	1.079	1.187	1.295	1.403	1.511	1.619	1.727	2.159	2.698	3.238	3.778
29	64.9		2.20E+05	0.579	0.811	0.926	0.984	1.042	1.158	1.274	1.389	1.505	1.621	1.737	1.853	2.316	2.895	3.474	4.053
30	67.1		2.28E+05	0.620	0.867	0.991	1.053	1.115	1.239	1.363	1.487	1.611	1.735	1.859	1.983	2.478	3.098	3.717	4.337
31	69.3	35	2.36E+05	0.662	0.926	1.058	1.125	1.191	1.323	1.455	1.588	1.720	1.852	1.985	2.117	2.646	3.308	3.969	4.631
32	71.6		2.43E+05	0.705	0.987	1.128	1.198	1.269	1.410	1.551	1.692	1.833	1.974	2.115	2.256	2.820	3.525	4.229	4.934
33	73.8		2.51E+05	0.750	1.050	1.199	1.274	1.349	1.499	1.649	1.799	1.949	2.099	2.249	2.399	2.999	3.748	4.498	5.248
34	76.1		2.58E+05	0.796	1.114	1.273	1.353	1.432	1.592	1.751	1.910	2.069	2.228	2.387	2.546	3.183	3.979	4.775	5.570
35	78.3	40	2.66E+05	0.843	1.181	1.349	1.434	1.518	1.687	1.855	2.024	2.193	2.361	2.530	2.698	3.373	4.216	5.060	5.903
36	80.5		2.74E+05	0.892	1.249	1.427	1.517	1.606	1.784	1.963	2.141	2.320	2.498	2.676	2.855	3.569	4.461	5.353	6.245
37	82.8		2.81E+05	0.942	1.319	1.508	1.602	1.696	1.885	2.073	2.262	2.450	2.639	2.827	3.016	3.770	4.712	5.654	6.597
38	85.0		2.89E+05	0.994	1.392	1.590	1.690	1.789	1.988	2.187	2.386	2.584	2.783	2.982	3.181	3.976	4.970	5.964	6.958
39	87.2		2.96E+05	1.047	1.466	1.675	1.780	1.885	2.094	2.303	2.513	2.722	2.932	3.141	3.351	4.188	5.235	6.282	7.329
40	89.5	45	3.04E+05	1.101	1.542	1.762	1.872	1.983	2.203	2.423	2.643	2.864	3.084	3.304	3.525	4.406	5.507	6.609	7.710
41	91.7		3.12E+05	1.157	1.620	1.851	1.967	2.083	2.314	2.546	2.777	3.009	3.240	3.472	3.703	4.629	5.786	6.943	8.100
42	94.0		3.19E+05	1.214	1.700	1.943	2.064	2.186	2.429	2.672	2.914	3.157	3.400	3.643	3.886	4.857	6.072	7.286	8.500
43	96.2		3.27E+05	1.273	1.782	2.037	2.164	2.291	2.546	2.800	3.055	3.309	3.564	3.818	4.073	5.091	6.364	7.637	8.910
44	98.4	50	3.34E+05	1.333	1.866	2.132	2.266	2.399	2.665	2.932	3.199	3.465	3.732	3.998	4.265	5.331	6.664	7.996	9.329
45	100.7		3.42E+05	1.394	1.952	2.230	2.370	2.509	2.788	3.067	3.346	3.624	3.903	4.182	4.461	5.576	6.970	8.364	9.758
46	102.9		3.50E+05	1.457	2.039	2.331	2.476	2.622	2.913	3.205	3.496	3.787	4.079	4.370	4.661	5.827	7.283	8.740	10.196
47	105.1		3.57E+05	1.521	2.129	2.433	2.585	2.737	3.041	3.345	3.650	3.954	4.258	4.562	4.866	6.083	7.603	9.124	10.645
48	107.4		3.65E+05	1.586	2.220	2.538	2.696	2.855	3.172	3.489	3.807	4.124	4.441	4.758	5.075	6.344	7.930	9.516	11.102
49	109.6	55	3.72E+05	1.653	2.314	2.645	2.810	2.975	3.306	3.636	3.967	4.297	4.628	4.958	5.289	6.611	8.264	9.917	11.570
50	111.8		3.80E+05	1.721	2.409	2.754	2.926	3.098	3.442	3.786	4.130	4.475	4.819	5.163	5.507	6.884	8.605	10.326	12.047
51	114.1		3.88E+05	1.791	2.507	2.865	3.044	3.223	3.581	3.939	4.297	4.655	5.013	5.372	5.730	7.162	8.953	10.743	12.534
52	116.3		3.95E+05	1.861	2.606	2.978	3.164	3.351	3.723	4.095	4.467	4.840	5.212	5.584	5.956	7.446	9.307	11.168	13.030
53	118.6	60	4.03E+05	1.934	2.707	3.094	3.287	3.481	3.867	4.254	4.641	5.028	5.414	5.801	6.188	7.735	9.668	11.602	13.536
54	120.8		4.10E+05	2.007	2.810	3.212	3.412	3.613	4.015	4.416	4.818	5.219	5.621	6.022	6.424	8.029	10.037	12.044	14.051

DRAG FORCE CALCULATIONS FOR VARIOUS WIND TUNNEL FREESTREAM VELOCITIES AND DRAG COEFFICIENTS.

IMAGE 3

WIDTH (m)	HEIGHT (m)
0.13925	0.10544

BLOCKAGE LESS THAN 10%

Diameter Dprojected (m)	0.13925
Area Projected (m^2)	0.01523
Density (kg/m^3)	1.2
Mu ($N\text{-}s/m^2$)	1.80E-05
Kinematic Viscosity	1.50E-05

			Cd	0.5	0.7	0.8	0.85	0.9	1	1.1	1.2	1.3	1.4	1.5	1.6	2	2.5	3	3.5
Tunnel Speed				Force															
m/s	MPH	Hz	RE #	lbs	lbs	lbs	lbs	lbs	lbs	lbs	lbs	lbs	lbs	lbs	lbs	lbs	lbs	lbs	lbs
0	0.0		0.00E+00	0.000	0.000	0.000	0.000	0.000	0.000	0.000	0.000	0.000	0.000	0.000	0.000	0.000	0.000	0.000	0.000
1	2.2		9.28E+03	0.001	0.001	0.002	0.002	0.002	0.002	0.002	0.002	0.003	0.003	0.003	0.003	0.004	0.005	0.006	0.007
2	4.5	2	1.86E+04	0.004	0.006	0.007	0.007	0.007	0.008	0.009	0.010	0.011	0.012	0.012	0.013	0.016	0.021	0.025	0.029
3	6.7	2	2.79E+04	0.009	0.013	0.015	0.016	0.017	0.018	0.020	0.022	0.024	0.026	0.028	0.030	0.037	0.046	0.055	0.065
4	8.9	4	3.71E+04	0.016	0.023	0.026	0.028	0.030	0.033	0.036	0.039	0.043	0.046	0.049	0.053	0.066	0.082	0.099	0.115
5	11.2		4.64E+04	0.026	0.036	0.041	0.044	0.046	0.051	0.056	0.062	0.067	0.072	0.077	0.082	0.103	0.128	0.154	0.180
6	13.4		5.57E+04	0.037	0.052	0.059	0.063	0.067	0.074	0.081	0.089	0.096	0.104	0.111	0.118	0.148	0.185	0.222	0.259
7	15.7		6.50E+04	0.050	0.070	0.081	0.086	0.091	0.101	0.111	0.121	0.131	0.141	0.151	0.161	0.201	0.252	0.302	0.352
8	17.9		7.43E+04	0.066	0.092	0.105	0.112	0.118	0.131	0.145	0.158	0.171	0.184	0.197	0.210	0.263	0.329	0.394	0.460
9	20.1		8.36E+04	0.083	0.116	0.133	0.141	0.150	0.166	0.183	0.200	0.216	0.233	0.250	0.266	0.333	0.416	0.499	0.582
10	22.4		9.28E+04	0.103	0.144	0.164	0.175	0.185	0.205	0.226	0.247	0.267	0.288	0.308	0.329	0.411	0.514	0.616	0.719
11	24.6		1.02E+05	0.124	0.174	0.199	0.211	0.224	0.249	0.273	0.298	0.323	0.348	0.373	0.398	0.497	0.621	0.746	0.870
12	26.8		1.11E+05	0.148	0.207	0.237	0.251	0.266	0.296	0.325	0.355	0.385	0.414	0.444	0.473	0.592	0.740	0.887	1.035
13	29.1	15	1.21E+05	0.174	0.243	0.278	0.295	0.312	0.347	0.382	0.417	0.451	0.486	0.521	0.555	0.694	0.868	1.041	1.215
14	31.3		1.30E+05	0.201	0.282	0.322	0.342	0.362	0.403	0.443	0.483	0.523	0.564	0.604	0.644	0.805	1.007	1.208	1.409
15	33.6		1.39E+05	0.231	0.324	0.370	0.393	0.416	0.462	0.508	0.555	0.601	0.647	0.693	0.740	0.924	1.155	1.387	1.618
16	35.8		1.49E+05	0.263	0.368	0.421	0.447	0.473	0.526	0.578	0.631	0.684	0.736	0.789	0.841	1.052	1.315	1.578	1.841
17	38.0	20	1.58E+05	0.297	0.416	0.475	0.505	0.534	0.594	0.653	0.712	0.772	0.831	0.891	0.950	1.187	1.484	1.781	2.078
18	40.3		1.67E+05	0.333	0.466	0.532	0.566	0.599	0.666	0.732	0.799	0.865	0.932	0.998	1.065	1.331	1.664	1.997	2.329
19	42.5		1.76E+05	0.371	0.519	0.593	0.630	0.667	0.742	0.816	0.890	0.964	1.038	1.112	1.187	1.483	1.854	2.225	2.595
20	44.7		1.86E+05	0.411	0.575	0.657	0.698	0.740	0.822	0.904	0.986	1.068	1.150	1.233	1.315	1.643	2.054	2.465	2.876
21	47.0		1.95E+05	0.453	0.634	0.725	0.770	0.815	0.906	0.996	1.087	1.178	1.268	1.359	1.449	1.812	2.265	2.718	3.171
22	49.2	25	2.04E+05	0.497	0.696	0.795	0.845	0.895	0.994	1.094	1.193	1.293	1.392	1.491	1.591	1.988	2.486	2.983	3.480
23	51.4		2.14E+05	0.543	0.761	0.869	0.924	0.978	1.087	1.195	1.304	1.413	1.521	1.630	1.739	2.173	2.717	3.260	3.803
24	53.7		2.23E+05	0.592	0.828	0.947	1.006	1.065	1.183	1.302	1.420	1.538	1.657	1.775	1.893	2.366	2.958	3.550	4.141
25	55.9		2.32E+05	0.642	0.899	1.027	1.091	1.155	1.284	1.412	1.541	1.669	1.797	1.926	2.054	2.568	3.210	3.852	4.494
26	58.2	30	2.41E+05	0.694	0.972	1.111	1.180	1.250	1.389	1.528	1.666	1.805	1.944	2.083	2.222	2.777	3.472	4.166	4.860
27	60.4		2.51E+05	0.749	1.048	1.198	1.273	1.348	1.498	1.647	1.797	1.947	2.097	2.246	2.396	2.995	3.744	4.493	5.241
28	62.6		2.60E+05	0.805	1.127	1.288	1.369	1.449	1.611	1.772	1.933	2.094	2.255	2.416	2.577	3.221	4.026	4.832	5.637
29	64.9		2.69E+05	0.864	1.209	1.382	1.468	1.555	1.728	1.900	2.073	2.246	2.419	2.591	2.764	3.455	4.319	5.183	6.047
30	67.1		2.79E+05	0.924	1.294	1.479	1.571	1.664	1.849	2.034	2.219	2.403	2.588	2.773	2.958	3.698	4.622	5.546	6.471
31	69.3	35	2.88E+05	0.987	1.382	1.579	1.678	1.777	1.974	2.172	2.369	2.566	2.764	2.961	3.159	3.948	4.935	5.922	6.909
32	71.6		2.97E+05	1.052	1.472	1.683	1.788	1.893	2.104	2.314	2.524	2.735	2.945	3.155	3.366	4.207	5.259	6.311	7.362
33	73.8		3.06E+05	1.119	1.566	1.790	1.901	2.013	2.237	2.461	2.684	2.908	3.132	3.356	3.579	4.474	5.593	6.711	7.830
34	76.1		3.16E+05	1.187	1.662	1.900	2.018	2.137	2.375	2.612	2.850	3.087	3.325	3.562	3.799	4.749	5.937	7.124	8.311
35	78.3	40	3.25E+05	1.258	1.761	2.013	2.139	2.265	2.516	2.768	3.020	3.271	3.523	3.775	4.026	5.033	6.291	7.549	8.807
36	80.5		3.34E+05	1.331	1.864	2.130	2.263	2.396	2.662	2.928	3.195	3.461	3.727	3.993	4.260	5.325	6.656	7.987	9.318
37	82.8		3.43E+05	1.406	1.969	2.250	2.390	2.531	2.812	3.093	3.375	3.656	3.937	4.218	4.500	5.624	7.031	8.437	9.843
38	85.0		3.53E+05	1.483	2.076	2.373	2.521	2.670	2.966	3.263	3.560	3.856	4.153	4.449	4.746	5.933	7.416	8.899	10.382
39	87.2		3.62E+05	1.562	2.187	2.500	2.656	2.812	3.124	3.437	3.749	4.062	4.374	4.687	4.999	6.249	7.811	9.373	10.936
40	89.5	45	3.71E+05	1.643	2.301	2.629	2.794	2.958	3.287	3.615	3.944	4.273	4.601	4.930	5.259	6.573	8.217	9.860	11.504
41	91.7		3.81E+05	1.727	2.417	2.763	2.935	3.108	3.453	3.798	4.144	4.489	4.834	5.180	5.525	6.906	8.633	10.359	12.086
42	94.0		3.90E+05	1.812	2.537	2.899	3.080	3.261	3.624	3.986	4.348	4.711	5.073	5.435	5.798	7.247	9.059	10.871	12.683
43	96.2		3.99E+05	1.899	2.659	3.039	3.229	3.418	3.798	4.178	4.558	4.938	5.318	5.697	6.077	7.596	9.496	11.395	13.294
44	98.4	50	4.08E+05	1.988	2.784	3.182	3.380	3.579	3.977	4.375	4.772	5.170	5.568	5.965	6.363	7.954	9.942	11.931	13.919
45	100.7		4.18E+05	2.080	2.912	3.328	3.536	3.744	4.160	4.576	4.992	5.408	5.824	6.240	6.656	8.320	10.399	12.479	14.559
46	102.9		4.27E+05	2.173	3.043	3.477	3.695	3.912	4.347	4.781	5.216	5.651	6.085	6.520	6.955	8.693	10.867	13.040	15.213
47	105.1		4.36E+05	2.269	3.176	3.630	3.857	4.084	4.538	4.992	5.445	5.899	6.353	6.807	7.260	9.076	11.344	13.613	15.882
48	107.4		4.46E+05	2.366	3.313	3.786	4.023	4.260	4.733	5.206	5.679	6.153	6.626	7.099	7.573	9.466	11.832	14.199	16.565
49	109.6	55	4.55E+05	2.466	3.453	3.946	4.192	4.439	4.932	5.425	5.919	6.412	6.905	7.398	7.891	9.864	12.330	14.796	17.263
50	111.8		4.64E+05	2.568	3.595	4.108	4.365	4.622	5.136	5.649	6.163	6.676	7.190	7.703	8.217	10.271	12.839	15.407	17.974
51	114.1		4.73E+05	2.672	3.740	4.274	4.542	4.809	5.343	5.877	6.412	6.946	7.480	8.015	8.549	10.686	13.358	16.029	18.701
52	116.3		4.83E+05	2.777	3.888	4.444	4.721	4.999	5.555	6.110	6.666	7.221	7.776	8.332	8.887	11.109	13.886	16.664	19.441
53	118.6	60	4.92E+05	2.885	4.039	4.616	4.905	5.193	5.770	6.347	6.924	7.501	8.078	8.655	9.232	11.541	14.426	17.311	20.196
54	120.8		5.01E+05	2.995	4.193	4.792	5.092	5.391	5.990	6.589	7.188	7.787	8.386	8.985	9.584	11.980	14.975	17.970	20.965

DRAG FORCE CALCULATIONS FOR VARIOUS WIND TUNNEL FREESTREAM VELOCITIES AND DRAG COEFFICIENTS.

IMAGE 4

WIDTH (m)	HEIGHT (m)
0.18114	0.084179

BLOCKAGE LESS THAN 10%

Diameter Dprojected (m)	0.18114
Area Projected (m^2)	0.02577
Density (kg/m^3)	1.2
Mu ($N\text{-}s/m^2$)	1.80E-05
Kinematic Viscosity	1.50E-05

			Cd																
				0.5	0.7	0.8	0.85	0.9	1	1.1	1.2	1.3	1.4	1.5	1.6	2	2.5	3	3.5
Tunnel Speed				Force															
m/s	MPH	Hz	RE #	lbs	lbs	lbs	lbs	lbs	lbs	lbs	lbs	lbs	lbs	lbs	lbs	lbs	lbs	lbs	lbs
0	0.0		0.00E+00	0.000	0.000	0.000	0.000	0.000	0.000	0.000	0.000	0.000	0.000	0.000	0.000	0.000	0.000	0.000	0.000
1	2.2		1.21E+04	0.002	0.002	0.003	0.003	0.003	0.003	0.004	0.004	0.005	0.005	0.005	0.006	0.007	0.009	0.010	0.012
2	4.5	2	2.42E+04	0.007	0.010	0.011	0.012	0.013	0.014	0.015	0.017	0.018	0.019	0.021	0.022	0.028	0.035	0.042	0.049
3	6.7	2	3.62E+04	0.016	0.022	0.025	0.027	0.028	0.031	0.034	0.038	0.041	0.044	0.047	0.050	0.063	0.078	0.094	0.109
4	8.9	4	4.83E+04	0.028	0.039	0.044	0.047	0.050	0.056	0.061	0.067	0.072	0.078	0.083	0.089	0.111	0.139	0.167	0.195
5	11.2		6.04E+04	0.043	0.061	0.070	0.074	0.078	0.087	0.096	0.104	0.113	0.122	0.130	0.139	0.174	0.217	0.261	0.304
6	13.4		7.25E+04	0.063	0.088	0.100	0.106	0.113	0.125	0.138	0.150	0.163	0.175	0.188	0.200	0.250	0.313	0.375	0.438
7	15.7		8.45E+04	0.085	0.119	0.136	0.145	0.153	0.170	0.187	0.204	0.221	0.238	0.255	0.273	0.341	0.426	0.511	0.596
8	17.9		9.66E+04	0.111	0.156	0.178	0.189	0.200	0.222	0.245	0.267	0.289	0.311	0.334	0.356	0.445	0.556	0.667	0.779
9	20.1		1.09E+05	0.141	0.197	0.225	0.239	0.253	0.282	0.310	0.338	0.366	0.394	0.422	0.450	0.563	0.704	0.845	0.985
10	22.4		1.21E+05	0.174	0.243	0.278	0.295	0.313	0.348	0.382	0.417	0.452	0.487	0.521	0.556	0.695	0.869	1.043	1.217
11	24.6		1.33E+05	0.210	0.294	0.336	0.358	0.379	0.421	0.463	0.505	0.547	0.589	0.631	0.673	0.841	1.051	1.262	1.472
12	26.8		1.45E+05	0.250	0.350	0.400	0.425	0.450	0.501	0.551	0.601	0.651	0.701	0.751	0.801	1.001	1.251	1.502	1.752
13	29.1	15	1.57E+05	0.294	0.411	0.470	0.499	0.529	0.587	0.646	0.705	0.764	0.822	0.881	0.940	1.175	1.469	1.762	2.056
14	31.3		1.69E+05	0.341	0.477	0.545	0.579	0.613	0.681	0.749	0.818	0.886	0.954	1.022	1.090	1.363	1.703	2.044	2.385
15	33.6		1.81E+05	0.391	0.547	0.626	0.665	0.704	0.782	0.860	0.939	1.017	1.095	1.173	1.251	1.564	1.955	2.346	2.737
16	35.8		1.93E+05	0.445	0.623	0.712	0.756	0.801	0.890	0.979	1.068	1.157	1.246	1.335	1.424	1.780	2.225	2.670	3.115
17	38.0	20	2.05E+05	0.502	0.703	0.804	0.854	0.904	1.005	1.105	1.205	1.306	1.406	1.507	1.607	2.009	2.511	3.014	3.516
18	40.3		2.17E+05	0.563	0.788	0.901	0.957	1.014	1.126	1.239	1.351	1.464	1.577	1.689	1.802	2.252	2.816	3.379	3.942
19	42.5		2.29E+05	0.627	0.878	1.004	1.067	1.129	1.255	1.380	1.506	1.631	1.757	1.882	2.008	2.510	3.137	3.765	4.392
20	44.7		2.42E+05	0.695	0.973	1.112	1.182	1.251	1.390	1.529	1.668	1.808	1.947	2.086	2.225	2.781	3.476	4.171	4.866
21	47.0		2.54E+05	0.766	1.073	1.226	1.303	1.380	1.533	1.686	1.840	1.993	2.146	2.299	2.453	3.066	3.832	4.599	5.365
22	49.2	25	2.66E+05	0.841	1.178	1.346	1.430	1.514	1.682	1.851	2.019	2.187	2.355	2.524	2.692	3.365	4.206	5.047	5.888
23	51.4		2.78E+05	0.919	1.287	1.471	1.563	1.655	1.839	2.023	2.207	2.390	2.574	2.758	2.942	3.678	4.597	5.516	6.436
24	53.7		2.90E+05	1.001	1.402	1.602	1.702	1.802	2.002	2.202	2.403	2.603	2.803	3.003	3.204	4.004	5.005	6.007	7.008
25	55.9		3.02E+05	1.086	1.521	1.738	1.847	1.955	2.173	2.390	2.607	2.824	3.042	3.259	3.476	4.345	5.431	6.518	7.604
26	58.2	30	3.14E+05	1.175	1.645	1.880	1.997	2.115	2.350	2.585	2.820	3.055	3.290	3.525	3.760	4.700	5.874	7.049	8.224
27	60.4		3.26E+05	1.267	1.774	2.027	2.154	2.281	2.534	2.787	3.041	3.294	3.548	3.801	4.054	5.068	6.335	7.602	8.869
28	62.6		3.38E+05	1.363	1.908	2.180	2.316	2.453	2.725	2.998	3.270	3.543	3.815	4.088	4.360	5.450	6.813	8.176	9.538
29	64.9		3.50E+05	1.462	2.046	2.339	2.485	2.631	2.923	3.216	3.508	3.800	4.093	4.385	4.677	5.847	7.308	8.770	10.232
30	67.1		3.62E+05	1.564	2.190	2.503	2.659	2.816	3.128	3.441	3.754	4.067	4.380	4.693	5.005	6.257	7.821	9.385	10.949
31	69.3	35	3.74E+05	1.670	2.338	2.672	2.839	3.006	3.340	3.675	4.009	4.343	4.677	5.011	5.345	6.681	8.351	10.021	11.692
32	71.6		3.86E+05	1.780	2.492	2.848	3.026	3.204	3.559	3.915	4.271	4.627	4.983	5.339	5.695	7.119	8.899	10.678	12.458
33	73.8		3.99E+05	1.893	2.650	3.028	3.218	3.407	3.785	4.164	4.542	4.921	5.300	5.678	6.057	7.571	9.463	11.356	13.249
34	76.1		4.11E+05	2.009	2.813	3.215	3.416	3.616	4.018	4.420	4.822	5.224	5.626	6.027	6.429	8.037	10.046	12.055	14.064
35	78.3	40	4.23E+05	2.129	2.981	3.407	3.619	3.832	4.258	4.684	5.110	5.536	5.961	6.387	6.813	8.516	10.645	12.774	14.903
36	80.5		4.35E+05	2.252	3.153	3.604	3.829	4.054	4.505	4.955	5.406	5.856	6.307	6.757	7.208	9.010	11.262	13.515	15.767
37	82.8		4.47E+05	2.379	3.331	3.807	4.045	4.283	4.759	5.235	5.710	6.186	6.662	7.138	7.614	9.517	11.897	14.276	16.655
38	85.0		4.59E+05	2.510	3.514	4.016	4.266	4.517	5.019	5.521	6.023	6.525	7.027	7.529	8.031	10.039	12.548	15.058	17.568
39	87.2		4.71E+05	2.644	3.701	4.230	4.494	4.758	5.287	5.816	6.344	6.873	7.402	7.931	8.459	10.574	13.218	15.861	18.505
40	89.5	45	4.83E+05	2.781	3.893	4.449	4.727	5.005	5.562	6.118	6.674	7.230	7.786	8.342	8.899	11.123	13.904	16.685	19.466
41	91.7		4.95E+05	2.922	4.090	4.675	4.967	5.259	5.843	6.428	7.012	7.596	8.180	8.765	9.349	11.686	14.608	17.530	20.451
42	94.0		5.07E+05	3.066	4.292	4.905	5.212	5.519	6.132	6.745	7.358	7.971	8.584	9.198	9.811	12.263	15.329	18.395	21.461
43	96.2		5.19E+05	3.214	4.499	5.142	5.463	5.784	6.427	7.070	7.713	8.355	8.998	9.641	10.283	12.854	16.068	19.282	22.495
44	98.4	50	5.31E+05	3.365	4.711	5.384	5.720	6.057	6.730	7.403	8.076	8.748	9.421	10.094	10.767	13.459	16.824	20.189	23.554
45	100.7		5.43E+05	3.519	4.927	5.631	5.983	6.335	7.039	7.743	8.447	9.151	9.855	10.558	11.262	14.078	17.597	21.117	24.636
46	102.9		5.55E+05	3.678	5.149	5.884	6.252	6.620	7.355	8.091	8.826	9.562	10.297	11.033	11.768	14.711	18.388	22.066	25.743
47	105.1		5.68E+05	3.839	5.375	6.143	6.527	6.911	7.679	8.446	9.214	9.982	10.750	11.518	12.286	15.357	19.196	23.036	26.875
48	107.4		5.80E+05	4.004	5.606	6.407	6.807	7.208	8.009	8.810	9.611	10.411	11.212	12.013	12.814	16.018	20.022	24.026	28.031
49	109.6	55	5.92E+05	4.173	5.842	6.677	7.094	7.511	8.346	9.181	10.015	10.850	11.684	12.519	13.354	16.692	20.865	25.038	29.211
50	111.8		6.04E+05	4.345	6.083	6.952	7.387	7.821	8.690	9.559	10.428	11.297	12.166	13.035	13.904	17.380	21.725	26.070	30.415
51	114.1		6.16E+05	4.521	6.329	7.233	7.685	8.137	9.041	9.945	10.849	11.753	12.658	13.562	14.466	18.082	22.603	27.123	31.644
52	116.3		6.28E+05	4.700	6.579	7.519	7.989	8.459	9.399	10.339	11.279	12.219	13.159	14.099	15.039	18.798	23.498	28.198	32.897
53	118.6	60	6.40E+05	4.882	6.835	7.811	8.300	8.788	9.764	10.741	11.717	12.693	13.670	14.646	15.623	19.528	24.410	29.292	34.175
54	120.8		6.52E+05	5.068	7.095	8.109	8.616	9.122	10.136	11.150	12.163	13.177	14.191	15.204	16.218	20.272	25.340	30.408	35.476

DRAG FORCE CALCULATIONS FOR VARIOUS WIND TUNNEL FREESTREAM VELOCITIES AND DRAG COEFFICIENTS.

IMAGE 5

WIDTH (m)	HEIGHT (m)
0.21581	0.08114

BLOCKAGE LESS THAN 10%

Diameter Dprojected (m)	0.21581
Area Projected (m^2)	0.03658
Density (kg/m^3)	1.2
Mu ($N\text{-}s/m^2$)	1.80E-05
Kinematic Viscosity	1.50E-05

			Cd																
				0.5	0.7	0.8	0.85	0.9	1	1.1	1.2	1.3	1.4	1.5	1.6	2	2.5	3	3.5
Tunnel Speed				Force															
m/s	MPH	Hz	RE #	lbs	lbs	lbs	lbs	lbs	lbs	lbs	lbs	lbs	lbs	lbs	lbs	lbs	lbs	lbs	lbs
0	0.0		0.00E+00	0.000	0.000	0.000	0.000	0.000	0.000	0.000	0.000	0.000	0.000	0.000	0.000	0.000	0.000	0.000	0.000
1	2.2		1.44E+04	0.002	0.003	0.004	0.004	0.004	0.005	0.005	0.006	0.006	0.007	0.007	0.008	0.010	0.012	0.015	0.017
2	4.5	2	2.88E+04	0.010	0.014	0.016	0.017	0.018	0.020	0.022	0.024	0.026	0.028	0.030	0.032	0.039	0.049	0.059	0.069
3	6.7	2	4.32E+04	0.022	0.031	0.036	0.038	0.040	0.044	0.049	0.053	0.058	0.062	0.067	0.071	0.089	0.111	0.133	0.155
4	8.9	4	5.75E+04	0.039	0.055	0.063	0.067	0.071	0.079	0.087	0.095	0.103	0.111	0.118	0.126	0.158	0.197	0.237	0.276
5	11.2		7.19E+04	0.062	0.086	0.099	0.105	0.111	0.123	0.136	0.148	0.160	0.173	0.185	0.197	0.247	0.308	0.370	0.432
6	13.4		8.63E+04	0.089	0.124	0.142	0.151	0.160	0.178	0.195	0.213	0.231	0.249	0.266	0.284	0.355	0.444	0.533	0.622
7	15.7		1.01E+05	0.121	0.169	0.193	0.206	0.218	0.242	0.266	0.290	0.314	0.338	0.363	0.387	0.484	0.604	0.725	0.846
8	17.9		1.15E+05	0.158	0.221	0.253	0.268	0.284	0.316	0.347	0.379	0.411	0.442	0.474	0.505	0.632	0.789	0.947	1.105
9	20.1		1.29E+05	0.200	0.280	0.320	0.340	0.360	0.400	0.440	0.480	0.520	0.560	0.599	0.639	0.799	0.999	1.199	1.399
10	22.4		1.44E+05	0.247	0.345	0.395	0.419	0.444	0.493	0.543	0.592	0.641	0.691	0.740	0.789	0.987	1.233	1.480	1.727
11	24.6		1.58E+05	0.299	0.418	0.478	0.507	0.537	0.597	0.657	0.716	0.776	0.836	0.896	0.955	1.194	1.493	1.791	2.090
12	26.8		1.73E+05	0.355	0.497	0.568	0.604	0.639	0.710	0.782	0.853	0.924	0.995	1.066	1.137	1.421	1.776	2.131	2.487
13	29.1	15	1.87E+05	0.417	0.584	0.667	0.709	0.750	0.834	0.917	1.001	1.084	1.167	1.251	1.334	1.668	2.085	2.502	2.918
14	31.3		2.01E+05	0.484	0.677	0.774	0.822	0.870	0.967	1.064	1.160	1.257	1.354	1.451	1.547	1.934	2.418	2.901	3.385
15	33.6		2.16E+05	0.555	0.777	0.888	0.944	0.999	1.110	1.221	1.332	1.443	1.554	1.665	1.776	2.220	2.775	3.330	3.886
16	35.8		2.30E+05	0.632	0.884	1.010	1.074	1.137	1.263	1.389	1.516	1.642	1.768	1.895	2.021	2.526	3.158	3.789	4.421
17	38.0	20	2.45E+05	0.713	0.998	1.141	1.212	1.283	1.426	1.569	1.711	1.854	1.996	2.139	2.281	2.852	3.565	4.278	4.991
18	40.3		2.59E+05	0.799	1.119	1.279	1.359	1.439	1.599	1.758	1.918	2.078	2.238	2.398	2.558	3.197	3.997	4.796	5.595
19	42.5		2.73E+05	0.891	1.247	1.425	1.514	1.603	1.781	1.959	2.137	2.316	2.494	2.672	2.850	3.562	4.453	5.344	6.234
20	44.7		2.88E+05	0.987	1.382	1.579	1.678	1.776	1.974	2.171	2.368	2.566	2.763	2.960	3.158	3.947	4.934	5.921	6.908
21	47.0		3.02E+05	1.088	1.523	1.741	1.850	1.958	2.176	2.393	2.611	2.829	3.046	3.264	3.481	4.352	5.440	6.528	7.616
22	49.2	25	3.17E+05	1.194	1.672	1.910	2.030	2.149	2.388	2.627	2.866	3.104	3.343	3.582	3.821	4.776	5.970	7.164	8.358
23	51.4		3.31E+05	1.305	1.827	2.088	2.219	2.349	2.610	2.871	3.132	3.393	3.654	3.915	4.176	5.220	6.525	7.830	9.135
24	53.7		3.45E+05	1.421	1.989	2.274	2.416	2.558	2.842	3.126	3.410	3.695	3.979	4.263	4.547	5.684	7.105	8.526	9.947
25	55.9		3.60E+05	1.542	2.159	2.467	2.621	2.775	3.084	3.392	3.700	4.009	4.317	4.626	4.934	6.167	7.709	9.251	10.793
26	58.2	30	3.74E+05	1.668	2.335	2.668	2.835	3.002	3.335	3.669	4.002	4.336	4.670	5.003	5.337	6.671	8.338	10.006	11.674
27	60.4		3.88E+05	1.798	2.518	2.878	3.057	3.237	3.597	3.957	4.316	4.676	5.036	5.395	5.755	7.194	8.992	10.791	12.589
28	62.6		4.03E+05	1.934	2.708	3.095	3.288	3.481	3.868	4.255	4.642	5.029	5.416	5.802	6.189	7.736	9.671	11.605	13.539
29	64.9		4.17E+05	2.075	2.905	3.320	3.527	3.735	4.149	4.564	4.979	5.394	5.809	6.224	6.639	8.299	10.374	12.448	14.523
30	67.1		4.32E+05	2.220	3.108	3.552	3.774	3.997	4.441	4.885	5.329	5.773	6.217	6.661	7.105	8.881	11.101	13.322	15.542
31	69.3	35	4.46E+05	2.371	3.319	3.793	4.030	4.267	4.742	5.216	5.690	6.164	6.638	7.112	7.586	9.483	11.854	14.225	16.595
32	71.6		4.60E+05	2.526	3.537	4.042	4.295	4.547	5.052	5.558	6.063	6.568	7.073	7.579	8.084	10.105	12.631	15.157	17.683
33	73.8		4.75E+05	2.687	3.761	4.298	4.567	4.836	5.373	5.910	6.448	6.985	7.522	8.060	8.597	10.746	13.433	16.119	18.806
34	76.1		4.89E+05	2.852	3.993	4.563	4.848	5.133	5.704	6.274	6.844	7.415	7.985	8.556	9.126	11.407	14.259	17.111	19.963
35	78.3	40	5.04E+05	3.022	4.231	4.835	5.138	5.440	6.044	6.649	7.253	7.857	8.462	9.066	9.671	12.088	15.110	18.132	21.154
36	80.5		5.18E+05	3.197	4.476	5.116	5.435	5.755	6.394	7.034	7.673	8.313	8.952	9.592	10.231	12.789	15.986	19.183	22.381
37	82.8		5.32E+05	3.377	4.728	5.404	5.741	6.079	6.755	7.430	8.106	8.781	9.456	10.132	10.807	13.509	16.887	20.264	23.641
38	85.0		5.47E+05	3.562	4.987	5.700	6.056	6.412	7.125	7.837	8.550	9.262	9.975	10.687	11.399	14.249	17.812	21.374	24.936
39	87.2		5.61E+05	3.752	5.253	6.004	6.379	6.754	7.505	8.255	9.006	9.756	10.506	11.257	12.007	15.009	18.761	22.514	26.266
40	89.5	45	5.75E+05	3.947	5.526	6.316	6.710	7.105	7.894	8.684	9.473	10.263	11.052	11.842	12.631	15.789	19.736	23.683	27.630
41	91.7		5.90E+05	4.147	5.806	6.635	7.050	7.465	8.294	9.123	9.953	10.782	11.612	12.441	13.270	16.588	20.735	24.882	29.029
42	94.0		6.04E+05	4.352	6.092	6.963	7.398	7.833	8.704	9.574	10.444	11.315	12.185	13.055	13.926	17.407	21.759	26.111	30.462
43	96.2		6.19E+05	4.561	6.386	7.298	7.754	8.211	9.123	10.035	10.948	11.860	12.772	13.684	14.597	18.246	22.807	27.369	31.930
44	98.4	50	6.33E+05	4.776	6.687	7.642	8.119	8.597	9.552	10.507	11.463	12.418	13.373	14.328	15.284	19.104	23.880	28.657	33.433
45	100.7		6.47E+05	4.996	6.994	7.993	8.493	8.992	9.991	10.990	11.990	12.989	13.988	14.987	15.986	19.983	24.978	29.974	34.970
46	102.9		6.62E+05	5.220	7.308	8.352	8.874	9.396	10.440	11.484	12.528	13.572	14.616	15.660	16.705	20.881	26.101	31.321	36.541
47	105.1		6.76E+05	5.450	7.629	8.719	9.264	9.809	10.899	11.989	13.079	14.169	15.259	16.349	17.439	21.798	27.248	32.698	38.147
48	107.4		6.91E+05	5.684	7.958	9.094	9.663	10.231	11.368	12.505	13.641	14.778	15.915	17.052	18.189	22.736	28.420	34.104	39.788
49	109.6	55	7.05E+05	5.923	8.293	9.477	10.070	10.662	11.846	13.031	14.216	15.400	16.585	17.770	18.954	23.693	29.616	35.539	41.463
50	111.8		7.19E+05	6.167	8.634	9.868	10.485	11.101	12.335	13.568	14.802	16.035	17.269	18.502	19.736	24.670	30.837	37.005	43.172
51	114.1		7.34E+05	6.417	8.983	10.267	10.908	11.550	12.833	14.117	15.400	16.683	17.967	19.250	20.533	25.667	32.083	38.500	44.917
52	116.3		7.48E+05	6.671	9.339	10.673	11.340	12.007	13.341	14.676	16.010	17.344	18.678	20.012	21.346	26.683	33.354	40.024	46.695
53	118.6	60	7.63E+05	6.930	9.702	11.088	11.781	12.474	13.860	15.246	16.631	18.017	19.403	20.789	22.175	27.719	34.649	41.579	48.508
54	120.8		7.77E+05	7.194	10.071	11.510	12.229	12.949	14.388	15.826	17.265	18.704	20.143	21.581	23.020	28.775	35.969	43.163	50.356

DRAG FORCE CALCULATIONS FOR VARIOUS WIND TUNNEL FREESTREAM VELOCITIES AND DRAG COEFFICIENTS.

IMAGE 6

WIDTH (m)	HEIGHT (m)
0.22357	0.0624

BLOCKAGE LESS THAN 10%

Diameter Dprojected (m)	0.22357
Area Projected (m^2)	0.03926
Density (kg/m^3)	1.2
Mu ($N\text{-}s/m^2$)	1.80E-05
Kinematic Viscosity	1.50E-05

				Cd															
				0.5	0.7	0.8	0.85	0.9	1	1.1	1.2	1.3	1.4	1.5	1.6	2	2.5	3	3.5
Tunnel Speed				Force															
m/s	MPH	Hz	RE #	lbs	lbs	lbs	lbs	lbs	lbs	lbs	lbs	lbs	lbs	lbs	lbs	lbs	lbs	lbs	lbs
0	0.0		0.00E+00	0.000	0.000	0.000	0.000	0.000	0.000	0.000	0.000	0.000	0.000	0.000	0.000	0.000	0.000	0.000	0.000
1	2.2		1.49E+04	0.003	0.004	0.004	0.005	0.005	0.005	0.006	0.006	0.007	0.007	0.008	0.008	0.011	0.013	0.016	0.019
2	4.5	2	2.98E+04	0.011	0.015	0.017	0.018	0.019	0.021	0.023	0.025	0.028	0.030	0.032	0.034	0.042	0.053	0.064	0.074
3	6.7	2	4.47E+04	0.024	0.033	0.038	0.041	0.043	0.048	0.052	0.057	0.062	0.067	0.071	0.076	0.095	0.119	0.143	0.167
4	8.9	4	5.96E+04	0.042	0.059	0.068	0.072	0.076	0.085	0.093	0.102	0.110	0.119	0.127	0.136	0.169	0.212	0.254	0.297
5	11.2		7.45E+04	0.066	0.093	0.106	0.113	0.119	0.132	0.146	0.159	0.172	0.185	0.199	0.212	0.265	0.331	0.397	0.463
6	13.4		8.94E+04	0.095	0.133	0.153	0.162	0.172	0.191	0.210	0.229	0.248	0.267	0.286	0.305	0.381	0.477	0.572	0.667
7	15.7		1.04E+05	0.130	0.182	0.208	0.221	0.234	0.259	0.285	0.311	0.337	0.363	0.389	0.415	0.519	0.649	0.778	0.908
8	17.9		1.19E+05	0.169	0.237	0.271	0.288	0.305	0.339	0.373	0.407	0.441	0.474	0.508	0.542	0.678	0.847	1.017	1.186
9	20.1		1.34E+05	0.214	0.300	0.343	0.365	0.386	0.429	0.472	0.515	0.558	0.600	0.643	0.686	0.858	1.072	1.287	1.501
10	22.4		1.49E+05	0.265	0.371	0.424	0.450	0.477	0.530	0.582	0.635	0.688	0.741	0.794	0.847	1.059	1.324	1.589	1.853
11	24.6		1.64E+05	0.320	0.449	0.513	0.545	0.577	0.641	0.705	0.769	0.833	0.897	0.961	1.025	1.281	1.602	1.922	2.243
12	26.8		1.79E+05	0.381	0.534	0.610	0.648	0.686	0.763	0.839	0.915	0.991	1.068	1.144	1.220	1.525	1.906	2.288	2.669
13	29.1	15	1.94E+05	0.447	0.626	0.716	0.761	0.805	0.895	0.984	1.074	1.163	1.253	1.342	1.432	1.790	2.237	2.685	3.132
14	31.3		2.09E+05	0.519	0.727	0.830	0.882	0.934	1.038	1.142	1.245	1.349	1.453	1.557	1.661	2.076	2.595	3.114	3.633
15	33.6		2.24E+05	0.596	0.834	0.953	1.013	1.072	1.191	1.311	1.430	1.549	1.668	1.787	1.906	2.383	2.979	3.574	4.170
16	35.8		2.38E+05	0.678	0.949	1.084	1.152	1.220	1.356	1.491	1.627	1.762	1.898	2.033	2.169	2.711	3.389	4.067	4.744
17	38.0	20	2.53E+05	0.765	1.071	1.224	1.301	1.377	1.530	1.683	1.836	1.989	2.142	2.295	2.448	3.061	3.826	4.591	5.356
18	40.3		2.68E+05	0.858	1.201	1.373	1.458	1.544	1.716	1.887	2.059	2.230	2.402	2.573	2.745	3.431	4.289	5.147	6.005
19	42.5		2.83E+05	0.956	1.338	1.529	1.625	1.720	1.912	2.103	2.294	2.485	2.676	2.867	3.059	3.823	4.779	5.735	6.690
20	44.7		2.98E+05	1.059	1.483	1.694	1.800	1.906	2.118	2.330	2.542	2.754	2.965	3.177	3.389	4.236	5.295	6.354	7.413
21	47.0		3.13E+05	1.168	1.635	1.868	1.985	2.102	2.335	2.569	2.802	3.036	3.269	3.503	3.736	4.670	5.838	7.006	8.173
22	49.2	25	3.28E+05	1.281	1.794	2.050	2.178	2.307	2.563	2.819	3.075	3.332	3.588	3.844	4.101	5.126	6.407	7.689	8.970
23	51.4		3.43E+05	1.401	1.961	2.241	2.381	2.521	2.801	3.081	3.361	3.642	3.922	4.202	4.482	5.602	7.003	8.403	9.804
24	53.7		3.58E+05	1.525	2.135	2.440	2.593	2.745	3.050	3.355	3.660	3.965	4.270	4.575	4.880	6.100	7.625	9.150	10.675
25	55.9		3.73E+05	1.655	2.317	2.648	2.813	2.979	3.309	3.640	3.971	4.302	4.633	4.964	5.295	6.619	8.274	9.928	11.583
26	58.2	30	3.88E+05	1.790	2.506	2.864	3.043	3.222	3.580	3.938	4.295	4.653	5.011	5.369	5.727	7.159	8.949	10.739	12.528
27	60.4		4.02E+05	1.930	2.702	3.088	3.281	3.474	3.860	4.246	4.632	5.018	5.404	5.790	6.176	7.720	9.650	11.581	13.511
28	62.6		4.17E+05	2.076	2.906	3.321	3.529	3.736	4.151	4.567	4.982	5.397	5.812	6.227	6.642	8.303	10.379	12.454	14.530
29	64.9		4.32E+05	2.227	3.117	3.563	3.785	4.008	4.453	4.899	5.344	5.789	6.235	6.680	7.125	8.907	11.133	13.360	15.586
30	67.1		4.47E+05	2.383	3.336	3.813	4.051	4.289	4.766	5.242	5.719	6.195	6.672	7.149	7.625	9.531	11.914	14.297	16.680
31	69.3	35	4.62E+05	2.544	3.562	4.071	4.325	4.580	5.089	5.598	6.106	6.615	7.124	7.633	8.142	10.177	12.722	15.266	17.810
32	71.6		4.77E+05	2.711	3.796	4.338	4.609	4.880	5.422	5.965	6.507	7.049	7.591	8.133	8.676	10.845	13.556	16.267	18.978
33	73.8		4.92E+05	2.883	4.037	4.613	4.901	5.190	5.766	6.343	6.920	7.496	8.073	8.650	9.226	11.533	14.416	17.299	20.183
34	76.1		5.07E+05	3.061	4.285	4.897	5.203	5.509	6.121	6.733	7.345	7.958	8.570	9.182	9.794	12.242	15.303	18.364	21.424
35	78.3	40	5.22E+05	3.243	4.541	5.189	5.514	5.838	6.487	7.135	7.784	8.433	9.081	9.730	10.379	12.973	16.217	19.460	22.703
36	80.5		5.37E+05	3.431	4.804	5.490	5.833	6.176	6.863	7.549	8.235	8.921	9.608	10.294	10.980	13.725	17.156	20.588	24.019
37	82.8		5.51E+05	3.625	5.074	5.799	6.162	6.524	7.249	7.974	8.699	9.424	10.149	10.874	11.599	14.498	18.123	21.747	25.372
38	85.0		5.66E+05	3.823	5.352	6.117	6.499	6.882	7.646	8.411	9.176	9.940	10.705	11.469	12.234	15.293	19.116	22.939	26.762
39	87.2		5.81E+05	4.027	5.638	6.443	6.846	7.249	8.054	8.859	9.665	10.470	11.276	12.081	12.886	16.108	20.135	24.162	28.189
40	89.5	45	5.96E+05	4.236	5.931	6.778	7.201	7.625	8.472	9.320	10.167	11.014	11.861	12.708	13.556	16.945	21.181	25.417	29.653
41	91.7		6.11E+05	4.451	6.231	7.121	7.566	8.011	8.901	9.791	10.681	11.572	12.462	13.352	14.242	17.802	22.253	26.704	31.154
42	94.0		6.26E+05	4.670	6.539	7.473	7.940	8.407	9.341	10.275	11.209	12.143	13.077	14.011	14.945	18.681	23.352	28.022	32.693
43	96.2		6.41E+05	4.895	6.854	7.833	8.322	8.812	9.791	10.770	11.749	12.728	13.707	14.686	15.665	19.582	24.477	29.372	34.268
44	98.4	50	6.56E+05	5.126	7.176	8.201	8.714	9.226	10.251	11.277	12.302	13.327	14.352	15.377	16.402	20.503	25.629	30.754	35.880
45	100.7		6.71E+05	5.361	7.506	8.578	9.114	9.650	10.723	11.795	12.867	13.940	15.012	16.084	17.156	21.446	26.807	32.168	37.530
46	102.9		6.86E+05	5.602	7.843	8.964	9.524	10.084	11.205	12.325	13.446	14.566	15.686	16.807	17.927	22.409	28.012	33.614	39.216
47	105.1		7.01E+05	5.849	8.188	9.358	9.943	10.527	11.697	12.867	14.036	15.206	16.376	17.546	18.715	23.394	29.243	35.091	40.940
48	107.4		7.15E+05	6.100	8.540	9.760	10.370	10.980	12.200	13.420	14.640	15.860	17.080	18.300	19.520	24.400	30.500	36.600	42.700
49	109.6	55	7.30E+05	6.357	8.900	10.171	10.807	11.442	12.714	13.985	15.257	16.528	17.799	19.071	20.342	25.428	31.784	38.141	44.498
50	111.8		7.45E+05	6.619	9.267	10.590	11.252	11.914	13.238	14.562	15.886	17.209	18.533	19.857	21.181	26.476	33.095	39.714	46.333
51	114.1		7.60E+05	6.886	9.641	11.018	11.707	12.396	13.773	15.150	16.527	17.905	19.282	20.659	22.036	27.546	34.432	41.318	48.205
52	116.3		7.75E+05	7.159	10.023	11.455	12.170	12.886	14.318	15.750	17.182	18.614	20.045	21.477	22.909	28.636	35.796	42.955	50.114
53	118.6	60	7.90E+05	7.437	10.412	11.899	12.643	13.387	14.874	16.362	17.849	19.336	20.824	22.311	23.799	29.748	37.185	44.623	52.060
54	120.8		8.05E+05	7.720	10.809	12.353	13.125	13.897	15.441	16.985	18.529	20.073	21.617	23.161	24.705	30.882	38.602	46.322	54.043

r

DRAG FORCE CALCULATIONS FOR VARIOUS WIND TUNNEL FREESTREAM VELOCITIES AND DRAG COEFFICIENTS.

IMAGE 7

WIDTH (m)	HEIGHT (m)
0.23301	0.05474

BLOCKAGE LESS THAN 10%

Diameter Dprojected (m)	0.23301
Area Projected (m^2)	0.04264
Density (kg/m^3)	1.2
Mu ($N\text{-}s/m^2$)	1.80E-05
Kinematic Viscosity	1.50E-05

				Cd															
				0.5	0.7	0.8	0.85	0.9	1	1.1	1.2	1.3	1.4	1.5	1.6	2	2.5	3	3.5
Tunnel Speed				Force															
m/s	MPH	Hz	RE #	lbs	lbs	lbs	lbs	lbs	lbs	lbs	lbs	lbs	lbs	lbs	lbs	lbs	lbs	lbs	lbs
0	0.0		0.00E+00	0.000	0.000	0.000	0.000	0.000	0.000	0.000	0.000	0.000	0.000	0.000	0.000	0.000	0.000	0.000	0.000
1	2.2		1.55E+04	0.003	0.004	0.005	0.005	0.005	0.006	0.006	0.007	0.007	0.008	0.009	0.009	0.012	0.014	0.017	0.020
2	4.5	2	3.11E+04	0.012	0.016	0.018	0.020	0.021	0.023	0.025	0.028	0.030	0.032	0.035	0.037	0.046	0.058	0.069	0.081
3	6.7	2	4.66E+04	0.026	0.036	0.041	0.044	0.047	0.052	0.057	0.062	0.067	0.072	0.078	0.083	0.104	0.129	0.155	0.181
4	8.9	4	6.21E+04	0.046	0.064	0.074	0.078	0.083	0.092	0.101	0.110	0.120	0.129	0.138	0.147	0.184	0.230	0.276	0.322
5	11.2		7.77E+04	0.072	0.101	0.115	0.122	0.129	0.144	0.158	0.173	0.187	0.201	0.216	0.230	0.288	0.359	0.431	0.503
6	13.4		9.32E+04	0.104	0.145	0.166	0.176	0.186	0.207	0.228	0.248	0.269	0.290	0.311	0.331	0.414	0.518	0.621	0.725
7	15.7		1.09E+05	0.141	0.197	0.225	0.240	0.254	0.282	0.310	0.338	0.366	0.395	0.423	0.451	0.564	0.705	0.846	0.986
8	17.9		1.24E+05	0.184	0.258	0.294	0.313	0.331	0.368	0.405	0.442	0.479	0.515	0.552	0.589	0.736	0.920	1.104	1.288
9	20.1		1.40E+05	0.233	0.326	0.373	0.396	0.419	0.466	0.512	0.559	0.606	0.652	0.699	0.745	0.932	1.165	1.398	1.631
10	22.4		1.55E+05	0.288	0.403	0.460	0.489	0.518	0.575	0.633	0.690	0.748	0.805	0.863	0.920	1.150	1.438	1.726	2.013
11	24.6		1.71E+05	0.348	0.487	0.557	0.592	0.626	0.696	0.766	0.835	0.905	0.974	1.044	1.114	1.392	1.740	2.088	2.436
12	26.8		1.86E+05	0.414	0.580	0.663	0.704	0.745	0.828	0.911	0.994	1.077	1.160	1.242	1.325	1.657	2.071	2.485	2.899
13	29.1	15	2.02E+05	0.486	0.680	0.778	0.826	0.875	0.972	1.069	1.166	1.264	1.361	1.458	1.555	1.944	2.430	2.916	3.402
14	31.3		2.17E+05	0.564	0.789	0.902	0.958	1.015	1.127	1.240	1.353	1.466	1.578	1.691	1.804	2.255	2.818	3.382	3.946
15	33.6		2.33E+05	0.647	0.906	1.035	1.100	1.165	1.294	1.424	1.553	1.682	1.812	1.941	2.071	2.588	3.235	3.882	4.530
16	35.8		2.49E+05	0.736	1.031	1.178	1.252	1.325	1.472	1.620	1.767	1.914	2.061	2.209	2.356	2.945	3.681	4.417	5.154
17	38.0	20	2.64E+05	0.831	1.164	1.330	1.413	1.496	1.662	1.828	1.995	2.161	2.327	2.493	2.660	3.325	4.156	4.987	5.818
18	40.3		2.80E+05	0.932	1.305	1.491	1.584	1.677	1.864	2.050	2.236	2.423	2.609	2.795	2.982	3.727	4.659	5.591	6.523
19	42.5		2.95E+05	1.038	1.453	1.661	1.765	1.869	2.076	2.284	2.492	2.699	2.907	3.115	3.322	4.153	5.191	6.229	7.267
20	44.7		3.11E+05	1.150	1.611	1.841	1.956	2.071	2.301	2.531	2.761	2.991	3.221	3.451	3.681	4.601	5.752	6.902	8.053
21	47.0		3.26E+05	1.268	1.776	2.029	2.156	2.283	2.537	2.790	3.044	3.298	3.551	3.805	4.058	5.073	6.341	7.610	8.878
22	49.2	25	3.42E+05	1.392	1.949	2.227	2.366	2.505	2.784	3.062	3.341	3.619	3.897	4.176	4.454	5.568	6.960	8.352	9.744
23	51.4		3.57E+05	1.521	2.130	2.434	2.586	2.738	3.043	3.347	3.651	3.956	4.260	4.564	4.868	6.085	7.607	9.128	10.649
24	53.7		3.73E+05	1.657	2.319	2.650	2.816	2.982	3.313	3.644	3.976	4.307	4.638	4.970	5.301	6.626	8.283	9.939	11.596
25	55.9		3.88E+05	1.797	2.516	2.876	3.056	3.235	3.595	3.954	4.314	4.673	5.033	5.392	5.752	7.190	8.987	10.785	12.582
26	58.2	30	4.04E+05	1.944	2.722	3.111	3.305	3.499	3.888	4.277	4.666	5.055	5.444	5.832	6.221	7.776	9.721	11.665	13.609
27	60.4		4.19E+05	2.097	2.935	3.354	3.564	3.774	4.193	4.612	5.032	5.451	5.870	6.290	6.709	8.386	10.483	12.579	14.676
28	62.6		4.35E+05	2.255	3.157	3.608	3.833	4.058	4.509	4.960	5.411	5.862	6.313	6.764	7.215	9.019	11.274	13.528	15.783
29	64.9		4.50E+05	2.419	3.386	3.870	4.112	4.354	4.837	5.321	5.805	6.288	6.772	7.256	7.740	9.675	12.093	14.512	16.930
30	67.1		4.66E+05	2.588	3.624	4.141	4.400	4.659	5.177	5.694	6.212	6.730	7.247	7.765	8.283	10.353	12.942	15.530	18.118
31	69.3	35	4.82E+05	2.764	3.869	4.422	4.698	4.975	5.527	6.080	6.633	7.186	7.738	8.291	8.844	11.055	13.819	16.582	19.346
32	71.6		4.97E+05	2.945	4.123	4.712	5.006	5.301	5.890	6.479	7.068	7.657	8.246	8.835	9.424	11.780	14.725	17.670	20.614
33	73.8		5.13E+05	3.132	4.385	5.011	5.324	5.637	6.264	6.890	7.516	8.143	8.769	9.396	10.022	12.527	15.659	18.791	21.923
34	76.1		5.28E+05	3.325	4.654	5.319	5.652	5.984	6.649	7.314	7.979	8.644	9.309	9.974	10.639	13.298	16.623	19.947	23.272
35	78.3	40	5.44E+05	3.523	4.932	5.637	5.989	6.341	7.046	7.751	8.455	9.160	9.864	10.569	11.274	14.092	17.615	21.138	24.661
36	80.5		5.59E+05	3.727	5.218	5.963	6.336	6.709	7.454	8.200	8.945	9.691	10.436	11.182	11.927	14.909	18.636	22.363	26.090
37	82.8		5.75E+05	3.937	5.512	6.299	6.693	7.087	7.874	8.662	9.449	10.236	11.024	11.811	12.599	15.748	19.686	23.623	27.560
38	85.0		5.90E+05	4.153	5.814	6.644	7.060	7.475	8.306	9.136	9.967	10.797	11.628	12.458	13.289	16.611	20.764	24.917	29.070
39	87.2		6.06E+05	4.374	6.124	6.999	7.436	7.874	8.748	9.623	10.498	11.373	12.248	13.123	13.998	17.497	21.871	26.245	30.620
40	89.5	45	6.21E+05	4.601	6.442	7.362	7.822	8.283	9.203	10.123	11.043	11.964	12.884	13.804	14.725	18.406	23.007	27.609	32.210
41	91.7		6.37E+05	4.834	6.768	7.735	8.218	8.702	9.669	10.636	11.603	12.569	13.536	14.503	15.470	19.338	24.172	29.006	33.841
42	94.0		6.52E+05	5.073	7.102	8.117	8.624	9.132	10.146	11.161	12.175	13.190	14.205	15.219	16.234	20.292	25.365	30.439	35.512
43	96.2		6.68E+05	5.318	7.445	8.508	9.040	9.572	10.635	11.699	12.762	13.826	14.889	15.953	17.016	21.270	26.588	31.905	37.223
44	98.4	50	6.83E+05	5.568	7.795	8.908	9.465	10.022	11.135	12.249	13.363	14.476	15.590	16.703	17.817	22.271	27.839	33.406	38.974
45	100.7		6.99E+05	5.824	8.153	9.318	9.900	10.483	11.647	12.812	13.977	15.142	16.306	17.471	18.636	23.295	29.118	34.942	40.766
46	102.9		7.15E+05	6.085	8.520	9.737	10.345	10.954	12.171	13.388	14.605	15.822	17.039	18.256	19.473	24.342	30.427	36.512	42.598
47	105.1		7.30E+05	6.353	8.894	10.165	10.800	11.435	12.706	13.976	15.247	16.517	17.788	19.059	20.329	25.411	31.764	38.117	44.470
48	107.4		7.46E+05	6.626	9.277	10.602	11.264	11.927	13.252	14.577	15.903	17.228	18.553	19.878	21.203	26.504	33.130	39.756	46.383
49	109.6	55	7.61E+05	6.905	9.667	11.048	11.739	12.429	13.810	15.191	16.572	17.953	19.334	20.715	22.096	27.620	34.525	41.430	48.335
50	111.8		7.77E+05	7.190	10.066	11.504	12.223	12.942	14.380	15.817	17.255	18.693	20.131	21.569	23.007	28.759	35.949	43.139	50.328
51	114.1		7.92E+05	7.480	10.472	11.968	12.716	13.464	14.960	16.456	17.953	19.449	20.945	22.441	23.937	29.921	37.401	44.881	52.362
52	116.3		8.08E+05	7.776	10.887	12.442	13.220	13.998	15.553	17.108	18.663	20.219	21.774	23.329	24.885	31.106	38.882	46.659	54.435
53	118.6	60	8.23E+05	8.078	11.310	12.925	13.733	14.541	16.157	17.772	19.388	21.004	22.620	24.235	25.851	32.314	40.392	48.470	56.549
54	120.8		8.39E+05	8.386	11.741	13.418	14.256	15.095	16.772	18.449	20.127	21.804	23.481	25.158	26.836	33.545	41.931	50.317	58.703

DRAG FORCE CALCULATIONS FOR VARIOUS WIND TUNNEL FREESTREAM VELOCITIES AND DRAG COEFFICIENTS.

IMAGE 8

WIDTH (m)	HEIGHT (m)
0.20777	0.08804

BLOCKAGE LESS THAN 10%

Diameter Dprojected (m)	0.20777
Area Projected (m^2)	0.03390
Density (kg/m^3)	1.2
Mu ($N\text{-}s/m^2$)	1.80E-05
Kinematic Viscosity	1.50E-05

Cd

				0.5	0.7	0.8	0.85	0.9	1	1.1	1.2	1.3	1.4	1.5	1.6	2	2.5	3	3.5
Tunnel Speed				Force															
m/s	MPH	Hz	RE #	lbs	lbs	lbs	lbs	lbs	lbs	lbs	lbs	lbs	lbs	lbs	lbs	lbs	lbs	lbs	lbs
0	0.0		0.00E+00	0.000	0.000	0.000	0.000	0.000	0.000	0.000	0.000	0.000	0.000	0.000	0.000	0.000	0.000	0.000	0.000
1	2.2		1.39E+04	0.002	0.003	0.004	0.004	0.004	0.005	0.005	0.005	0.006	0.006	0.007	0.007	0.009	0.011	0.014	0.016
2	4.5	2	2.77E+04	0.009	0.013	0.015	0.016	0.016	0.018	0.020	0.022	0.024	0.026	0.027	0.029	0.037	0.046	0.055	0.064
3	6.7	2	4.16E+04	0.021	0.029	0.033	0.035	0.037	0.041	0.045	0.049	0.054	0.058	0.062	0.066	0.082	0.103	0.123	0.144
4	8.9	4	5.54E+04	0.037	0.051	0.059	0.062	0.066	0.073	0.080	0.088	0.095	0.102	0.110	0.117	0.146	0.183	0.220	0.256
5	11.2		6.93E+04	0.057	0.080	0.091	0.097	0.103	0.114	0.126	0.137	0.149	0.160	0.171	0.183	0.229	0.286	0.343	0.400
6	13.4		8.31E+04	0.082	0.115	0.132	0.140	0.148	0.165	0.181	0.198	0.214	0.230	0.247	0.263	0.329	0.412	0.494	0.576
7	15.7		9.70E+04	0.112	0.157	0.179	0.190	0.202	0.224	0.246	0.269	0.291	0.314	0.336	0.359	0.448	0.560	0.672	0.784
8	17.9		1.11E+05	0.146	0.205	0.234	0.249	0.263	0.293	0.322	0.351	0.380	0.410	0.439	0.468	0.585	0.732	0.878	1.024
9	20.1		1.25E+05	0.185	0.259	0.296	0.315	0.333	0.370	0.407	0.445	0.482	0.519	0.556	0.593	0.741	0.926	1.111	1.297
10	22.4		1.39E+05	0.229	0.320	0.366	0.389	0.412	0.457	0.503	0.549	0.595	0.640	0.686	0.732	0.915	1.143	1.372	1.601
11	24.6		1.52E+05	0.277	0.387	0.443	0.470	0.498	0.553	0.609	0.664	0.719	0.775	0.830	0.885	1.107	1.383	1.660	1.937
12	26.8		1.66E+05	0.329	0.461	0.527	0.560	0.593	0.659	0.724	0.790	0.856	0.922	0.988	1.054	1.317	1.646	1.976	2.305
13	29.1	15	1.80E+05	0.386	0.541	0.618	0.657	0.696	0.773	0.850	0.927	1.005	1.082	1.159	1.237	1.546	1.932	2.319	2.705
14	31.3		1.94E+05	0.448	0.627	0.717	0.762	0.807	0.896	0.986	1.076	1.165	1.255	1.345	1.434	1.793	2.241	2.689	3.137
15	33.6		2.08E+05	0.514	0.720	0.823	0.875	0.926	1.029	1.132	1.235	1.338	1.441	1.543	1.646	2.058	2.572	3.087	3.601
16	35.8		2.22E+05	0.585	0.820	0.937	0.995	1.054	1.171	1.288	1.405	1.522	1.639	1.756	1.873	2.341	2.927	3.512	4.098
17	38.0	20	2.35E+05	0.661	0.925	1.057	1.123	1.189	1.322	1.454	1.586	1.718	1.850	1.982	2.115	2.643	3.304	3.965	4.626
18	40.3		2.49E+05	0.741	1.037	1.185	1.259	1.334	1.482	1.630	1.778	1.926	2.074	2.223	2.371	2.963	3.704	4.445	5.186
19	42.5		2.63E+05	0.825	1.156	1.321	1.403	1.486	1.651	1.816	1.981	2.146	2.311	2.476	2.641	3.302	4.127	4.953	5.778
20	44.7		2.77E+05	0.915	1.280	1.463	1.555	1.646	1.829	2.012	2.195	2.378	2.561	2.744	2.927	3.659	4.573	5.488	6.402
21	47.0		2.91E+05	1.008	1.412	1.613	1.714	1.815	2.017	2.218	2.420	2.622	2.823	3.025	3.227	4.034	5.042	6.050	7.059
22	49.2	25	3.05E+05	1.107	1.549	1.771	1.881	1.992	2.213	2.435	2.656	2.877	3.099	3.320	3.541	4.427	5.534	6.640	7.747
23	51.4		3.19E+05	1.210	1.693	1.935	2.056	2.177	2.419	2.661	2.903	3.145	3.387	3.629	3.871	4.838	6.048	7.258	8.467
24	53.7		3.32E+05	1.317	1.844	2.107	2.239	2.371	2.634	2.898	3.161	3.424	3.688	3.951	4.215	5.268	6.585	7.902	9.220
25	55.9		3.46E+05	1.429	2.001	2.287	2.430	2.572	2.858	3.144	3.430	3.716	4.002	4.287	4.573	5.717	7.146	8.575	10.004
26	58.2	30	3.60E+05	1.546	2.164	2.473	2.628	2.782	3.091	3.401	3.710	4.019	4.328	4.637	4.946	6.183	7.729	9.274	10.820
27	60.4		3.74E+05	1.667	2.334	2.667	2.834	3.000	3.334	3.667	4.001	4.334	4.667	5.001	5.334	6.668	8.335	10.002	11.669
28	62.6		3.88E+05	1.793	2.510	2.868	3.048	3.227	3.585	3.944	4.302	4.661	5.020	5.378	5.737	7.171	8.963	10.756	12.549
29	64.9		4.02E+05	1.923	2.692	3.077	3.269	3.461	3.846	4.231	4.615	5.000	5.384	5.769	6.154	7.692	9.615	11.538	13.461
30	67.1		4.16E+05	2.058	2.881	3.293	3.498	3.704	4.116	4.527	4.939	5.351	5.762	6.174	6.585	8.232	10.290	12.348	14.406
31	69.3	35	4.29E+05	2.197	3.076	3.516	3.736	3.955	4.395	4.834	5.274	5.713	6.153	6.592	7.032	8.790	10.987	13.185	15.382
32	71.6		4.43E+05	2.341	3.278	3.746	3.981	4.215	4.683	5.151	5.620	6.088	6.556	7.024	7.493	9.366	11.707	14.049	16.390
33	73.8		4.57E+05	2.490	3.486	3.984	4.233	4.482	4.980	5.478	5.976	6.474	6.972	7.470	7.968	9.960	12.451	14.941	17.431
34	76.1		4.71E+05	2.643	3.701	4.229	4.494	4.758	5.287	5.815	6.344	6.873	7.401	7.930	8.459	10.573	13.217	15.860	18.503
35	78.3	40	4.85E+05	2.801	3.922	4.482	4.762	5.042	5.602	6.162	6.723	7.283	7.843	8.403	8.963	11.204	14.005	16.807	19.608
36	80.5		4.99E+05	2.963	4.149	4.741	5.038	5.334	5.927	6.520	7.112	7.705	8.298	8.890	9.483	11.854	14.817	17.781	20.744
37	82.8		5.12E+05	3.130	4.382	5.009	5.322	5.635	6.261	6.887	7.513	8.139	8.765	9.391	10.017	12.521	15.652	18.782	21.912
38	85.0		5.26E+05	3.302	4.623	5.283	5.613	5.943	6.604	7.264	7.924	8.585	9.245	9.906	10.566	13.207	16.509	19.811	23.113
39	87.2		5.40E+05	3.478	4.869	5.565	5.912	6.260	6.956	7.651	8.347	9.043	9.738	10.434	11.129	13.912	17.390	20.868	24.345
40	89.5	45	5.54E+05	3.659	5.122	5.854	6.220	6.585	7.317	8.049	8.781	9.512	10.244	10.976	11.707	14.634	18.293	21.951	25.610
41	91.7		5.68E+05	3.844	5.381	6.150	6.534	6.919	7.688	8.456	9.225	9.994	10.763	11.531	12.300	15.375	19.219	23.063	26.906
42	94.0		5.82E+05	4.034	5.647	6.454	6.857	7.260	8.067	8.874	9.681	10.487	11.294	12.101	12.907	16.134	20.168	24.201	28.235
43	96.2		5.96E+05	4.228	5.919	6.765	7.187	7.610	8.456	9.301	10.147	10.993	11.838	12.684	13.529	16.912	21.140	25.368	29.595
44	98.4	50	6.09E+05	4.427	6.198	7.083	7.526	7.968	8.854	9.739	10.624	11.510	12.395	13.281	14.166	17.707	22.134	26.561	30.988
45	100.7		6.23E+05	4.630	6.483	7.409	7.872	8.335	9.261	10.187	11.113	12.039	12.965	13.891	14.817	18.521	23.152	27.782	32.413
46	102.9		6.37E+05	4.838	6.774	7.742	8.225	8.709	9.677	10.645	11.612	12.580	13.548	14.515	15.483	19.354	24.192	29.031	33.869
47	105.1		6.51E+05	5.051	7.072	8.082	8.587	9.092	10.102	11.112	12.123	13.133	14.143	15.153	16.164	20.204	25.256	30.307	35.358
48	107.4		6.65E+05	5.268	7.376	8.429	8.956	9.483	10.537	11.590	12.644	13.698	14.751	15.805	16.859	21.073	26.342	31.610	36.878
49	109.6	55	6.79E+05	5.490	7.686	8.784	9.333	9.882	10.980	12.078	13.176	14.274	15.372	16.470	17.568	21.961	27.451	32.941	38.431
50	111.8		6.93E+05	5.717	8.003	9.146	9.718	10.290	11.433	12.576	13.720	14.863	16.006	17.150	18.293	22.866	28.583	34.299	40.016
51	114.1		7.06E+05	5.947	8.326	9.516	10.111	10.705	11.895	13.084	14.274	15.463	16.653	17.842	19.032	23.790	29.737	35.685	41.632
52	116.3		7.20E+05	6.183	8.656	9.893	10.511	11.129	12.366	13.603	14.839	16.076	17.312	18.549	19.786	24.732	30.915	37.098	43.281
53	118.6	60	7.34E+05	6.423	8.992	10.277	10.919	11.562	12.846	14.131	15.415	16.700	17.985	19.269	20.554	25.692	32.115	38.538	44.961
54	120.8		7.48E+05	6.668	9.335	10.668	11.335	12.002	13.335	14.669	16.003	17.336	18.670	20.003	21.337	26.671	33.339	40.006	46.674

t

Appendix D: Sample of collected drag force data output from the LabVIEW virtual instrument for Model 8 at a freestream tunnel velocity of 18 m/s. (Please refer to enclosed compact disk for complete data set.)

Image 8 @ 18 m/s		
Drag Force (Kg)	Time(s)	Pressure (inH20)
2.173	0	-0.782
2.402	0.638	-0.782
2.246	1.222	-0.782
2.125	1.811	-0.782
2.161	2.398	-0.782
2.39	2.985	-0.782
2.342	3.57	-0.782
2.294	4.16	-0.782
2.258	4.749	-0.782
2.306	5.337	-0.782
2.21	5.927	-0.782
2.318	6.514	-0.782
2.354	7.103	-0.782
2.137	7.693	-0.782
2.222	8.282	-0.782
2.234	8.872	-0.782
2.161	9.462	-0.782
2.234	10.054	-0.782
2.246	10.644	-0.782
2.161	11.236	-0.782
2.21	11.827	-0.782
2.137	12.417	-0.782
2.27	13.009	-0.782
2.234	13.6	-0.782
2.198	14.192	-0.782
2.222	14.783	-0.782
2.246	15.375	-0.782
2.414	15.968	-0.782
2.234	16.559	-0.782
2.185	17.152	-0.782
2.342	17.745	-0.782
2.45	18.338	-0.782
2.173	18.93	-0.782
2.258	19.524	-0.782
2.246	20.117	-0.782
2.149	20.711	-0.782
2.21	21.302	-0.782
2.27	21.898	-0.782
2.185	22.491	-0.782
2.258	23.086	-0.782
2.198	23.678	-0.782
2.366	24.273	-0.782

Drag reading with no tunnel speed and model attached (Kg)
1.081

Average Drag reading at speed (Kg)
2.25365

Temperature=80 F

Actual Average Drag Force (Kg)
1.17265

Actual Average Drag Force (lb)
2.585251161

Standard Deviation (Kg)
0.076958303

Error bar values (+/-)
0.010883548

2.366	24.867	-0.782
2.185	25.46	-0.782
2.234	26.053	-0.782
2.246	26.647	-0.782
2.33	27.243	-0.782
2.234	27.838	-0.782
2.318	28.432	-0.782
2.246	29.027	-0.782
2.366	29.622	-0.782
2.39	30.217	-0.782
2.258	30.811	-0.782
2.366	31.407	-0.782
2.366	32.001	-0.782
2.173	32.596	-0.782
2.222	33.189	-0.782
2.173	33.786	-0.782
2.137	34.383	-0.782
2.27	34.976	-0.782
2.354	35.574	-0.782
2.294	36.17	-0.782
2.33	36.765	-0.782
2.306	37.361	-0.782
2.234	37.956	-0.782
2.354	38.552	-0.782
2.318	39.147	-0.782
2.294	39.742	-0.782
2.354	40.338	-0.782
2.294	40.933	-0.782
2.366	41.53	-0.782
2.161	42.127	-0.782
2.089	42.722	-0.782
2.258	43.319	-0.782
2.149	43.917	-0.782
2.125	44.512	-0.782
2.185	45.109	-0.782
2.234	45.707	-0.782
2.294	46.302	-0.782
2.246	46.9	-0.782
2.366	47.498	-0.782
2.306	48.094	-0.782
2.185	48.691	-0.782
2.149	49.289	-0.782
2.234	49.886	-0.782
2.198	50.483	-0.782
2.234	51.08	-0.782
2.198	51.676	-0.782
2.246	52.274	-0.782
2.27	52.87	-0.782

2.198	53.468	-0.782
2.222	54.064	-0.782
2.258	54.661	-0.782
2.258	55.259	-0.782
2.282	55.855	-0.782
2.27	56.451	-0.782
2.402	57.05	-0.782
2.282	57.646	-0.782
2.27	58.244	-0.782
2.27	58.841	-0.782
2.246	59.438	-0.782
2.173	60.036	-0.782
2.246	60.633	-0.782
2.282	61.231	-0.782
2.438	61.83	-0.782
2.21	62.427	-0.782
2.294	63.024	-0.782
2.234	63.622	-0.782
2.294	64.219	-0.782
2.198	64.817	-0.782
2.089	65.415	-0.782
2.354	66.011	-0.782
2.173	66.609	-0.782
2.198	67.207	-0.782
2.354	67.803	-0.782
2.21	68.403	-0.782
2.294	69.002	-0.782
2.246	69.598	-0.782
2.21	70.196	-0.782
2.354	70.794	-0.782
2.462	71.391	-0.782
2.258	71.989	-0.782
2.222	72.586	-0.782
2.246	73.183	-0.782
2.258	73.778	-0.782
2.318	74.38	-0.782
2.258	74.978	-0.782
2.294	75.574	-0.782
2.366	76.173	-0.782
2.234	76.772	-0.782
2.282	77.371	-0.782
2.426	77.969	-0.782
2.258	78.568	-0.782
2.27	79.167	-0.782
2.161	79.764	-0.782
2.198	80.364	-0.782
2.185	80.963	-0.782
2.125	81.561	-0.782

2.282	82.16	-0.782
2.161	82.758	-0.782
2.185	83.356	-0.782
2.282	83.955	-0.782
2.378	84.554	-0.782
2.414	85.153	-0.782
2.306	85.751	-0.782
2.246	86.35	-0.782
2.258	86.948	-0.782
2.378	87.547	-0.782
2.294	88.147	-0.782
2.282	88.746	-0.782
2.318	89.345	-0.782
2.222	89.945	-0.782
2.198	90.545	-0.782
2.234	91.145	-0.782
2.234	91.75	-0.782
2.294	92.349	-0.782
2.185	92.948	-0.782
2.137	93.549	-0.782
2.21	94.148	-0.782
2.173	94.747	-0.782
2.45	95.346	-0.782
2.198	95.945	-0.782
2.077	96.546	-0.782
2.21	97.144	-0.782
2.306	97.744	-0.782
2.306	98.343	-0.782
2.21	98.943	-0.782
2.366	99.544	-0.782
2.234	100.143	-0.782
2.318	100.743	-0.782
2.21	101.344	-0.782
2.198	101.945	-0.782
2.234	102.545	-0.782
2.234	103.144	-0.782
2.33	103.744	-0.782
2.354	104.345	-0.782
2.246	104.947	-0.782
2.161	105.548	-0.782
2.234	106.148	-0.782
2.27	106.748	-0.782
2.294	107.348	-0.782
2.258	107.949	-0.782
2.234	108.55	-0.782
2.198	109.15	-0.782
2.258	109.752	-0.782
2.077	110.351	-0.782

2.173	110.952	-0.782
2.137	111.553	-0.782
2.294	112.154	-0.782
2.222	112.755	-0.782
2.246	113.355	-0.782
2.246	113.954	-0.782
2.234	114.556	-0.782
2.161	115.157	-0.782
2.354	115.759	-0.782
2.258	116.359	-0.782
2.185	116.96	-0.782
2.173	117.561	-0.782
2.149	118.162	-0.782
2.198	118.763	-0.782

Appendix E: Stock Material Pricing

DELRIN (ACETAL)

Plastics Unlimited
10/31/05
Pricing on Natural Delrin (Round Stock)

10 " dia $365.33/ft - Standard Length 36"
so on this you would rec. 1 pc 3 ft
* & 1 pc 1 ft
6" dia x 18" long material in stock
$181.20/pc
2" dia x 12" material in stock $27.16/ft

Would have to order the 10" dia in just 3-4 days to get.

Thanks again

Wendy

TriStar Plastics

Brian,

Here is the information that you requested.

8” dia. Natural Acetal rod - $258.00/ft.

9” dia. Natural Acetal rod - $312.46/ft.

10” dia. Natural Acetal rod - $382.70/ft.

I would have to order all three of these. It would take 2-3 days for it to hit my dock once we get it on order.

Please let me know if you have any questions or if you need anything else from me.

Thank you,
Brian

Brian Parath
Branch Manager
Tri Star Plastics Corp.
phone - 800-323-3311, ext. 3209
fax - 508-845-1200
cell - 508-847-8645

ALUMINUM

Yarde Metals
11/1/05
Sales Quote:

> |ITEM |Quantity |Order Units|
> --
> 6061-T651-RD 2.0000 x 12' 0" 1 Pieces
@ $ 118.00 ea
> 6061-T651-RD 6.0000 x 12' 0" 1.5 Feet
@ $ 168.00 ea
> 6061-T6511-RD 10.0000 x 12' 0" 3.5 Feet
@ $ 774.00 ea

thank you,

Dave Chisholm
Sales
Yarde Metals
David.Chisholm@Yarde.com
Ph: 800-376-2011
Fx; 603-635-1282

Pricing from Drop Zone:

Aluminum 6061-T6 Round Stock

10.125" x 30.5" $426.70
9.0" x 27.5" $292.40
7.2" x 7.375" $49.50

Rough estimate of stock size needed:

Stock dia (inches)	max dia. (inches)	height (inches)	boss height (inches)	total height (inches)	stock height rounded up (inches)
2	1.278	5.634	3	8.63	10
6	4.489	4.953	3	7.95	9
6	5.482	4.151	3	7.15	9
9	7.131	3.315	3	7.31	9
9	8.497	3.193	3	7.19	9
9	8.802	2.457	3	5.45	7
10	9.174	2.154	3	5.15	7
9	8.180	3.466	3	7.46	9

Delrin cost estimate: approx. $1,600
Aluminum cost *estimate: approx. $1,1*00

Material request correspondence with Dr. Kenneth Desabrais at the Natick Soldier Center:

Checking into now. I will get back to you guys in a few days with more details.

Ken

-----Original Message-----
From: Day, Brian P [mailto:brianday@WPI.EDU]
Sent: Friday, November 04, 2005 3:33 PM
To: kenneth.desabrais@natick.army.mil
Cc: dropteam@WPI.EDU
Subject: Material and Tooling Request

Ken,

The machine shop gave us a request for tooling and we also have some initial material requests so we can get going on our simplest shapes (shape 1 & 2). Could you order these for us?

The machine shop would like:

From MSC:
ER-11 Collet Extension
MSC #: 84904523
Cost: $105.95
Shank dia.: .625"
overall length: 6.67"

Material from Plastics Unlimited:
Sales Rep: Wendy

Natural Delrin

6" dia x 18" long   material in stock $181.20/pc

2" dia x 12"   material in stock $27.16/ft

NOTE: These prices do not include shipping

Thanks,

Brian
Justin
Matt

Guys,

Your first order from Plastics Unlimited is in ME office, I think. I also have the collet extension from MSC. I'll leave it in the small office tonight near the wind tunnel where I store all my stuff. Ask Prof. Johari to let you in the office to get
it.

I'm going to put your second order from Plastics Unlimited in system today.

I'll be on-campus next week if you have any questions.

Have a good weekend.

Ken

-----Original Message-----
From: Day, Brian P [mailto:brianday@WPI.EDU]
Sent: Wednesday, November 16, 2005 4:29 PM
To: kenneth.desabrais@natick.army.mil
Cc: dropteam@WPI.EDU
Subject: Additional Material Request

Ken,

In addition to the material you have already ordered, we will need the following:

Acetal (delrin or equivalent)

ITEM 1:
3 ft length of 9" dia Acetal $312.46/ft
From Tri Star Plastics in Shrewsbury
If you order this size from Plastics Unlimited it will cost $343.22/ft

ITEM 2:
1 ft length 10" dia Acetal $365.33/ft
From Plastics Unlimited in Worcester
If you order this size from Tri Star it will cost $382.70/ft

According to these companies, Acetal stock of this size does not come in square blocks.

Thanks,

Justin, Matt, Brian